NANO-MODIFIED SLAG-BASED CEMENTITIOUS COMPOSITES REINFORCED WITH MULTI-SCALE FIBER SYSTEMS

by
Omar Mohamed Mahmoud Hosny Abdelrahim Youssef

A Thesis submitted to the Faculty of Graduate Studies of
The University of Manitoba
In partial fulfillment of the requirements of the degree of

Master of Science

Department of Civil Engineering

University of Manitoba

Winnipeg

ABSTRACT

This thesis responds to the need for improving the overall performance of concrete infrastructure to achieve longer service life, fewer cycles of repair, and reduced life-cycle costs. Novel high-performance fiber-reinforced cementitious composites were developed, which comprised high content (50%) slag by mass of the base binder as well as nano-silica (NS) or nano-crystalline cellulose (NCC). In addition, nano-fibrillated cellulose (NFC), and a novel form of basalt fiber strands protected by polymeric resins: basalt fiber pellets (BFP), representing nano-/micro- and macro-fibers, respectively were incorporated in the composites. The response surface method was used in the statistical modeling part to evaluate the impact of key factors (NS, NCC, NFC, BFP) on the performance of 15 mixtures. The composites were assessed in terms of setting times, early- and late-age compressive strength, flexural performance, and resistance to freezing-thawing cycles, and the bulk trends were corroborated by fluid absorption, thermogravimetry and microscopy tests. Moreover, selected high-performance composites were extracted from laboratory testing and numerical optimization scenarios to access their suitability as a repair/overlay option for concrete flatwork.

While the addition of BFP reduced the compressive and flexural capacity of the composites by an average of 20% and 37%, respectively, after 28 days, the co-existence of NCC and/or NFC alleviated this trend. Furthermore, all nano-modified composites with multi-scale fibers showed notable improvement in terms of post-cracking flexural performance (residual strength up to 7.9 MPa, and toughness up to 46.8 J) and resistance to ingress of fluids (absorption less than 2.5%) and frost action (durability factor more than 90%. Generally, all composites selected for use as a repair/overlay option showed superior qualities: high mechanical and durability properties, as well as mechanical compatibility

with substrate concrete. In particular, composites incorporating (up to 3.75%) NS and (0.0375–0.1) NCC in slag-based composites, with (0.25–0.375) NFC and (4.5%) BFP, which can be an effective option for flatwork toppings requiring balance between high-strength, ductility and durability.

Dedication

Every stage in life teases your mind to think about different

perspectives

of the journey you are living.

It reshapes your thoughts and direct them to one single fact,

which is

To **Allah** we belong and to Him we will return.

This work is dedicated to:

My Parents, Mohamed and Samar,

My Sister, Nour,

My Grandparents, may their soul rest in Allah’s mercy,

And my uncle, Khaled

Acknowledgements

Alhamdulillah, glory be to the Almighty Allah, the All-Powerful, Most Gracious, and Most Merciful. To whom I would like to thank for giving me the strength and guidance to complete this thesis. After that, I would like to thank our Prophet Muhammad SAAWS, who fulfilled the message of Allah and advised the people and guided us to the moral life we enjoy today.

I appreciate all of the hard work and assistance my supervisor, Prof. Mohamed T. Bassuoni, has given me during my study. I am dedicating the quality of this work to Dr. Bassuoni's great degree of commitment, immense knowledge, and enthusiasm. This success would not have been attainable without his mentorship.

Moreover, I would like to specially thank Dr. Ahmed Ghazy for his mentorship, guidance, and constant support. Also, I appreciate the support I received from Dr. Ahmed Yasien for his professional attitude and hard work in assisting me during my work stages. I also want to acknowledge the efforts of the McQuade Heavy Structures Laboratory staff, for their technical assistance during the planning and testing phases.

I am grateful for the financial support by the Natural Sciences and Engineering Research Council of Canada (NSERC), Performance Biofilaments, and the City of Winnipeg.

Finally, to the two most important people in my life, Mohamed M. Hosny and Samar A. Hassan, I would like to express my sincere gratitude for their moral guidance and religious enlightenment throughout my whole life. I appreciate their endless support, love, kindness, and prayers. May Allah bring our hearts together in this life and the hereafter.

TABLE OF CONTENTS

LIST OF TABLES

LIST OF FIGURES

NOTATIONS

AEA Air entrainment admixture

ANOVA Analysis of Variance

BF Basalt Fiber

BFP Basalt fiber pellets

Ca^{++} Calcium Ion

$CaCl_2$ Calcium Chloride

CC conventional concrete

CCD Central Composite Design

CF Cellulose fiber

CH Calcium hydroxide

COW City of Winnipeg

CNC Cellulose-nano crystals

C-S-H Calcium-silicate-hydrate

C/S Calcium-to-Silicate Ratio

DF Durability Factor

EDX Energy dispersive X-ray analysis

f'c 28d 28 Days Compressive Strength

f'c 3d 3 Days Compressive Strength

FCCD Face-Centered Composite Design

FST Final Setting Time

FRP Fiber-reinforced polymer

FRCC Fiber-reinforced cementitious Composite

GGBFS Ground granulated blast furnace slag

GU General Use Cement

HPFRCC High-performance fiber-reinforced cementitious composites

HRWRA High-range water reducing Agent

IST Initial Setting Time

ITZ Interfacial transition zone

MFC Micro-fibrillated cellulose

NaCl Sodium Chloride

NS Nano-silica

NCC Nano-crystalline cellulose

NFC Nano-fibrillated cellulose

OH- Hydroxyl Ion

R^2 Coefficient of Determination

RH Relative Humidity

RSM Response Surface Method

SCMs Supplementary Cementitious Materials

SEM Scanning electron microscopy

TGA Thermogravimetric analysis

UHPC Ultrahigh performance concrete

w/b Water-To-Binder Ratio

x Experimental Value

X_i Independent Variable

y The Statistical Model Response (Predicted)

$\beta 0$ Model Intercept

β_i Linear Regression Coefficients

β_{ii} Quadratic Regression Coefficients

β_{ij} Interaction Regression Coefficients

ϵ Model Random Error

CHAPTER 1: INTRODUCTION

1.1 Overview

Environmental challenges such as global warming and energy consumption usually accompany the growth of concrete infrastructure, which is essential to ensure the continued economic growth of different countries. In light of world strategies to deal with environmental concerns, the concrete industry is experiencing pressing need towards adopting sustainable approaches to reduce the carbon footprint and increase eco-efficiency such as replacing cement with supplementary cementitious materials (SCMs) (Cheah & Ramli, 2014; Sanchez & Sobolev, 2010). The performance of concrete infrastructure (e.g., bridge decks, pavements, runways, etc.) depends on various factors such as the rheological, mechanical as well as durability properties of the used materials. Moreover, the exposure conditions and loading configurations have a significant impact on the service life of concrete structures. These interrelated parameters may result in the initiation and propagation of cracks in concrete, and consequently affect its overall performance and longevity (Safiuddin et al., 2018).

Brittleness, exposure conditions and loading configurations typically result in the initiation and propagation of cracks in concrete, and consequently affect its overall performance and longevity. Hence, numerous studies have been conducted to introduce high-performance fiber-reinforced cementitious composites (HPFRCC) in which fibers are a crucial component to control cracking and enhance tensile performance including post-cracking behavior and ductility (e.g., Azzam et al., 2019a; Spadea et al., 2015; Kang and Kim, 2011). HPFRCC can be employed in a suite of concrete applications such as production of thinner and lighter structural elements, beam-column joints,

retrofitting/strengthening of flexural sides of elements, toping of heavy-duty flatwork (e.g., parking structures), etc.

HPFRCC incorporating high-volume SCMs, such as slag, typically has improved durability with the added sustainability benefits of preserving natural resources, reducing energy consumption, improving air quality and offering a waste management option (Mehta & Monteiro, 2014). However, there is still lack of confidence in using higher volumes of SCMs in concrete among various stakeholders mainly due to performance limitations including delay in setting time and slow strength development which adversely affect construction schedules and hence projects' budgets (e.g., Eco Smart Foundation, 2007). Due to their ultrafine nature, nanomaterials (size scale of 1-100 billionth of a meter in any dimension) can vigorously speed-up the kinetics of cement hydration, impart pozzolanic reactivity (nano-silica, nano-clay) and efficiently refine the pore structure in the matrix (Sanchez & Sobolev, 2010). Their application in cementitious binders (nano-modification) has shown great potential to mitigate the performance issues associated with the use of higher volumes of SCMs and create innovative types of sustainable cement-based products with superior performance. For instance, findings from previous studies showed that addition of 1-6% nano-silica or 5-20% nano-calcium carbonate by mass of binder has an accelerating effect on early-age properties (hydration, setting time and strength development) of cementitious systems incorporating 30-50% fly ash or slag as a cement replacement (e.g., Ghazy, Bassuoni, Maguire, et al., 2016; Bentz et al., 2012; Zhang et al., 2012).

Macro-fiber reinforcement is usually used to enhance the cementitious matrices' ductility through bridging of macro-cracks (Mexasa et al., 2011). Comparatively, nano- and micro-scale fibers may interlink the cementitious matrix and successfully bridge the

nano-/micro-cracks (Siddique & Mehta, 2014). For instance, numerous studies were carried out to develop fiber-reinforced cementitious composites (FRCC) with improved flexural performance such as post-cracking behavior and fracture toughness (Azzam et al., 2019a; Spadea et al., 2015; S.-T. Kang & Kim, 2011; Hsie et al., 2008;).

Recently, it has been shown that cellulose-based nanomaterials [nano-crystalline cellulose (NCC), and nano-fibrillated cellulose (NFC)] can improve the characteristics of cementitious materials (Balea et al., 2019; Cao et al., 2016; Moon et al., 2011). These sustainable and biodegradable nanomaterials have high surface area and aspect ratio, low density, low thermal expansion coefficient, and low cost compared to other nanomaterials [e.g., nano-silica, carbon nanotubes] (Sharip and Ariffin, 2019; Moon et al., 2011). However, there is still dearth of information on the effect of cellulose-based nanomaterials on different types of HPFRCC (e.g., high-strength types) and their interaction in the mixtures with high volume SCMs or other types of fibers.

Basalt fibers have been used as a reinforcement in cementitious materials due to their mechanical characteristics (strength up to 4,000 MPa, modulus of elasticity up to 100 GPa), non–corrosive nature, high thermal resistance and low cost compared to other types of fibers [e.g., carbon, glass, steel] (Yi et al., 2021; J. J. Lee et al., 2014). However, degradation of basalt fibers in alkaline media, such as cement-based matrices with high pH, was reported due to reactions between the silicate component in the fibers and alkaline pore solution, which had negative effects on strength and durability of the hardened cementitious matrix (C. Jiang et al., 2014). Therefore, a novel form of encapsulated basalt fiber strands in a protective polymeric resin (e.g. epoxy, polyamide, etc.) known as basalt fiber pellets (BFP) has been recently introduced to mitigate this performance risk

(Mahmoud et al., 2017). HPFRCC incorporating BFP may offer a viable option for a suite of applications, which warrants focused research in this direction.

1.2 Need for Research

Concerted efforts at the University of Manitoba have led to the development of slag-based (50%) cementitious composites modified with 6% nano-silica, meeting Category 1 high-volume SCM concrete according to the Canadian Standards Association, (2019) and reinforced with a novel class of non-metallic fibers [BFP] (Mahmoud et al., 2017). These composites showed high-performance in terms of high strength and ductility as well as high resistance to ingress of fluids, alkaline environments and frost action without/with de-icing salts (Azzam et al., 2021; Azzam et al., 2022; Bedwiy et al., 2022). Yet, further aspects such as other binder formulations based on sustainable nanomaterials and their interactions with BFP still require exploration.

This thesis is part of an ongoing program led by the Cementitious Materials Research Group at the University of Manitoba. It was conducted to investigate the performance of these composites based on new binder formulations incorporating nano-crystalline cellulose and nano-fibrillated cellulose, and their interactions with high-content slag, nano-silica and BFP. The effects of these key parameters were evaluated by experiments (fresh, hardened, and durability properties) and statistical modeling, which were augmented by thermogravimetry and microscopy analyses. In addition, the optimization of binder formulations with muti-scale fiber systems to address volume stability, bonding and compatibility between these novel high-performance composites with substrate concrete are still unknown. Hence, it was studied in this program. Data from this thesis is essential to informatively assess the suitability and resiliency of these

innovative composites for applications requiring balance of strength, ductility and longevity (e.g., repair/overlay of flatwork).

1.3 Objectives of Research

The primary objectives of this master's thesis are to develop novel HPFRCC and examine their potential as a repair/overlay option for concrete flatwork applications. The precise goals of this research are to:

- develop high-volume slag-based nano-modified cementitious composites comprising BFP without/with nanomaterials (NS, NCC, NFC) and assess their fresh, hardened, fluid transport properties and durability characteristics.
- capture the effect of key parameters of mix designs such as dosages of nanomaterials (NS and NCC), and macro/micro fibers (BFP and NFC).
- introduce optimized scenarios for these composites and test their suitability for repair/overlay applications of concrete flatwork.

1.4 Scope of Research

To achieve the aforementioned objectives, this master's thesis was divided into two stages as described below:

Phase I: slag-based cementitious composites incorporating nano-silica, nano-cellulose material and basalt pellets.

In this phase, a statistical model was established to investigate the effect of changing the proposed materials' dosages and combinations on HPFRCC performance. The impact of mix design parameters on the performance of composites was assessed using the Response Surface Method (RSM), which is based on Face-Centered Composite Design (FCCD). Three factors were considered in the generated models: nanoparticles [NS (0 to 6% addition by mass of binder) and NCC (0 to 0.1% by mass of binder)], NFC (0 to 0.5%

by volume of composite), and BFP (0 to 4.5% by volume of composite) dosages. These parameters were examined at the model's factorial levels of 1 and -1, respectively. By adding more points to the model's factorial set, this technique relies on increasing the precision of forecasting the response space. In order to account for any potential quadratic effects of each variable, a central point, at the intermediate level (0), for each component was also incorporated in the constructed models. Hence, 15 mixtures were cast, and the mixtures' performance was assessed based on fresh properties (air content and setting time), hardened properties (compressive strength and flexural behavior [pre-and post-cracking at 28 days], as well as durability (absorption, freezing/thawing resistance), which were augmented by thermogravimetry and microscopy analyses. Additionally, optimal combinations for repair/overlay applications were found through the numerical optimization scheme conducted herein.

Phase II: nano-modified slag-based cementitious composites reinforced with multi-scale fiber systems as a repair/overlay option

In Phase II, four selected HPFRCC mixtures, as well as two optimized mixtures derived from the optimization scenarios in Phase I were extracted to investigate their potential to be used as a repair/overlay option for concrete flatwork. The mixtures contained a constant BFP dosage of 4.5% (by volume of composite) to attain the highest flexural performance. Tests regarding fresh, mechanical, durability, and compatibility properties were performed to ensure that the qualities of the selected mixture are complying with the target application. The fresh properties included mortar flow, flow retention, air content and setting time. The compressive strength development and flexural toughness of the composites up to 28 days of curing were evaluated to assess the evolution of mechanical capacity with time. The fluid transport properties and durability of the mixtures were

assessed using rapid chloride penetrability test, and resistance to salt-frost scaling. To assess the compatibility between substrate concrete and the HPFRCC, restrained shrinkage and pull-off tests were performed.

1.5 Structure of the Thesis

This thesis consists of six chapters, described as follows:

- CHAPTER 1 contains introduction, main needs for research, significance of the proposed work, objectives and scope of work.
- CHAPTER 2 provides comprehensive literature review on HPFRCC, the effect of SCM in cementitious composites, the effect of using multi-scale cellulosic products, and BFP effects on the performance of HPFRCC.
- CHAPTER 3 describes the adopted statistical modelling approach, methodology, innovative materials, and mixtures used in the testing program. Also, it provides comprehensive details of the test specifications and setups used in Phases I and II.
- CHAPTER 4 includes the results and discussion of the statistical models developed in Phase I and the fresh, hardened and durability properties of HPFRCC. Also, it features a numerical optimization exercise to identify the mixtures used in Phase II.
- CHAPTER 5 presents the results and discussion of Phase II on utilizing nano-modified cementitious composites as a repair/overlay option for flatwork applications to achieve balanced early-age and long-term performance.
- CHAPTER 6 includes conclusive summary of the major findings for the entire thesis and lists the proposed recommendations for future research.

CHAPTER 2: LITERATURE REVIEW

Today's concrete technology faces an unparalleled push toward maximizing eco-efficient construction materials in light of Canadian policies for dealing with environmental challenges such as natural resource depletion and energy consumption constantly accompanying the growth of the concrete industry. In this context, the increased need for high-performance materials resulted in the creation of a new generation of fiber-reinforced cementitious composites, pushing the boundaries of multifunctional engineering qualities that lead to increased eco-efficiency. This can help to reduce issues linked to its manufacturing, structure, and producing high-quality output. In order to minimize brittle failure and enhance the desired properties of concrete, fibers can be added to concrete to enhance tensile strength, flexural performance, post-cracking behavior, and energy absorption capacity. Some types of fibers are also included in concrete for structural member repair, rehabilitation, and retrofitting. Incorporation of numerous natural and synthetic fibers into cementitious composites have also been the subject of in-depth studies across the world, and improvements in these materials are seen as crucial stages toward the attainment of sustainable building developments (Balagopal et al., 2022).

2.1. Overview of Fiber-reinforced cementitious composites (FRCC)

Fiber-reinforced cementitious composites (FRCC) are a group of materials made up of a cementitious-based matrix that has been augmented with fibers. Fibers can greatly enhance the mechanical characteristics of cement-based materials, such as tensile strength, ductility, and impact resistance, making them more useful in a variety of concrete flatwork applications, including construction, infrastructure, and transportation.

Cement, fine aggregate, and different types of fibers are the main components that make up FRCC. Several different fiber types are used for both commercial and

experimental purposes. The two categories of fibers that are now on the market include fibers with a low elasticity modulus but a high elongation property, these types of natural and synthetic fibers including nano-fibrillated cellulose, polyethylene, and polypropylene tend not to increase stiffness, but they do increase strength and plastic shrinkage resistance through different mechanisms. The other category of fibers with high elasticity modulus such as steel, basalt, and carbon fibers are used primarily to increase the strength, toughness, and stiffness of composites.

One of the most commonly used types of FRCCs is steel fiber-reinforced concrete (SFRC). SFRC is known for its high strength, durability, and ability to resist cracking and spalling. It is widely used on industrial floors, airport runways, and other heavy-duty applications. Jhatial et al., (2018) found that the use of steel fibers in SFRC can improve its compressive strength by up to 20% and its flexural strength by up to 20%. Another type of FRCC is glass fiber-reinforced concrete (GFRC). GFRC is known for its high flexural strength and ability to be molded into complex shapes. It is commonly used in architectural cladding and decorative applications such as statues and fountains. The use of glass fibers in GFRC can also improve its fire resistance, making it a suitable material for use in fire-exposed areas. Polymer fiber-reinforced cementitious composites (PFRCs) are a class of FRCCs that use synthetic fibers as reinforcement. These fibers are made of various polymers such as polypropylene, polyethylene, and nylon. PFRCs are commonly used in bridge decks, pavements, and other infrastructure projects.

Basalt fibers, a relatively new form of fiber, are presented to industry. Mined basalt rocks must be heated to 1,400°C. After that, the molten rocks are forced out of tiny nozzles to create continuous basalt fiber threads. They have great flexural properties, and thermal, stability, and are environmentally safe as they are non-toxic fibers. Iyer et al., (2015)

investigated how the addition of basalt fibers at various sizes and doses affected the mechanical properties of composites in a similar manner to composites reinforced with steel fibers.

2.2. High-Performance Fiber-Reinforced Cementitious composites (HPFRCC)

High-Performance Fiber-Reinforced Cementitious composites (HPFRCC) are the evolution of FRCC and have gained popularity in the building sector in recent years. The materials employed in HPFRCC are determined by the required properties and the accessibility of suitable locally produced inexpensive substitute materials. Concrete is a common building material that is often weak in tension and frequently prone to cracking from different sources of deterioration such as impact loading and shrinkage cracks. To resist fractures from spreading, multi-scaled discrete fibers can be incorporated into concrete. Although there is more interest in using HPFRCC in concrete constructions, there are some lingering questions about how fibers affect the characteristics of concrete. Therefore, extensive studies in the last three decades were conducted to evaluate the performance of HPFRCC including (Abtahi et al., 2010; Ardanuy et al., 2015; Azzam et al., 2021; Mechtcherine, 2012; Zheng, 1995), which provides a wide range of knowledge defining the main properties of HPFRCC.

Numerous HPFRCCs were developed to understand and control the behavior of such composites. One of the key factors investigated was the mechanical properties of HPFRCC composites incorporating single and hybrid fiber systems. For instance, Köksal et al., (2008) investigated how steel fibers affected the compressive strength of FRCC incorporating silica fume. Three different percentages were employed to examine the effects of silica fume, including 5, 10, and 15% with two different fiber contents: 0.5 and 1.0%. According to this study, the compressive strengths of steel FRCCs with 15% silica

fume increased up to 118%, when 1% steel fiber content was added compared to the control specimen.

The inclusion of steel fiber composition and mineral admixtures into high-performance concrete (HPC) and the behavior of composites was monitored by Kaïkea et al., (2014), where 10% and 20% by weight of cement, respectively, silica fume and blast-furnace slag were employed as two different types of mineral admixtures. A commercially employed steel fiber was also incorporated into the mixture. The compressive strength of HPC was significantly impacted by the presence of steel fiber. The compressive strength of the mix with 20% slag increased by around 30% as a result of the inclusion of 2% steel fiber content.

Another study that utilized a combination of 0.25% palm fiber, or a combination of 0.5% palm fiber and synthetic fiber with steel fiber (total fiber content of 2%), was found to be highly effective in enhancing the elastic modulus of concrete. These fiber combinations resulted in a 44% and 52% increase, respectively, in the static modulus of elasticity of concrete. This can be attributed to the stronger bond development between the matrix and the fiber fraction (Kayali et al., 2003, Nataraja et al., 1999).

2.3. Role of Supplementary Cementitious Materials (SCM) in Cementitious Composites

In general, supplementary cementitious materials (SCMs) such as ground granulated blast furnace slag (GGBFS), fly ash, and silica fume (SF) are added to concrete to improve the mechanical and durability properties of cementitious composites (He et al., 2018; Jang et al., 2017; Heidari & Tavakoli, 2013), in addition to cost reduction and improvement of the workability of fresh concrete.

In order to develop HPFRCC, it is crucial to have a thorough understanding of how the matrix and fibers interact, as well as the different traits of such composites, in order to control the composite's behavior. Therefore, researchers have explored the impact of incorporating various supplementary cementitious minerals in cementitious composite mixtures to enhance the matrix. The most commonly used minerals are fly ash and slag (Yang et al., 2007). Zhu et al., (2012) investigated the use of 70% mineral admixtures, including fly ash and ground granulated blast furnace slag. The results showed that the combination of mineral admixtures in high-performance cementitious composites (HPCC) can achieve the necessary strain-hardening performance as well as a tensile strain capacity of over 2.5% after 90 days. In addition, the combination of slag and fly ash was found to significantly increase the compressive strength, particularly at early stages. For example, the compressive strength of the mixture with 40% fly ash and 30% slag was 45% and 60% higher compared to the mixture with only 70% fly ash as the total binder.

The impact of GGBFS on the mechanical strength depends primarily upon the type, fineness, activity index, and proportion of slag used in the concrete (Mohamed, 2019; Islam et al., 2014). In general, slag-blended concrete develops lower strength at the initial curing period, i.e., 1–5 days, when compared to control concrete. However, a gradual increase in strength can be observed after 7 and 28 days (Samad & Shah, 2017). The incorporation of GGBS in cement paste helps to transform the larger pores into smaller pores, resulting in a decrease in the permeability of the concrete. It has been reported that this reduction of permeability is achieved due to the replacement level of slag increasing from 40 to 65% of the total cementitious material (Gruyaert et al., 2013). The yielded results may be influenced by factors such as curing temperature, curing time, and the ratio of water to binder (Castellano et al., 2016). It has been found that maintaining a water-to-binder ratio

of 0.30 can enhance the strength of GGBFS blended cement concrete with a 40% cement replacement level.

In terms of durability, partial replacement of cement by GGBFS could decrease permeability, and enhance water transport properties of cementitious composites. Also, it could increase resistance to freeze-thaw cycles, chloride penetrability, and expansion. Incorporation of GGBFS with adequate curing methods and periods resulted in the formation of a dense and impermeable microstructure (Ke et al., 2017). Adding GGBFS to cement paste helps to make the pores in the concrete smaller, which leads to a decrease in its permeability (N. K. Lee & Lee, 2013). Research has shown that this effect is achieved when the amount of slag used as a replacement increases from 40 to 65% of the total cement material (Teng et al., 2013). Concrete with granulated slag may require a reduced concrete cover to protect reinforcing bars from corrosion. Studies have also shown that slag concrete has comparable resistance to freeze-thaw actions compared to conventional concrete (Wawrzeńczyk et al., 2018). Studies by Bakharev et al., (2001) and Khan & Sarker, (2019) have found that using GGBFS in alkali-activated concrete reduces expansion when compared to regular concrete, likely due to a lower calcium/silicate ratio and higher aluminate/silicate ratio.

2.4. Role of Nanoparticles in Cementitious Composites

Despite the ecological and engineering benefits of SCMs in concrete, the use of SCMs as a cement replacement in cementitious composites is typically limited to dosages between 15 or 20%. The slow rate of strength gain and microstructural development at early-age are considered to be the major issues that deter its wider use and acceptance (Malhotra et al. 2000). However, these performance limitations associated with the use of slowly reactive pozzolans (e.g. GGBFS) can be mitigated by incorporation of nanoparticles (size scale of

1-100 billionth of a meter) in concrete (Said et al. 2012). Nanoparticles (e.g. nano-silica) have been applied in concrete research and proven to enhance fresh and hardened properties by modifying the structure of the cementitious matrix at the nano and micro levels (Ghazy et al. 2016; Said et al. 2012). Therefore, their application in concrete may have a greater potential to produce innovative types of cementitious composites with superior performance in harsh environments.

Nano-silica can accelerate the hydration of cement by creating additional surfaces for early precipitation of hydration products (Hou et al. 2013; Korpa et al. 2008). Also, it has been shown that commercial nano-silica sols (originally dispersed to their primary sizes) form small enough agglomerates to impart a filler effect in the cementitious matrix (Oertel et al. 2013; Kong et al., 2012). All these factors might have contributed to improving the early-age strength (up to 7 days) of nano-modified cementitious matrix even for mixtures incorporating high dosages of SCMs.

2.5. Cementitious Composites Reinforced with Basalt Fibers

In recent years, cementitious composites reinforced with basalt fiber have drawn more interest as a viable substitute for conventional reinforced concrete. Basalt fibers, which are made of volcanic rock, have desirable qualities including high tensile strength and great chemical resistance that are similar to those of conventional glass fibers. Basalt fibers, on the other hand, are more eco-friendly because they come from a naturally available resource and don't require the high energy usage needed to produce glass fibers.

Studies have shown that basalt fiber pellets can enhance cementitious composites' mechanical qualities, such as tensile strength, flexural strength, and toughness. For instance, according to studies by Iyer et al., (2015) and C. Jiang et al., (2014), basalt fiber pellets added to concrete enhanced its tensile strength by up to 25%. Another study by

Jalasutram et al., (2017) discovered that adding basalt fibers increased the flexural tensile strength by 75% and toughness was increased by three folds with reference to normal cement-based composites.

In addition, it has been demonstrated that basalt fibers enhance cementitious composites' durability. For instance, Branston et al., (2016) and Ghazy, et al., (2016) employed basalt fibers to increase composite's resistance to shrinkage and crack formation. The results demonstrated that basalt fibers were successful in efficiently preventing cracks formation by minimizing free shrinkage and limiting the propagation of developing cracks. Zhao et al., (2017) studied the resistance of composites incorporating basalt fibers to impact failure after exposure to freezing and thawing cycles. It was found that basalt fiber tripled the resilience of composites to initial crack development from inbound damages and cyclic exposures to frost actions.

The use of basalt fiber pellets in cementitious composites also offers potential environmental benefits. As previously mentioned, basalt fibers are derived from a natural, abundant resource and do not require the high energy consumption necessary for glass fiber production. In addition, this can potentially reduce the carbon footprint of the concrete industry and efficiently contribute to the Canadian 2050 net-zero Emissions plan.

2.6. Role of Nano - Cellulosic Fibers and Crystals in Cementitious Composites

Bacterial nanocellulose (BNC), nano-fibrillated cellulose (NFC) (also known as cellulose nanofibrils, micro-fibrillated celluloses), and nano-crystalline cellulose (NCC) are the common types of Nanocelluloses. The first group is made biotechnologically by bacteria; the second group is made mechanically; and the third group is made chemically by hydrolysis treatments (Klemm et al., 2018). Delamination in high-pressure homogenizers, microfluidizers, and other equipment produces nanofibrils. To make the operation go more

smoothly and avoid clogging the equipment, different procedures can be used to pre-treat plant material such as charged groups' electrostatically driven swelling, oxidative treatments, carboxymethylation, peridine-1-oxyl reagent TEMPO, and mild acids or enzymatic treatments (Klemm et al., 2018).

Cellulose is biodegradable, renewable, and non-petroleum-based; therefore, it has a strong environmental appeal. These properties are critical in the civil construction sector, which consumes a lot of natural resources and produces a lot of CO_2. As a result, the use of NFC in cementitious matrices can help to make construction products more environmentally friendly.

It's important to know that NFC is referred to by several terms in the literature. Nanofibrils, microfibrils, nanofibers, nanocellulose, micro fibrillated cellulose, and cellulose nano fibers. However, the names nano-fibrillated cellulose and micro-fibrillated cellulose (MFC) are not interchangeable. Fibers with lower sizes (between 4 and 20 nm) are usually termed as NFC and bigger diameters (between 10 and 100 nm) are termed as MFC during the defibrillation process. However, this distinction is not always taken into account, and both names are used interchangeably in the literature, which may lead to a misunderstanding (Guimarães et al., 2015; Moon et al., 2011). Biodegradability, high surface area, high surface area/volume ratio, big aspect ratio, better mechanical capabilities, low thermal expansion coefficient (Guimarães et al., 2015), low density, and inexpensive price when compared to other inorganic nanofibers (Sharip & Ariffin, 2019b) have all piqued people's interest in NFC.

Nanocellulose has been shown to drastically alter the characteristics of cementitious materials, and it has the potential to be employed for a variety of applications (Balea et al., 2019b; Cao et al., 2016b). If a sufficient dose is utilized, Nanocellulose can

be employed to improve the mechanical characteristics of cementitious materials (Akhlaghi et al., 2020; Mazlan et al., 2020; Barnat-Hunek et al., 2019; Hisseine et al., 2019). It should be noted; however, that if a large dose of nanocellulose is utilized, agglomeration may develop, compromising mechanical qualities. In such circumstances, a dispersion procedure (e.g., sonication) for nanocellulose is required to increase its influence on mechanical characteristics (Cao et al., 2016b).

In addition, the right dose of Nanocellulose can minimize cementitious material shrinkage, especially when the water-to-cement (w/c) ratio is low (H.-J. Lee et al., 2019). The agglomeration of Nanocellulose generated by a large dose may have a detrimental impact, similar to the effect on mechanical qualities in this case an increased shrinkage will be experienced. Nanocellulose also has a variety of additional uses, including increasing the ductility of strain-hardening cementitious composites (Hisseine & Tagnit-Hamou, 2020).

2.6.1 Structure of Nano Fibrillated/Crystalline Cellulose

To understand the structure of cellulose, **Fig. 1.1 (a)** illustrates how cellulose is made up of a linear chain with two molecules of anhydroglucose joined together by an oxygen atom covalently attached to the C1 of a glucose molecule and the C4 of the neighboring molecule. The microfibrils (elementary fibrils) are formed when different chains connect via hydrogen bonds and van der Waals forces.

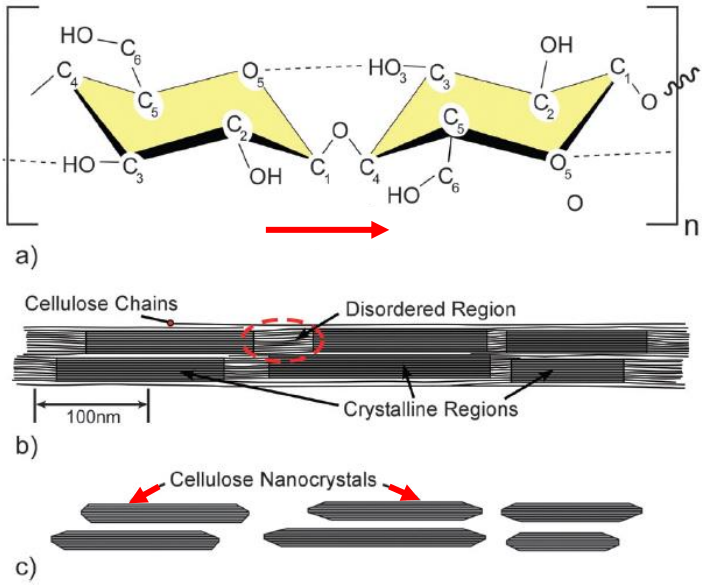

Figure 2. 1: Schematics of (a) single cellulose chain repeat unit, (b) cellulose microfibril showing the crystalline and amorphous regions ((adopted from Eyley and Thielemans 2014), and (c) cellulose nanocrystals after acid hydrolysis dissolved the disordered regions (adopted from Moon et al. 2011).

This type of link is known as b-1–4 glycosidic, and the basic unit can be repeated 10,000 to 15,000 times. Furthermore, the linear cellulose chain is stabilized by hydrogen bonds formed between hydroxyl groups and oxygen from nearby glucose molecules (Moon et al., 2011). As shown in **Fig. 2.1 (b)**, NFCs contain crystalline and amorphous regions. The crystalline areas are made up of cellulose chains that have been aggregated by a complicated network of hydrogen bonds and van der Walls forces that keep them stable. Amorphous zones are caused by faults in the structure caused by alterations in the aggregation process (Lavoine et al., 2012; Habibi et al., 2010). Acid hydrolysis can eliminate these amorphous areas, resulting in the production of nano-crystalline cellulose (Eyley & Thielemans, 2014), as illustrated in **Fig. 2.1 (c)**.

2.6.2 Effect of NFC/NCC on Mechanical Properties

NFCs have been effectively employed to improve the mechanical characteristics of cement-based composites. For instance, Peters et al., (2010) utilized commercial NFC (Sigmacell 101) to study the fabrication of reactive powder concrete. By weight of cement, the NFC content was 1%, 3%, and 5%, respectively. When compared to the non-reinforced material, the reinforcement of 3% of MFC resulted in a little improvement in tensile strength and a 50% increase in fracture energy (**Fig. 2.2**).

Stephenson (2011) tested ultra-high-performance concretes with NFC levels of 0.1, 0.5, and 1.0 % (by weight of cement) and found that the 0.5 % NFC offered the best fracture qualities and greatly reduced shrinkage at the early ages of the composites. In this study, the compressive strength was not affected by the NFC concentration, since only minor improvements in this mechanical attribute were seen in compression testing. Santos et al., (2021) employed NFC in cement pastes with diameters ranging from 20 to 100 nm (concentrations ranging from 0.10 % to 0.40 % by volume of cement). They discovered that adding 0.15 % NFC by volume of cement with a water-cement ratio of 0.50 increased compressive and flexural strength by 20% and 15%, respectively.

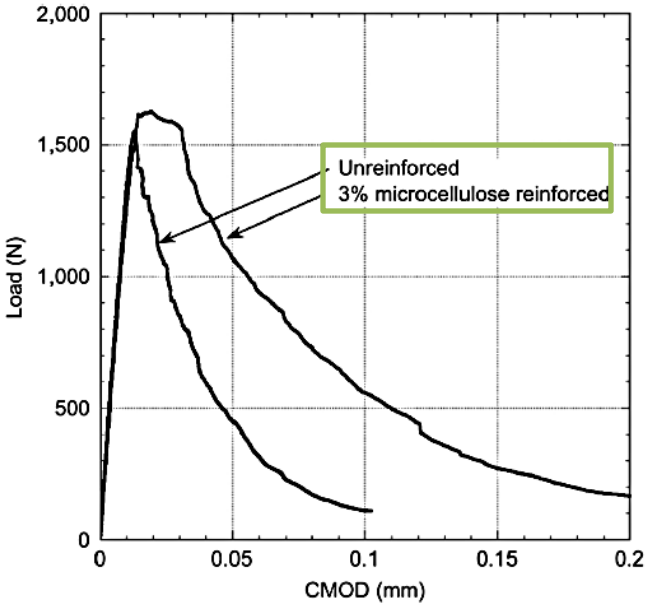

Figure 2. 2: Load–deformation curve of specimens with and without NFC (adopted from Peters et al., 2010)**.**

Onuaguluchi et al., (2014) utilized NFC with sizes ranging from 5 to 10 nm and General Use Limestone (GUL) cement. By weight of cement, NFC was 0.05 %, 0.1 %, 0.2 %, and 0.4 %. The addition of merely 0.1 % NFC resulted in the greatest gain in flexural strength by 106% (**Fig. 2.3**). The thermal, mechanical, and microstructural characteristics of pastes containing NFC were investigated by Mejdoub et al., (2017). To ease defibrillation and improve NFC dispersion within the cement matrix, the cellulose fibers were subjected to a TEMPO-mediated oxidation pre-treatment. As reported by Onuaguluchi et al., (2014), the diameters obtained ranged from 5 to 10 nm. By weight of cement, the NFC concentrations of the pastes were 0.01 %, 0.05 %, 0.1 %, 0.2 %, 0.3 %, and 0.5 %. The inclusion of 0.3 % NFCs resulted in a matrix that was denser and had less porosity. As a result, the addition of 0.3 % NFC resulted in the greatest improvement in compressive strength (43 %) (**Fig. 2.4**).

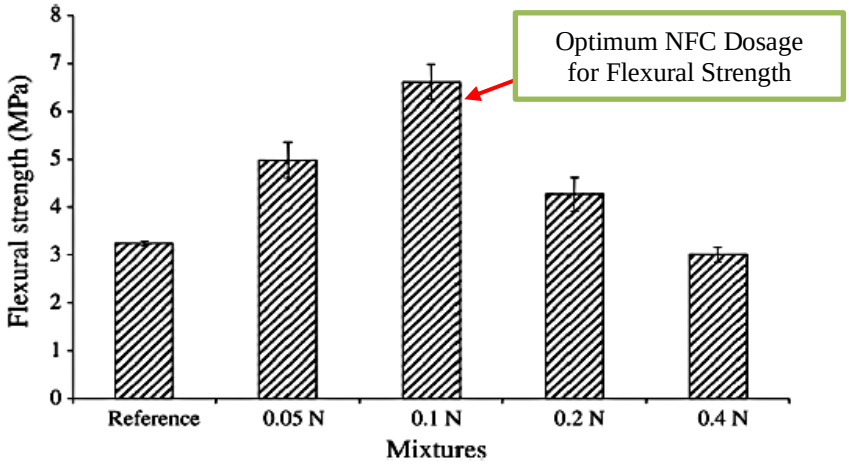

Figure 2. 3: Flexural strength after 28 days (adopted from Onuaguluchi et al., 2014)

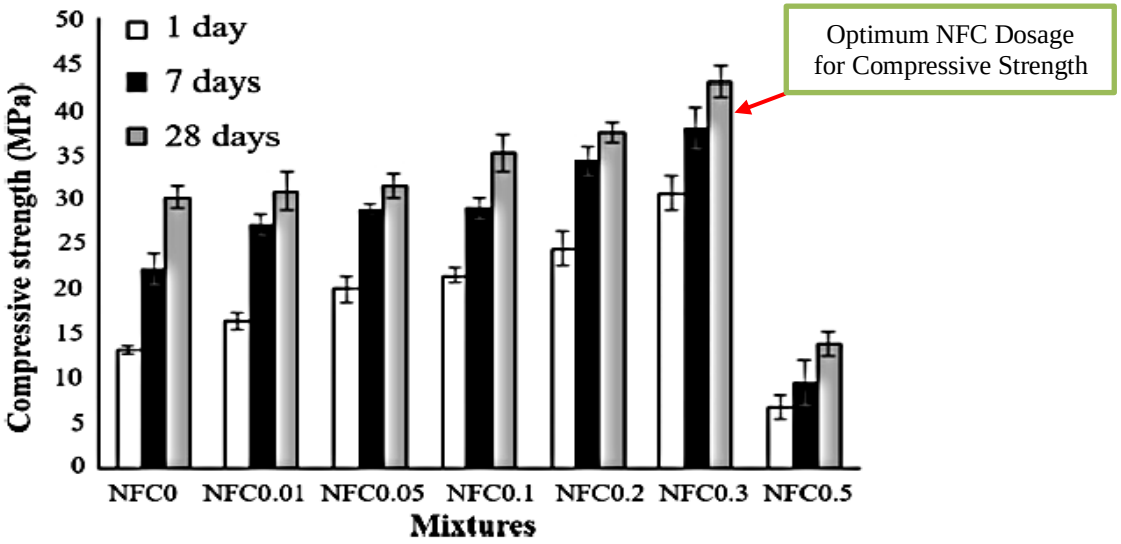

Figure 2. 4: compressive strength for cement pastes reinforced with different NFC dosages (adopted from Onuaguluchi et al., 2014)

Sun et al., (2016) introduced NFC to oil well cement pastes in concentrations ranging from 0.04 % to 0.28 % (by weight of cement) and found that the 0.04 % NFC content offered the greatest flexural strength enhancement, where it increased by 20.7%. The addition of NFC to low-alkali cement was explored by Hoyos et al., (2019). The NFC

manufacturing method produced a limited number of fibers with sizes greater than 100 nm and the majority of fibers with diameters less than 100 nm. NFC was added to cement pastes at concentrations of 0.1 %, 0.2 %, 0.3 %, and 0.4 % by weight of cement. In the combinations containing 0.4 % NFC, there was a greater degree of hydration. Claramunt et al., (2019) investigated the impact of various NFC and NCC concentrations (varying from 0.1 to 0.8 % by weight of cement) on calcium aluminate cement (CAC) and ordinary Portland cement (OPC) matrices. NFC sizes ranged from 25 to 500 nm, whereas NCC diameters also ranged from 25 to 500 nm. The authors discovered that minor additions of 0.1 % and 0.2 % nanocelluloses resulted in the greatest gains in flexural strength of 28%.

Reixach et al., (2019) made cement pastes with varying amounts of lignocellulosic micro/nanofibers with diameters of around 28 nm (0.0 %, 0.5 %, 1.0 %, 1.5 %, and 2.0 % by weight of cement). Flexural strength was measured after 7, 14, and 28 days on the specimens. All of the doses studied resulted in increased flexural strength, according to the authors. At 28 days of curing, the larger improvements (25%) occurred for nanofiber concentrations of 1.0 % and 1.5 %. This high dosage can be attributed to the usage of small-sized NFC with respect to other papers. Kamasamudram et al., (2021) recently explored the possible application of several types of NFC (pure NFC, silica-coated NFC, and lignin-containing NFC) for increasing the mechanical performance of cement pastes. In all of the case situations, a constant concentration of NFC of 0.1 % (by weight of cement) was applied. The cement pastes' 90-day compressive strength was not affected by pure NFC or lignin-containing NFC, but the silica-coated NFC offered a 13 % strength improvement. Furthermore, pure NFC increased flexural strength by up to 70%, followed by lignin-containing NFC (increases by up to 40 %). However, the flexural strength of the cement pastes was not significantly improved by silica-coated NFC.

Santos et al., (2021) examined the mechanical characteristics of cement-based composites with NFC levels ranging from 0.01 % to 5.00 % (by mass of cement). The lowest NFC concentration was 0.01 % (by mass of cement), resulting in a minor reduction in the porosity of cement-based products and a modest increase in compressive strength. However, an analysis of the experimental results shows that the value of various mechanical properties (e.g., compressive strength, tensile strength, flexural strength, modulus of elasticity, and so on) tends to increase as the NFC content increases, despite the fact that excessive NFC dosage will reduce the mechanical performance of the cement-based composites due to inhomogeneous dispersion and detrimental agglomeration of nanomaterials. The maximum amount of NFC supported by cement-based materials was 5.00 % (by mass of cement), according to the present literature. NFC content was observed to frequently lead to inadequate workability. Furthermore, the best mechanical qualities were found when the NFC concentration was between 0.10 % and 3.00 % (by mass of cement), according to the research. The varied mix proportions, NFC features, techniques of NFC dispersion, type and concentration of dispersing agents, and attributes of the raw materials utilized to make the cement composites are the key causes for the varying optimal NFC contents reported in these investigations. NFC produced the most substantial mechanical benefits by increasing compressive strength by 43 %, flexural strength by 106 %, modulus of elasticity by 5%, flexural modulus by 71 %, and fracture energy by 50 %. The next part provides a full explanation of the mechanics that underpin these enhancements.

2.6.3 NFC/NCC effect on durability

To determine the durability of cement-based composites containing NFCs, some researchers investigated their resistance to physical attacks (freezing and thawing) (Barnat-Hunek et al., 2019), accelerated aging (Claramunt et al., 2019; da Costa Correia et al., 2018; Ardanuy et al., 2012), and resistance to chloride permeability of such composites (Goncalves et al., 2020).

Diffusion, capillary suction, permeation, and convective flow are all involved in the penetration and transport of soluble chlorides into concrete and are linked by the coarser capillary pore structure (i.e., 10 nm to 10 m) (Jennings et al., 2002) and/or microcracks within the system (Cao et al., 2019; Al-Saleh, 2015; Mitchell et al., 2012). A portion of the chloride is physically absorbed by the calcium silicate hydrate, C-S-H gel, during this movement. The tricalcium aluminate, C_3A, and the tetra calcium alumina-ferrite, C_4AF, are chemically linked to the calcium aluminate compounds of cement, creating chloroaluminates, or Friedel's salt. Steel rebar corrosion is thus limited to the freely existent parcel of dissolved chloride ions in the aqueous phase of cement-based systems (Angst et al., 2009). However, depending on an increase in alkalinity and a favorable temperature, the above-mentioned bound chlorides may be released into the pore solution. Therefore, studying the role of NFC in resisting the permeability of chlorides was necessary.

Goncalves et al. (2020) examined the ingress of chloride ions in accordance with the Rapid Chloride Penetration Test (ASTM C1202-22, 2022) and further assessed by colorimetry. Three variants of NFC, differing in carboxylate content (0.13–1.13 mmol/g of fiber), were added to CSA Type GU cement mortars at up to 0.5% volume fraction, to examine their effect on the transport of chloride ions. Besides the standard test using rapid chloride penetration, chloride ingress was further evaluated through colorimetry, by

spraying 0.1 N $AgNO_3$ solution on the fractured surfaces of the specimens. The transport of chloride ions is greatly reduced when NFC is added to cement mortar. The decrease in the electric charge in the RCPT was confirmed as shown in **Fig. 2.5 (a)**, and the decrease in the chloride front measured by colorimetry is shown in **Fig. 2.5 (b)**. The reduction is favored when the NFC is grafted with [COOH] groups. The NFC#1.13 resulted in a 50% reduction in both the electrical charge and the depth of chloride infiltration at the maximum tested 0.5 percent volume fraction.

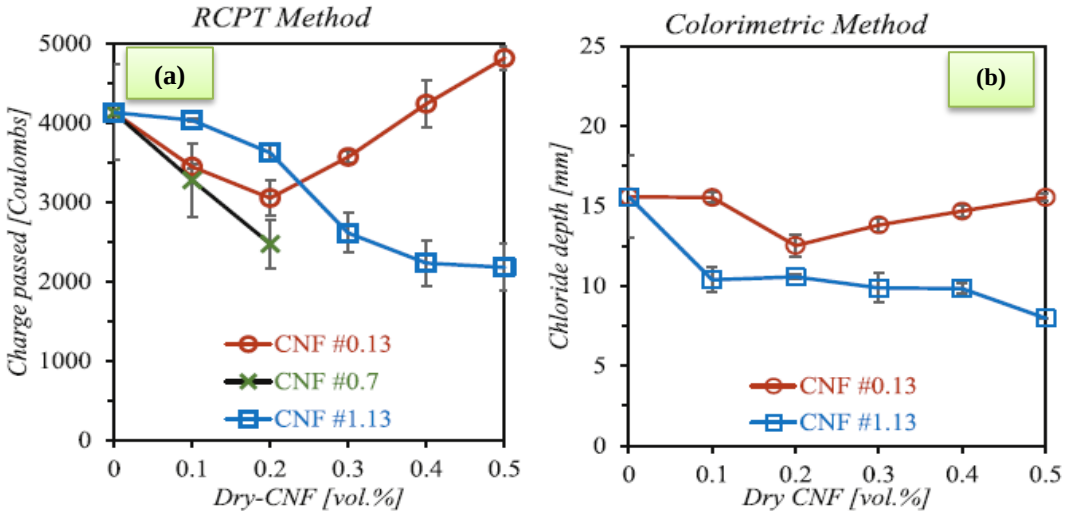

Figure 2. 5: (a) Electrical resistance to chloride ion ingress (RCPT) as per (ASTM C1202-22, 2022) in mortars dosed with various NFC fractions and NFC types, and (b) Free-chloride depth penetration of mortars dosed with various NFC fractions as per $AgNO_3$-based colorimetric method (adopted from Goncalves et al., 2020).

Freezing and thawing (F/T) damage is a well-known cause of concrete deterioration. To summarize its mechanism, when water freezes, it expands about 9 percent. As the water in moist concrete freezes, it produces pressure in the pores of the concrete. If the pressure developed exceeds the tensile strength of the concrete, the cavity will dilate and rupture. The accumulative effect of successive freeze-thaw cycles and

disruption of paste and aggregate can eventually cause expansion and cracking, scaling, and crumbling of the concrete.

Barnat-Hunek et al. (2019) investigated the incorporation of 0.5% and 1% of both NFC and NCC in 12 cubic samples with an edge length of 100 mm which were subjected to a frost resistance test after being saturated with water. At a temperature of − 20˚ C, the samples were frozen for 4 hours. The samples were then thawed to +20˚ C for 4 hours. 100 cycles of freezing and thawing were performed on the samples, and the mass loss and compressive strength decrease were measured in comparison to the reference samples, which were kept in water at a temperature of + 20˚ C throughout the experiment. The mass loss after 100F/T cycles was more pronounced in the case of NCC; in both concretes, it significantly dropped as the amount of added nanocellulose increased. In the case of the NFC 0.5 mixture, the mass loss of the sample reached over 80%, while in NFC 1%, the loss was 58-fold lower. They concluded that the freezing-thawing resistance of concrete could be increased with the increase of NFCs, which was verified by the less pronounced mass loss and compressive strength decrease after 100 F/T cycles. Compared to NCCs, the mass loss of concrete in the case of NFCs was less pronounced, whereas the compressive strength decrease was more significant.

Claramunt et al. (2015) used accelerated aging experiments to assess the durability of cement mortars including combinations of varying contents (0 %, 2 %, 4 %, 6 %, and 8 % by mass of cement representing samples 1 to 5, respectively) of conventional pulps and NFC. After being treated to 20 wet/dry accelerated aging cycles. The wet/dry cycle used was 96 h of soaking in water at room temperature followed by 72 h of drying in an oven provided with open-air circulation at 60 °C. Specimens containing greater levels of NFCs showed increases in flexural strength of up to 16%, increases in modulus of elasticity of up

to 55 %, and retained their original fracture energy values, as shown in **Fig. 2.6**. After age, however, specimens with a larger concentration of standard pulps had lower flexural strength and fracture energy values. The researchers found that NFCs were able to assure increases in fiber bonding owing to age effects while also improving interfacial zone densification.

Ardanuy et al. (2012) evaluated the impact of sisal fiber diameters on the durability of mortar that had been exposed to accelerated aging. Sisal pulp fibers with a diameter of 15.9 mm were employed, as well as NFC with sizes ranging from 25 to 250 nm. In cement composites comprising exclusively NFCs as natural reinforcements, a 4 percent NFC content (by weight of cement) was employed. The specimens were treated to 5 wet-dry cycles after 7 days of cure. After these cycles, specimens containing NFCs showed a 7% increase in flexural strength, a 15% rise in flexural modulus, and a 15% decrease in fracture energy. Control specimens lacking NFCs, on the other hand, had a 6% reduction in flexural strength, a 44 percent rise in flexural modulus, and a 15% reduction in fracture energy. As a result, NFCs showed a small considerable benefit in the durability of the cement composites.

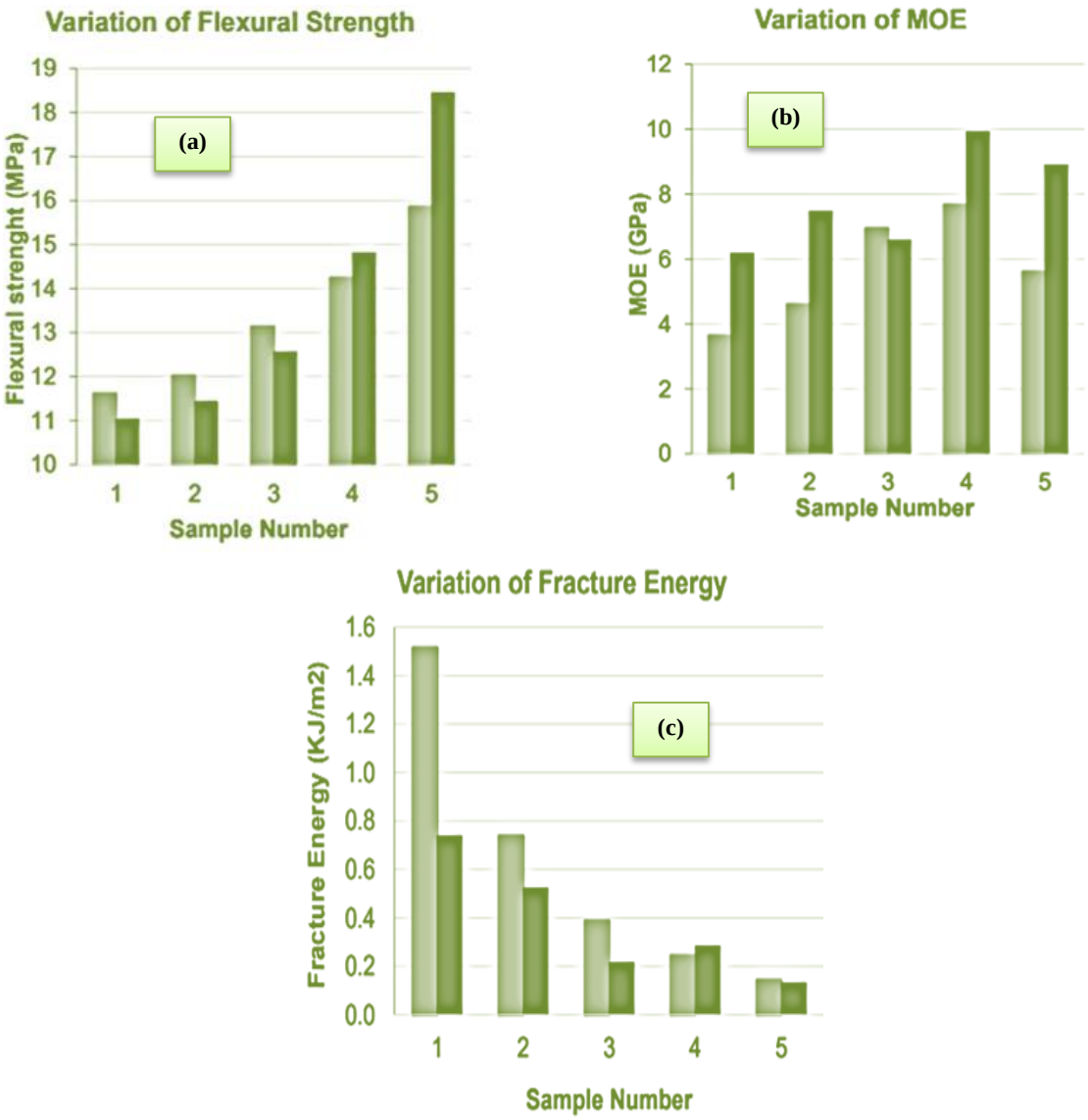

Figure 2. 6: a) variations of flexural strength, b) variation of MOE, and c) variation of fracture energy (adopted from Claramunt et al., 2015)

Claramunt et al. (2019) studied different cement matrices containing NFC concentrations ranging from 0.10 % to 8.00 % (by weight of cement). The lowest NFC concentration previously studied was 0.1 % (by mass of cement), which was shown to be capable of preventing accelerated aging-related mechanical degradation of flexural strength and elastic modulus. Other NFC concentrations, such as 0.2 %, 0.4 %, and 0.8 %

(by mass of cement), yielded similar results (Claramunt et al., 2019). However, a comparison of the experimental results of other studies suggests that increasing the NFC concentration up to 8% (by mass of cement) caused the mechanical properties of cement-based composites to increase after accelerated aging (e.g., flexural strength, flexural modulus, modulus of elasticity).

Goncalves et al. (2019) also reported that samples with the highest NFCs concentration presented the lowest chloride penetration. Therefore, the effects of high NFC contents on the durability of cement matrices seem to be different from the effects observed on their mechanical performance, since higher NFC dosage provided the highest increases in mechanical properties after aging, the highest decreases in sulfate penetration, and chloride resistance. The testing results showed that the highest NFC concentrations had the best durability qualities. For example, composites containing 8% of NFCs (by mass of cement) showed the greatest gains in mechanical characteristics owing to aging effects. Composites containing 0.5 % (by volume) NFC had the highest improvement in chloride resistance. The influence of NFC on the durability of cementitious matrices has just recently been studied and the majority of the research on durability referenced in this review was published in 2019 and 2022. Despite the lack of research on the subject, it can be concluded that NFC can improve aggressive agent resistance through improved cement matrix refinement, nucleation effects, bridging effects, and microcrack prevention. As reported by Goncalves et al., (2019), NFCs produce a cementitious matrix that is more compact and less permeable to aggressive agents.

2.6.4 Mechanisms of NFC/NCC in Cement Matrices

The various interaction mechanisms of NFC integrated into cement matrices are discussed in this section. According to the studies discussed in the preceding section, NFCs have a superior influence on cementitious composites' mechanical strength. Such performance can be due to higher hydration in the matrices as shown by numerous studies: (Mazlan et al., 2020; Hoyos et al., 2019; Mejdoub et al., 2017; Onuaguluchi et al., 2014). NFCs function as nucleation sites, causing the hydration process to ramp up. As a result, the degree of hydration and the generation of hydrated products including portlandite, ettringite and calcium silicate hydrate (C-S-H) tend to increase in the presence of NFC (Mejdoub et al., 2017). The degree of cement hydration rises as the NFC content of the composites increases.

C-S-H crystals were developing in and around NFCs using the water held by the nanocellulose as observed by Hoyos et al., (2019). When researching the addition of NCC in cementitious matrices, Cao et al., (2016b) postulated a short-circuit diffusion mechanism (SCD), which the authors ascribed to this finding. **Fig. 2.7 (a-b)** depicts this method. Hydrated products (C-S-H) create a shell around the cement particle during curing, slowing the hydration process inside the particle. NCC attaches to the cement particles and establishes a water transport route into the unhydrated particle when present in the paste. As a result, this would improve the matrix's hydration. Although this process has been postulated for NCC, it has been maintained by some writers who have utilized NFC in the cementitious matrix as an explanation for the higher hydration seen in cement-based composites (Bakkari et al., 2019; Goncalves et al., 2019; Hoyos et al., 2019).

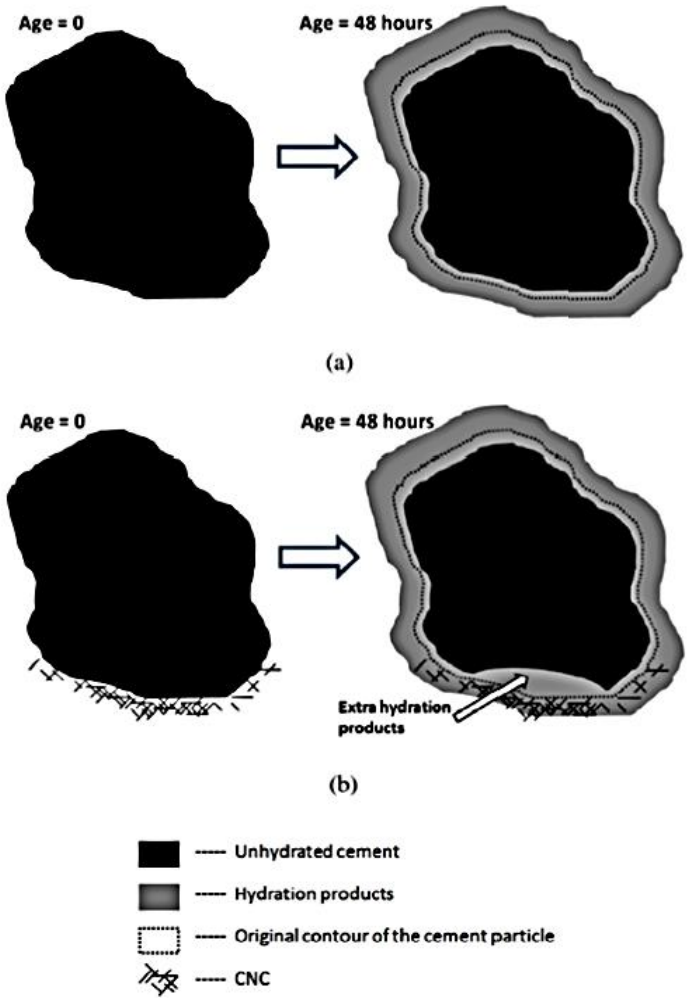

Figure 2. 7: Short-circuit diffusion mechanism for CNC and NFC (adopted from Hoyos et al., 2019)**.**

The bridging effect, in which the fibers intercept the fractures in the matrix, stopping their propagation, increasing the fracture energy, and avoiding brittle failure, is another mechanism that explains the improvement in mechanical characteristics (Fonseca et al., 2019). **Fig. 2.8** depicts this impact, which corresponds to Peters et al., (2010)'s findings. The bridging effect's contributions toward improving the mechanical characteristics of composites appear to be related to their age. Because the framework of the hydrated system is highly organized at later ages, a better link between NFCs and the

cementitious matrix is produced, which improves the adhesion of the fibers into the hydrated system (Hisseine et al., 2020).

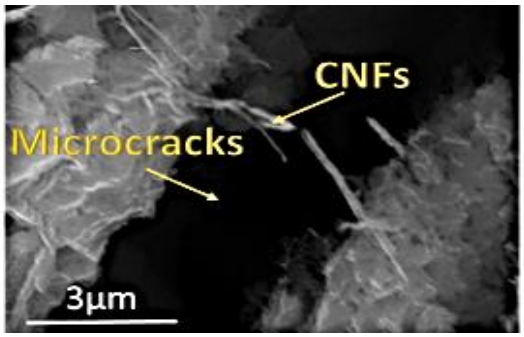

Figure 2. 8: SEM image capturing the Bridging effect of NFC (adopted from Sun et al., 2017)**.**

2.7. Statistical analysis and experimental design

Due to the existence of several dosages of admixtures, supplemental cementitious materials (SCMs), fibers, and nanomaterials that might alter the performance of concrete, optimization techniques for concrete mixtures based on statistical analysis have become extremely necessary. A statistical technique known as "design of experiments" is used to set up a matrix of experimental runs to examine the effects of multiple factors rather than just one, as well as the interactions between these factors and specific responses, which can help us better understand certain conditions (Montgomery, 2017; Ghezal & Khayat, 2002).

Factorial design is the most popular research approach used to investigate the interaction of the main and independent variables of one or more outcome variable(s) of a constructed system. However, it has some downsides, such as the requirement for a significant number of runs when numerous components are present. As a result, this procedure may be time- and money-consuming. Additionally, not all runs of the full factorial design must be completed in order to arrive at a model with high confidence and reliability (Montgomery, 2017). Therefore, when it comes to statistical analysis and the

optimization process while taking into account a large number of elements, different modelling methods are used such as the response surface method (RSM).

In order to create and optimize a process, RSM analyses the impact of many elements and how they interact with the desired response. RSM's primary goal is to identify the conditions under which various variables can best achieve the desired result (Ghafari et al., 2014). The two most popular RSM design methodologies, central composite design (CCD) and face-centered composite design (FCCD) have been used in a variety of concrete studies (Yasien & Bassuoni, 2022; Shahab-ud-Din et al., 2018; Al-alaily & Hassan, 2016; S.-C. Kang et al., 2010).

The FCCD has an experimental sequence divided into three parts, as illustrated in **Fig. 2.9**, a two-level factorial design with data points chosen for the design including the edges of the design space representing all +1 and -1 design points, a point in the center of all factors, and axial points laying on the boundary of the design matrix (Montgomery, 2017). The CCD follows the same experimental sequence, except for the axial points, which, exceed the design space with constant -α and α values (Ferdosian & Camões, 2017). However, FCCD shows more practicality for this thesis's work, as the boundaries are limited within the permissible space of a practical design block. For instants, if one of the factors used is a type of fiber where levels are between -1 and 1 responding to dosages of 0 and 4.5%, respectively. Therefore, CCD is not a possible option, as it is not practical to have a dosage at a level beyond -1 where the dosage will have a negative value, which is not possible.

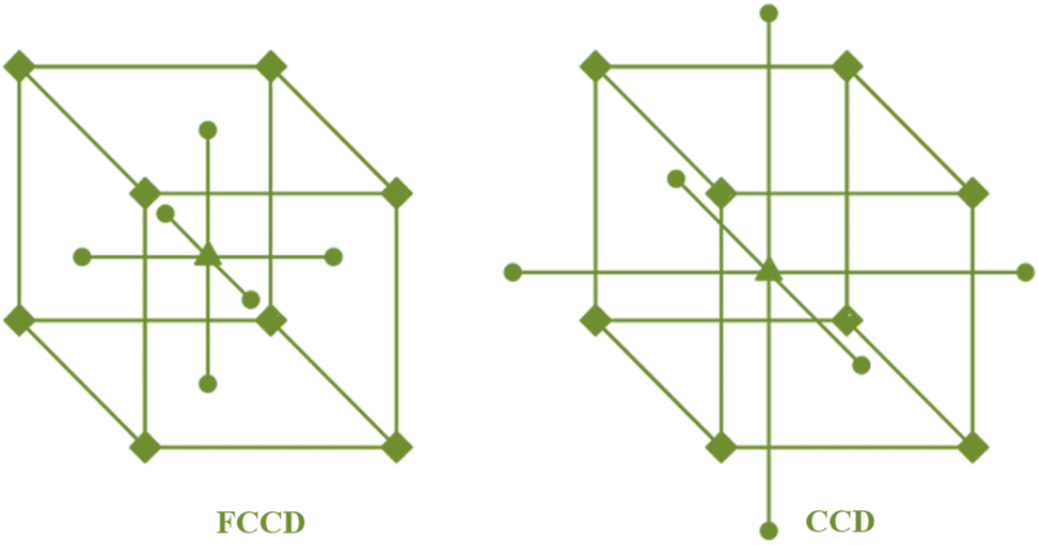

Figure 2. 9: FCCD and CCD design points (adopted from Montgomery, 2017).

Shahab-ud-Din et al. (2018) developed a statistical model using RSM to predict the fresh and Hardened characteristics of fly ash–based geopolymers and the effect of altering the molarity of sodium hydroxide (varied from 8M to 16M), sodium silicate to sodium hydroxide ratio (ranged from 1 to 2.5) and curing temperature (45℃ to 90 ℃). The specified factors and their interactions were all found to be statistically significant (*P-value* 0.05). Additionally, the model's parameters were optimized, and the optimum mix was validated by experimental results in terms of compressive strength, to conclude that the RSM was successful in predicting the proper outcome. This shows that any target value of the response from the potential combination of factors can be selected using the RSM to construct the experiment for different mixtures.

Köksal et al. (2022) employed the response surface method approach to examine the toughness and splitting tensile strength of steel fiber-reinforced concrete (SFRC). The experiment's independent variables included the volume fraction of steel fiber, the aspect ratio, and the quantity of silica fume employed as a substitute for cement. The dependent variables were SFRC mechanical characteristics derived through experimentation. The

optimization yielded the optimal steel fiber volume of 0.70% and the silica fume concentration of 15% for both aspect ratios. The author concluded that RSM is a reliable approach to examining the properties of SFRC and optimizing factors such as ductility and cost.

There is a dearth of knowledge in this field despite the significance of statistical analysis models to better understand and optimize various parameters including multi-scaled fibers, and nanomaterials dose, which might have a tangible impact on nano-modified fiber-reinforced cementitious composites.

2.8. Closure

HPFRCC has superior properties to that of FRCC, making it suitable for various construction projects. There is a growing demand for this type of high-strength, high-ductility cement-based composite that incorporates metallic or non-metallic fibers, particularly for repairing and strengthening structures, in order to address the weakness of traditional concrete. Recently, cellulose and basalt fibers have been used extensively in various applications due to their high performance and have been considered a better alternative in cement-based composites to other fibers such as synthetic and steel fibers. BFP, a new class of non-metallic basalt fibers, has shown great potential when used in cement-based composites, similar to the commonly used metallic fibers such as steel fibers. However, there is still a lack of research on the use of BFP in different construction and repair work for concrete applications.

The goal of flatwork system repair and restoration techniques is to improve the concrete slabs' quality or/and the substrate layer's structural strength. These repair solutions use a variety of cement-based combinations, both with and without fiber reinforcement. This encourages the usage of HPFRCC reinforced with multi-scaled combinations of fibers

and nanomaterials to maximize the properties of composites in the desired application(s). Hence, statistical modeling can analyze and optimize the dosages of materials being used in composites to reach a target function tailored for each application individually. Thus, further research should be done to better understand the effect of using these materials and their combinations on the properties and durability of composites produced for concrete flatwork applications and repair systems.

To date, the behavior of nano-modified cementitious composites incorporating a combination of NFC and BFP at different dosages is still unknown and has not been investigated. Thus, this thesis is dedicated to investigating and better understanding the effects of using these materials and the combination between them on the properties of composites. These combinations have promising expectations to enhance concrete's microstructure and strength development while decreasing the carbon footprint of the concrete industry and ultimately reducing repair cycles, cost, and time over the life cycles of concrete flat work. Hence, leading to the production of durable specialty concrete for different construction applications.

CHAPTER 3: METHODOLOGY

3.1 Statistical Model

The Response Surface Method (RSM), based on Face-Centered Composite Design (FCCD) was used to evaluate the influence of mixture design parameters on the performance of composites. Three parameters adopted in the developed models were: nano-particle types, nano-fibrillated cellulose (NFC) dosage, and basalt fiber pellets (BFP) dosage. They were investigated at two levels (1 and -1) representing the factorial part of the model. The method used depends on improving the accuracy of predicting the response space by considering additional points to the factorial set of the model. Accordingly, a central point, at the intermediate level (0), for each factor was included in the developed models to capture the quadratic effect of each variable, if any. Furthermore, the central point was repeated three times to improve the overall reliability of the model, as well as account for the model's experimental error (Montgomery, 2017). Hence, 15 mixtures were cast to establish the models which consist of the factorial part (2^3=8 mixtures), the axial part (2×3=6 mixtures), as well as the central point mixture.

The mixtures had a constant total binder of 700 kg/m^3 and *w/b* ratio of 0.3. A combination of NCC and NS was added to the different composites at a ratio of 1:0 to 0:1 [ranging from 0–0.1% for NCC (in addition to the mass of the binder) and 0–6% for NS (in addition to the mass of the binder), while NFC had a range of 0–0.5% (in addition to the mass of the binder)]. In addition, BFP's dosages varied within the mixes between 0–4.5% (by volume of composite), and a combination of NCC and NS was added to different composites at a ratio of 1:0 to 0:1 [ranging from 0–0.1% for NCC (in addition to the mass of the binder) and 0–6% for NS (in addition to the mass of the binder)]. **Table 3.1** represents the adopted variable's dosages and the corresponding codes. The dosages of slag, cement,

w/b, NS, NFC, NCC, and BFP were chosen based on previous studies (e.g., Kamasamudram et al., 2021a; Santos et al., 2021; Azzam et al., 2019b; Mejdoub et al., 2017; Ghazy et al., 2016; Onuaguluchi et al., 2014; Stephenson, 2011; Peters et al., 2010;) and trial batches. The independent responses modeled were: initial (IST) and final (FST) setting times, 7 and 28 days compressive strengths, flexural toughness, and resistance to freezing and thawing cycles (durability factor) which represent the composites' fresh, hardened, and durability properties.

Table 3. 1: Codes and values of parameters investigated

Parameter	Coding Values		
	-1	0	+1
BFP (%)	0	2.25	4.5
NFC (%)	0	0.25	0.5
Nanoparticles: NCC (%)/NS (%)	0:6	0.05:3	0.1:0

Note: BFP dosage is represented by volume of the composite, while NFC, NCC, and NS dosages are represented by mass of the binder (as an addition).

3.2 Experimental program

3.2.1 Materials

The base components of the binders were general use (GU) cement and Grade 100 slag, which meet the CSA-A3001 requirements (Canadian Standards Association, 2013). A water-based nano-silica sol (NS) with a 50% solid content of SiO_2 particles was also used as an addition to the binder. **Table 3.2** lists the physical and chemical parameters of the binders' constituents. The nano-fibrillated cellulose (NFC) used was produced via mechanically refining natural cellulose fibers, while nano-crystalline cellulose (NCC) was extruded chemically by hydrolysis. The NFC used was in wet form, with 20% solid content. The basalt fiber pellets consisted of 16-μm basalt roving encased in polyamide resin with the fiber component accounting for 60% of the pellet's composition. **Table 3.3** lists the

properties of NCC, NFC, and BFP. The composites were produced using locally available river sand that had a continuous gradation of 0–600 μm and a fineness modulus of 2.9, as per ASTM C136/136M, (2014). In addition, according to ASTM C128, (2014), the absorption and specific gravity of the fine aggregate were 1.5 and 2.6 %, respectively. A high-range water-reducing admixture (HRWRA) based on Poly carboxylic acid and complying with ASTM C494/C494M, (2017) Type F was added to achieve a flow diameter of 180±20 mm. Also, an air-entraining admixture complying with ASTM C260, (2010), was incorporated in all mixtures to achieve a fresh air content of 6 ±1%. The materials used for both Phases I and II were the same.

Table 3. 2: Physical and chemical properties of the GU cement, slag, and nano-silica

Aspect	GU Cement	Slag	Nano-silica
Chemical composition			
SiO_2 (%)	19.22	33.40	99.17
Al_2O_3 (%)	5.01	13.40	0.39
Fe_2O_3 (%)	2.33	0.76	0.02
CaO (%)	63.22	42.70	--
MgO (%)	3.31	5.30	0.21
SO_3 (%)	3.01	2.40	--
Na_2Oeq. (%)	0.12	0.30	0.20
Physical properties			
Specific gravity	3.15	2.87	1.1
Mean particle size (μm)	13.15	11.45	35×10^{-3}
Fineness (m^2/kg)	390	492	80,000

Note: The properties of all materials have been provided by the manufacturers.

Table 3. 3: Properties of NCC, NFC, and BFP

Parameter	NCC	NFC	BFP
Length (mm)	$50\text{-}800\times10^{-6}$	100×10^{-3}	36
Diameter/width (mm)	$5\text{-}40\times10^{-6}$	80×10^{-6}	1.8
Aspect ratio	1.25-160	1250	20
Specific gravity	1.5	1.5	1.7
Tensile strength (MPa)	--	115	2,300
Elastic modulus (GPa)	--	12	65

Note: The properties of all materials have been provided by the manufacturers.

3.2.2 Procedures

3.2.2.1 Phase I: Slag-based cementitious composites incorporating nano-silica, nano-cellulose material and basalt pellets

In this Phase, fifteen mixtures were cast, cured, and tested. An ID is given for each mixture where one or more letters identify the type of material used followed by a number indicating the dosage. The given letters are defined as follows: Basalt fiber pellets (B), Nano-fibrillated cellulose (NFC), and finally, letters refereeing to the nanoparticles: S for NS, C for NCC and SC for NS+NCC. The mixtures IDs, coding, and proportions are listed in **Table 3.4**.

Constituent materials were mixed in a mechanical concrete mixer at a speed of 60 rpm. According to the manufacturer's mixing guideline and trial batches, a specific sequence of mixing was adopted to produce homogeneous mixtures. Firstly, the dry constituents were mixed then the needed water, admixtures, and NCC and/or nano-silica were added while mixing until the composites achieved uniformity. The BFPs were then added, and the ingredients were mixed to ensure that the pellets were distributed evenly.

Once a uniform consistency was achieved, the NFC was added, and the mixing further continued for 10 minutes. The entire process took about 15 - 20 min. After casting the composites in molds, all specimens were consolidated using a vibrating table. Polyethylene sheets were used to cover the surface of the specimens for 24 h. Subsequently, the specimens were demolded and cured in a standard room maintained at 22±2°C and relative humidity of more than 95% until testing.

3.1.1.1 Phase II: Nano-modified slag-based cementitious composites reinforced with multi-scale fiber systems as a repair/overlay option

Based on Phase I, four mixtures were selected representing the domain of key experimental variables, in addition to two mixtures derived from the numerical optimization to evaluate the suitability of the nano-modified cementitious composites as a repair/overlay option. The mixtures IDs and proportions are listed in **Table 3.5**. The mixing sequence adopted in Phase II was identical to that used in Phase I.

Table 3. 4: Mixtures IDs, coding, and proportions per cubic meter

Mixture ID	Coding	Cement (kg)	Slag (kg)	Water (kg)*	Fine Agg. (kg)	NS (kg)	NCC (kg)	NFC (kg)	BFP (kg)
B4.5-NFC0.5-C	1, 1, 1	350	350	210	1190	0	0.70	3.50	78
B4.5-NFC0.5-S	1, 1, -1	350	350	180	1105	42	0	3.50	78
B0-NFC0.5-C	-1, 1, 1	350	350	210	1305	0	0.70	3.50	0
B0-NFC0.5-S	-1, 1, -1	350	350	180	1225	42	0	3.50	0
B4.5-NFC0-C	1, -1, 1	350	350	210	1195	0	0.70	0	78
B4.5-NFC0-S	1, -1, -1	350	350	180	1115	42	0	0	78
B0-NFC0-C	-1, -1, 1	350	350	210	1315	0	0.70	0	0
B0-NFC0-S	-1, -1, -1	350	350	180	1235	42	0	0	0
B2.25-NFC0-SC	0, -1, 0	350	350	195	1215	21	0.35	0	39
B2.25-NFC0.5-SC	0, 1, 0	350	350	195	1210	21	0.35	3.50	39
B4.5-NFC0.25-SC	1, 0, 0	350	350	195	1150	21	0.35	1.75	78
B0-NFC0.25-SC	-1, 0, 0	350	350	195	1270	21	0.35	1.75	0
B2.25-NFC0.25-C	0, 0, 1	350	350	210	1250	0	0.70	1.75	39
B2.25-NFC0.25-S	0, 0, -1	350	350	180	1170	42	0	1.75	39
B2.25-NFC0.25-SC	0, 0, 0	350	350	195	1210	21	0.35	1.75	39

*Adjusted amount of mixing water considering the water content of NS (50% solid content) and/or NFC (20% solid content).

Table 3. 5: Selected mixtures for repair

Mixture ID	Cement (kg)	Slag (kg)	Water (kg)*	Fine Agg. (kg)	NS (kg)	NCC (kg)	NFC (kg)	BFP (kg)
B4.5-NFC0.5-C	350	350	210	1190	0	0.70	3.50	78
B4.5-NFC0.5-S	350	350	180	1105	42	0	3.50	78
B4.5-NFC0-C	350	350	210	1195	0	0.70	0	78
B4.5-NFC0-S	350	350	180	1115	42	0	0	78
B4.5-NFC0.25-C	350	350	210	1190	0	0.70	1.75	78
B4.5-NFC0.375-S3.75/C0.0375	350	350	190	1140	26	0.25	2.70	78

*Adjusted amount of mixing water considering the water content of NS (50% solid content) and/or NFC (20% solid content).

3.1.2 Testing

For the fresh properties, the mortar flow and retention were performed according to ASTM C230/C230M, (2014) and the initial and final setting times of the composites were assessed following ASTM C403/C403M, (2016). Fresh mortar without pellets was placed in a container at room temperature, and the penetration resistance was determined by standard needles at regular time intervals.

The mechanical properties were evaluated based on compressive and flexural strength tests. The compressive strength of the mixtures was evaluated by testing triplicate cylinders (100×200 mm) at early- and later ages complying with ASTM C39/C39M, (2018). The flexural behavior was determined at 28 days by testing triplicate prisms (100×100×350) according to ASTM C1609/C1609M, (2012); hence, a servo-controlled closed-loop testing machine was used, where the displacement rate relied on the measured net mid-span deflection of the prism. The flexural performance was assessed based on the first cracking strength, peak strength, residual strength at spans *L/600* (0.5 mm) and *L/150* (2 mm), as well as toughness, which was calculated as the area under the

load-deflection curve (P-δ) up to a deflection of span L/150. The flexural test setup is shown in **Fig. 3.1**.

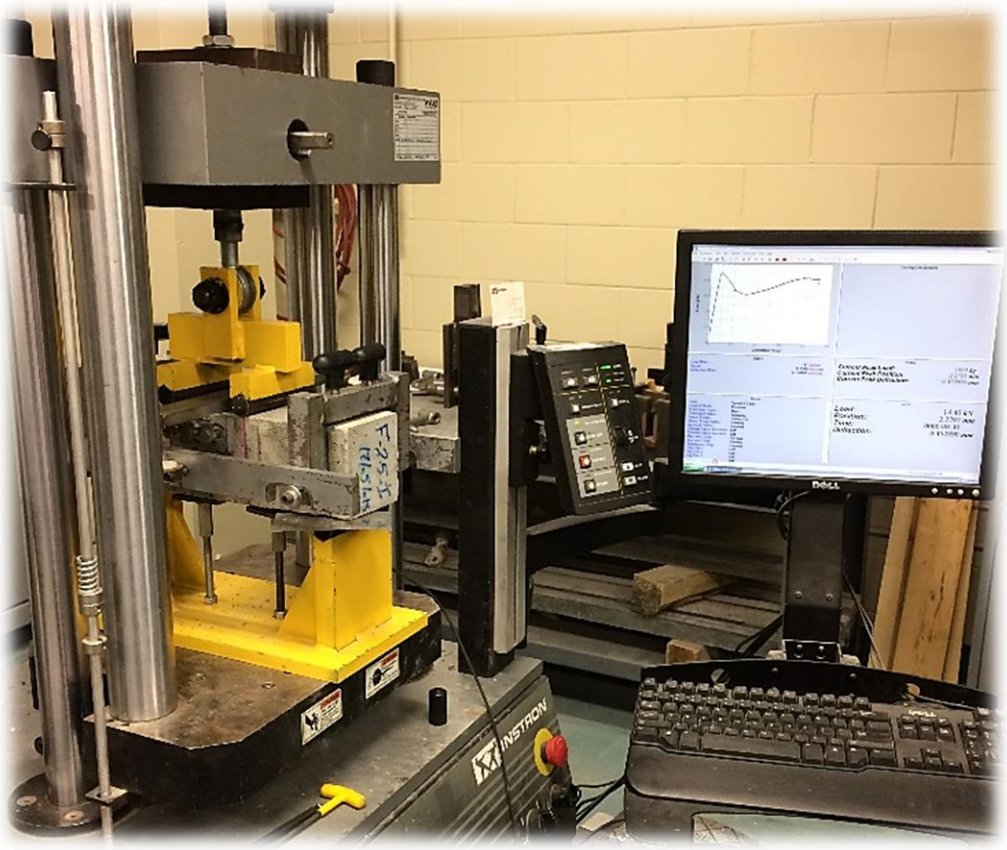

Figure 3. 1: Flexural test setup.

The penetrability of selected mixtures was assessed by performing a fluid absorption test based on a test procedure introduced by Tiznobaik and Bassuoni (2018). After 28 days of curing, three concrete discs (75×50 mm) were put in an oven at 50°C and 40% RH until a constant mass was achieved. Subsequently, specimens were then left for 6 hours in a sealed desiccator operated at vacuum pressure (85 kPa). Each specimen was then freely submerged in a 4% calcium chloride ($CaCl_2$) solution for 6 hours, then the absorption was measured to the closest 0.01 g as the percentage change in mass of the specimens relative to the initial dry masses after 1, 5, 10, 20, 40, 80, 160 and 360 minutes.

In addition, the fluid transport properties within the composites were evaluated by performing the rapid chloride penetration test (RCPT), as per ASTM C1202-22, (2022), on triplicate disc specimens (100×50 mm) to determine the passing charges in addition to the depth of chloride penetration into specimens. The test setup for the RCPT is illustrated in **Fig. 3.2**. The specimens were split in half and sprayed with a 0.1M silver nitrate solution, which creates a white silver chloride precipitate within 15 minutes. The average depth of the white precipitate was then measured at five locations along each half. The depth indicates the ease with which external fluids can enter the microstructure, and consequently the microstructure's continuity of the matrix.

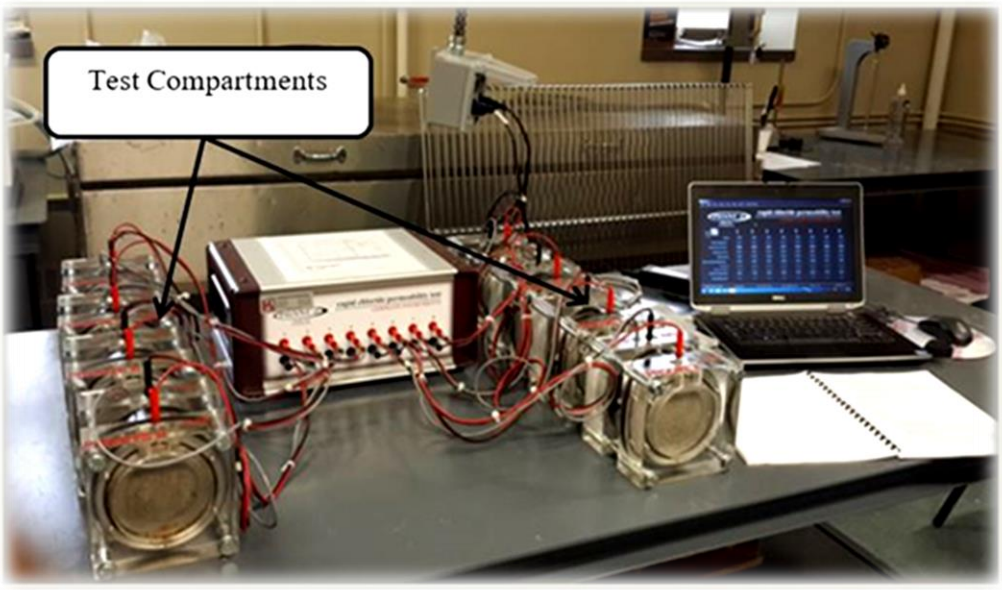

Figure 3. 2: Test setup for RCPT.

The resistance of the different mixtures to freezing-thawing (F/T) cycles was evaluated based on the durability factor (*DF*) of triplicate prisms (75×75×285) mm as stipulated by ASTM C666, Procedure A, which was calculated using ultra-pulse velocity (UPV) with 54 kHz transducers in accordance to ASTM C597, (2016). The duration of one F/T cycle was 12 hours: freezing at −18±1°C for 7 h and thawing at 4±1°C for 3.5 h, and

45 min. to ramp to the minimum freezing temperature or the maximum thawing temperature. Every two weeks, the samples were brought outside of the environmental chamber (**Fig. 3.3**) for visual observation and to measure the change in relative dynamic modulus of elasticity (RE_d) of the concrete specimens. The durability factor was calculated according to the following equation (**Eq. 3.1**):

$$DF = PN/M \quad \textbf{(Eq. 3. 1)}$$

where, *DF* = durability factor of the test specimen;

P = relative dynamic modulus of elasticity from UPV at N cycles, %;

N = number of cycles at which *P* reaches the specified minimum value of 60 % for discontinuing the test or the specified number of cycles at which the exposure is to be terminated, whichever is less; and

M = specified number of cycles at which the exposure is to be terminated (300 cycles).

The resistance of triplicate concrete slabs (250×250×100 mm) to salt-frost scaling was evaluated as per ASTM C672 (2012). The specimens were exposed to 50 F/T cycles, where each cycle consisted of ponding (3 to 5 mm) the surface of specimens with 4% calcium chloride solution for 16 h at a temperature of -18±2°C, followed by thawing at 23±2°C for 8 h. The resistance to surface scaling of concrete was assessed qualitatively by visual examination and quantitatively by weighing the scaled mass of specimens' surfaces.

Figure 3. 3: Environmental chamber used for F/T exposure.

Restrained shrinkage and pull-off tests were carried out to assess the compatibility between the substrate/parent concrete and the nano-modified (repair) concrete created in this work. Duplicate Concrete slabs (250×250×130 mm) were cast for both experiments, acting as the parent concrete for repair/overlay regime (400 kg/m^3 GU cement with 15% fly ash replacement at w/b of 0.4), which is a typical mix design of concrete pavement used

by the City of Winnipeg (COW) in Manitoba (CW 3310-R17, 2015). To remove any remaining shrinkage strain, the slabs were subsequently stored in laboratory conditions for 450 days after being kept within the curing room (21°C and >95% RH) for 7 days. The substrate concrete, which served as the surface of each slab, was wire-brushed and cleaned. The roughened surface was dampened before the repair/overlay layer (70 mm) was put on top. Four demec points were mounted to the repair/overlay layer's surface after casting by 1 hour in order to measure the composites' restricted shrinkage. A dial gauge extensometer was used to measure the shrinking of the repair/overlay layer for 28 days while it was curing. In order to track the cumulative shrinkage of the repair/overlay layer, the specimens were then transferred to a hot/dry exposure of 40°C and 35%RH and shrinkage was monitored and measured up to 180 days. The adopted scheme for the restrained shrinkage test accurately represented a crucial repair/overlay scenario with a high surface-to-volume ratio at the joint position in concrete pavement [Frentress and Harrington, 2012]. Furthermore, the pull-off test slabs were partially cored to assess the bond strength and failure mode (**Fig. 3.4**) between the parent concrete and repair/overlay layer in accordance with CSA A23.2-6B (2019) after 28 days of curing.

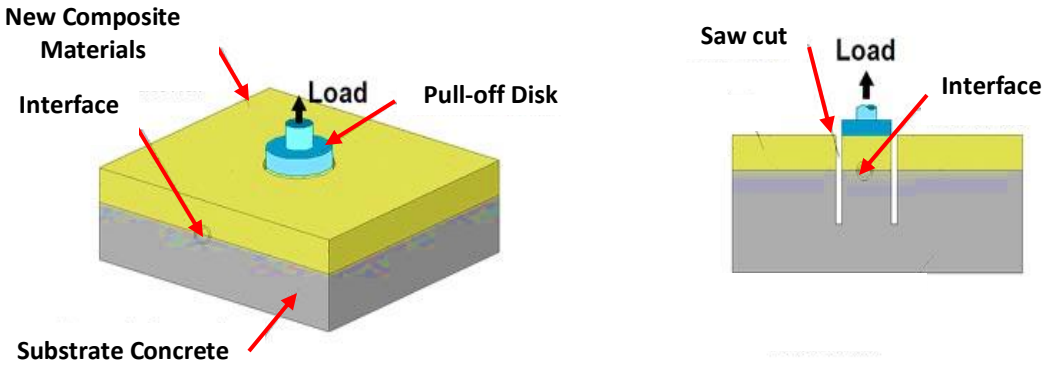

Figure 3. 4: Schematic for pull-off test.

The microstructural characteristics were assessed for selected composites to elucidate the trends obtained from the bulk tests. The thermogravimetric analysis (TGA) was conducted at a constant heating rate of 10°C/min on powder samples that were extracted from the composites to evaluate the hydration and pozzolanic activities by monitoring the portlandite (CH) quantities in the cementitious matrix up to 91 days. The CH was calculated by determining the percentage drop of an ignited mass of the TG curves at a temperature range of 400 to 450°C and multiplying it by 4.11 (ratio of the molecular mass of CH to that of water). The DSC device is shown in **Fig. 3.5**. Moreover, after 28 days of curing, scanning electron microscopy (SEM) associated with elemental dispersive X-ray (EDX) analysis was performed on fracture fragments, which were extracted from untested specimens to visually capture the effect of the adopted parameters on the performance of the different composites. The SEM samples were coated with a fine layer of carbon before performing the analysis to make the surface conductive and to improve the sample imaging. A visual representation of the used SEM is shown in **Fig. 3.6**.

Figure 3. 5: DSC instrument where the powder samples were tested.

Figure 3. 6: Scanning electron microscopy (SEM).

CHAPTER 4: RESULTS AND DISCUSSION OF PHASE I

4.1 Derived Statistical Models

The obtained test results, listed in **Table 4.1,** of the aforementioned responses for the cementitious composites, were statistically analyzed including fresh properties (initial [*IST*] and final [*FST*] setting times), early/later age hardened properties (3 [*f'c* 3d] and 28 days [*f'c* 28d] compressive strengths), flexural performance at 28 days (toughness [*T*]) and resistance to frost action (durability factor [*DF*]). All responses followed a general model, which can be expressed by (**Eq. 4.1**):

$$y = \beta_0 + \Sigma\, \beta_i X_i + \Sigma\, \beta_{ij} X_i X_j + \Sigma\, \beta_{ii} X_i X_i + \epsilon \qquad \textbf{(Eq. 4. 1)}$$

where, y*:* response;

X_i*:* independent variable;

β_0*:* model intercept (constant);

β_i*:* (i= 1, 2, 3): linear regression coefficients of each factor;

β_{ij}*:* (i= 1, 2, 3; j= 2, 3; i > j): interaction regression coefficients of each factor;

β_{ii}*:* (i = 1, 2, 3): quadratic regression coefficients of each factor; and

ϵ*:* random error for uncontrolled factors.

All responses were mapped based on the input parameters, which were utilized to determine the coefficients of the models following a non-linear regression analysis (polynomial function). The presented equations (**Eqs. 4.2 to 4.7**) are expressed in terms of the significant factors and their interactions which were determined using the analysis of variance (ANOVA) method. A factor is considered significant if its probability is lower than 0.05, which means that there is less than a 5% chance (or 95% confidence level) that a tested response surpasses the value of the specified coefficient. Accordingly, *P-values*

>0.05 indicate that a factor has an insignificant effect on the measured response; thus, it was eliminated from the equations. This criterion maximizes the models' coefficient of determination (R^2), i.e., best fit (Montgomery, 2017).

The models' best-fit responses were generated using a statistical analysis package, Design Expert version 13 (2022). Furthermore, the models' coefficients and significant variables extracted from ANOVA are listed in **Table 4.5.** Hence, the response equations are as follows:

$$IST\ [min] = 274.4 + 53.5 \times B + 40 \times NFC + 21.9 \times B \times NFC \quad \textbf{(Eq. 4. 2)}$$

$$FST\ [min] = 413.2 + 75.5 \times \mathrm{B} + 55.5 \times \mathrm{NFC} + 26.9 \times \mathrm{B} \times \mathrm{NFC} \quad \textbf{(Eq. 4. 3)}$$

$$(f'c\ 3d)^{-2}\ [MPa] = 0.0007 + 0.0002 \times B - 0.0001 \times NFC - 0.0001 \times SC \quad \textbf{(Eq. 4. 4)}$$

$$\frac{1}{(f'c\ 28d)}\ [MPa] = 0.0128 + 0.0012 \times B - 0.0006 \times NFC - 0.0004 \times SC + 0.0007 \times NFC^2 \quad \textbf{(Eq. 4. 5)}$$

$$(T)^{\frac{1}{2}}\ [J] = 5.4 + 2.7 \times B - 1.1 \times B^2 - 0.1538 \times NFC^2 - 0.2369 \times SC^2 \quad \textbf{(Eq. 4. 6)}$$

$$DF\ [\%] = 92.6 - 2.2 \times B + 1.5 \times NFC + 1.3 \times B \times NFC + 3.0 \times B^2 \quad \textbf{(Eq. 4. 7)}$$

Predictions for a response at specific values of each element can be made using these equations, which are expressed in terms of coded values. According to a unit change in the factor value, each coefficient shows the expected change in response. By comparing the coefficients of the elements, coded equations help to determine the relative importance of the factors. Indeed, the models' validity is limited by the high- and low-level factors (+1 to -1) of the experimental variables. To illustrate the interactive relationships among the different variables, three exemplar graphs were plotted from each response, where the effect of the high and low levels of each factor can be visually captured.

Table 4. 1: Summary of the bulk test results

Mixture ID	IST (min)	FST (min)	$f'c$ 3d (MPa)	$f'c$ 28d (MPa)	T (J)	DF (%)
B4.5-NFC0.5-C	380 (2.2)	550 (2.4)	38 (2.1)	74 (3.1)	43.0 (4.2)	98 (2.6)
B4.5-NFC0.5-S	390 (2.5)	580 (2.1)	36 (2.3)	72 (2.2)	45.0 (4.8)	96 (3.1)
B0-NFC0.5-C	235 (3.4)	360 (4.1)	49 (2.8)	90 (1.4)	0.8 (2.1)	100 (2.8)
B0-NFC0.5-S	240 (2.2)	370 (2.7)	45 (0.9)	83 (0.7)	2.1 (2.2)	100 (3.2)
B4.5-NFC0-C	250 (4.1)	385 (2.4)	33 (0.7)	70 (1.4)	42.0 (2.2)	93 (4.3)
B4.5-NFC0-S	280 (2.8)	425 (3.2)	31 (1.7)	62 (4.9)	43.0 (4.4)	90 (2.9)
B0-NFC0-C	200 (2.2)	305 (4.3)	42 (1.8)	79 (2.8)	1.6 (2.5)	100 (3.6)
B0-NFC0-S	210 (4.1)	320 (2.9)	38 (2.8)	76 (2.9)	1.5 (3.8)	99 (1.7)
B2.25-NFC0-SC	230 (3.6)	350 (3.6)	36 (3.3)	72 (4.6)	26.5 (2.7)	92 (2.1)
B2.25-NFC0.5-SC	325 (3.4)	480 (2.1)	41 (2.3)	76 (2.2)	26.7 (4.1)	95 (4.4)
B4.5-NFC0.25-SC	340 (3.2)	510 (2.4)	35 (2.2)	72 (2.3)	46.8 (2.9)	96 (3.2)
B0-NFC0.25-SC	220 (2.2)	340 (2.7)	51 (3.8)	92 (4.4)	2.6 (2.1)	96 (2.7)
B2.25-NFC0.25-C	300 (1.4)	450 (3.4)	40 (4.8)	76 (3.3)	25.5 (3.1)	95 (2.2)
B2.25-NFC0.25-S	270 (2.5)	405 (2.7)	38 (2.0)	74 (2.3)	26.0 (2.4)	93 (3.4)
B2.25-NFC0.25-SC	260 (2.9)	390 (2.1)	37 (1.4)	79 (1.4)	30.0 (4.6)	92 (1.5)
B2.25-NFC0.25-SC	265 (2.2)	400 (2.8)	38 (3.5)	79 (2.2)	29 (2.9)	92 (2.2)
B2.25-NFC0.25-SC	270 (3.6)	405 (3.4)	37 (3.1)	80 (2.7)	29 (2.2)	92 (1.9)

Note: The Values in parentheses represent the standard deviations.

Table 4. 2: Models' derived coefficients from ANOVA

Multiplied by	$(IST)^{-2}$	FST	$(f'c\ 3d)^{-2}$	$\frac{1}{(f'c\ 28d)}$	$(T)^{\frac{1}{2}}$	DF
Intercept	**274.4**	**413.2**	**0.0007**	**0.0128**	**5.4**	**92.6**
B	**53.5**	**75.5**	**0.0002**	**0.0012**	**2.7**	**-2.2**
NFC	**40**	**55.5**	**-0.0001**	**-0.0006**	0.0101	**1.5**
SC	-2.5	-5	**-0.0001**	**-0.0004**	-0.0791	0.8
B * NFC	**21.9**	**26.9**	--	-0.0001	0.0467	**1.3**
B * SC	-3.1	-5.6	--	-0.0001	0.0359	0.5
NFC * SC	3.1	1.9	--	0.0001	-0.0836	-0.3
B^2	--	--	--	-0.0005	**-1.1**	**3.0**
NFC^2	--	--	--	**0.0007**	**-0.1538**	0.5141
SC^2	--	--	--	0.0005	**-0.2369**	1.0
R^2	**0.9667**	**0.9609**	**0.9283**	**0.9495**	**0.9990**	**0.9163**

Note: significant values are bolded.

4.2 Setting Time

The results of IST and FST, which were determined according to ASTM C403/C403M, (2016), varied between 3.3 to 6.5 h and 5.1 to 9.7 h, respectively (**Table 4.1**). The derived **Eq.4.2** indicates that the IST response was significantly influenced by BFP and NFC dosages, while the type of nanoparticle showed an insignificant effect. The BFP (coefficient of 53.5) dosage had the dominant effect on the IST response compared with the NFC (coefficient of 40) dosage. Similarly, the FST response expressed by **Eq.4.3** showed the same trend with BFP and NFC coefficients of 75.5 and 55.5, respectively. Despite, the high dosages of HRWRA needed for target flow of the slag–based composites, the FST for most composites remained below the lower limit of the documented range for binders incorporating high volumes of supplementary cementitious materials (SCMs), which typically shows FST within the range of 9 to 12 h (Neville, 2011).

The isoresponses shown in **Figs. 4.1(a-c)** and **Figs. 4.2(a-c)** map the trends from the IST and FST models, respectively. Increasing the dosages of BFP led to extending the IST and FST of the composites. For instance, the incorporation of 4.5% BFP in mixture B0-NFC0-S to produce mixture B4.5-NFC0-S increased the IST and FST by 33%. Likewise, the amalgamation of NFC in the different composites delayed the setting times but to a lesser extent in comparison with BFP. For example, composite B0-NFC0.5-C achieved longest IST and FST by 18% compared to that of the counterpart composite without NFC (B0-NFC0-C), which were 3.3 h and 5.1 h, respectively. This can be ascribed to the extra amount of HRWRA required to maintain the composites' target flowability, especially when comprising macro-fibers; thus, an increase in the rate of admixture bleeding in the fresh composites may reduce the resistance of the superficial layer within the active depth of the penetrating needles in the setting time test.

Although the type of nanoparticles used herein was not a significant factor affecting the skeletal rigidity of the composites, the presence of these materials was essential to achieve acceptable hardening rates through different mechanisms, as shown in Section 4.6, especially with the coexistence of high dosages of a latent hydraulic binder (slag). These patterns align with the results of previous studies on nano-modified concrete incorporating high volumes of SCMs (X. Jiang et al., 2022; Azzam et al., 2019a; Motahari Karein et al., 2017).

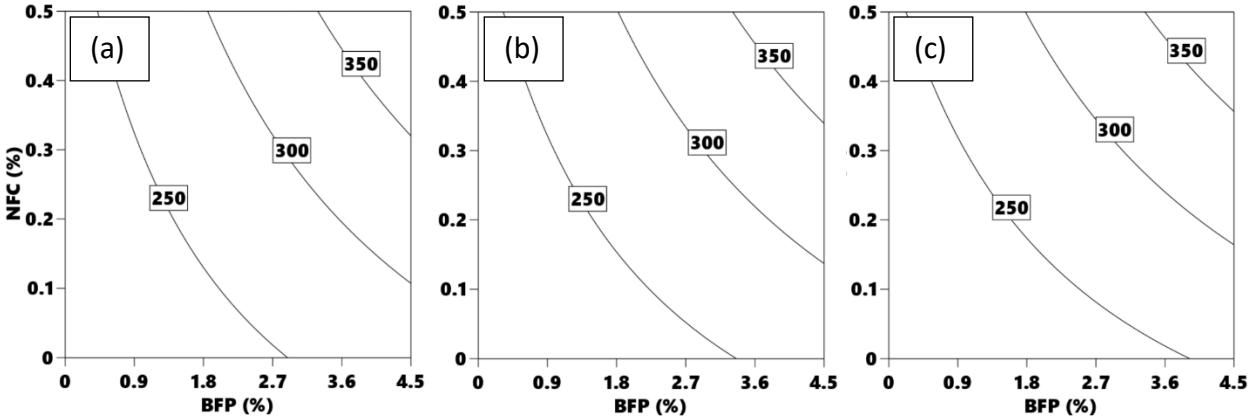

Figure 4. 1: IST isoresponse curves (min): (a) 6% nano-silica, (b) 3% nano-silica with 0.05% nano-crystalline cellulose, and (c) 0.1% nano-crystalline cellulose.

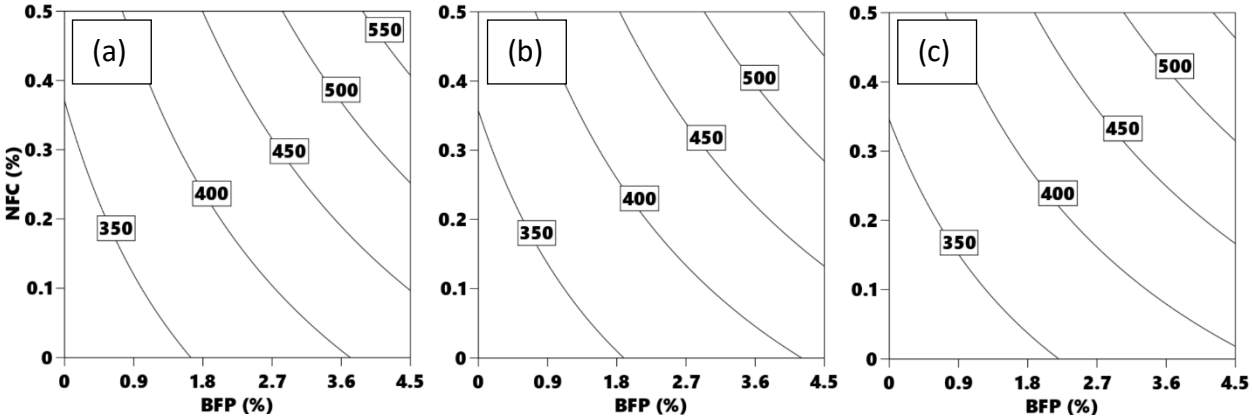

Figure 4. 2: FST isoresponse curves (min): (a) 6% nano-silica, (b) 3% nano-silica with 0.05% nano-crystalline cellulose, and (c) 0.1% nano-crystalline cellulose.

4.3 Compressive Strength

As listed in **Table 4.1**, all composites, which contained 50% slag, achieved compressive strengths more than 30 MPa at early-age, whilst the 28 days mechanical capacity varied between 62 to 92 MPa, which qualifies the proposed composites for a variety of infrastructure applications (e.g., patch repair and overlays for bridges and pavements). This proves the capability of the incorporated nanomaterials (NS, NCS, or NCC) to mitigate the drawback of using high-volume slag on strength development. As depicted in the isoresponse curves [**Figs. 4.3(a-c)** and **4.4(a-c)**] and the associated statistical models described by **Eqs. 4.4** and **4.5**, the compressive strength at both early- and late-ages was significantly affected by the adopted parameters. Both 3-days and 28-days compressive strengths experienced similar statistical significance trends, designated by the magnitudes of regression coefficients. Hence, the BFP exhibited the most significant impact on strength, followed by the NFC and nanomaterials type.

As shown in the isoresponse curves, it can be noted that irrespective of the mix design settings, the inclusion of BFP notably reduced the composites' compressive strength values. For instance, adding BFP to composite B0-NFC0.5-C and B0-NFC0.5-S to produce mixtures B4.5-NFC0.5-C and B4.5-NFC0.5-S reduced the compressive strength at 3 and 28 days by an average of 21% and 16%, respectively. A similar trend was reported by (Azzam et al., 2019a) for fly ash- and slag-based cementitious composites comprising BFP, which can be attributed to the ITZs created by BFP in the matrix, acting as stress concentrators/weak links, thus reducing its mechanical capacity.

In contrast, cementitious composites comprising NFC yielded higher compressive strengths than that of corresponding composites without NFC (**Figs. 4.3 and 4.4**). For example, the addition of 0.5% NFC by mass of composite B0-NFC0-S binder to produce

composite B0-NFC0.5-S increased the 3- and 28-days compressive strengths by 18 and 9%, respectively. This can be ascribed to the short circuit diffusion mechanism of NFC, which improves the hydration of the cementitious matrices, as will be substantiated in Section 4.6. This highlights the potential of NFC to alleviate the negative effect of BFP macro-fibers on the composites' mechanical capacity.

The amalgamation of NCC in the composites achieved a slight increase in compressive strength than its counterpart NS and the effect was elevated with the dosage of nanomaterials. For instance, composite B0-NFC0-C achieved a higher compressive strength than its counterpart composite B0-NFC0-S as it increased the 3- and 28-days compressive strength by 6 and 13%, respectively. Both NCC and NS provide nucleation surfaces for hydrations products to precipitate on at early-age; however, the short circuit diffusion mechanism of NCC might achieve better development in the composites' microstructure.

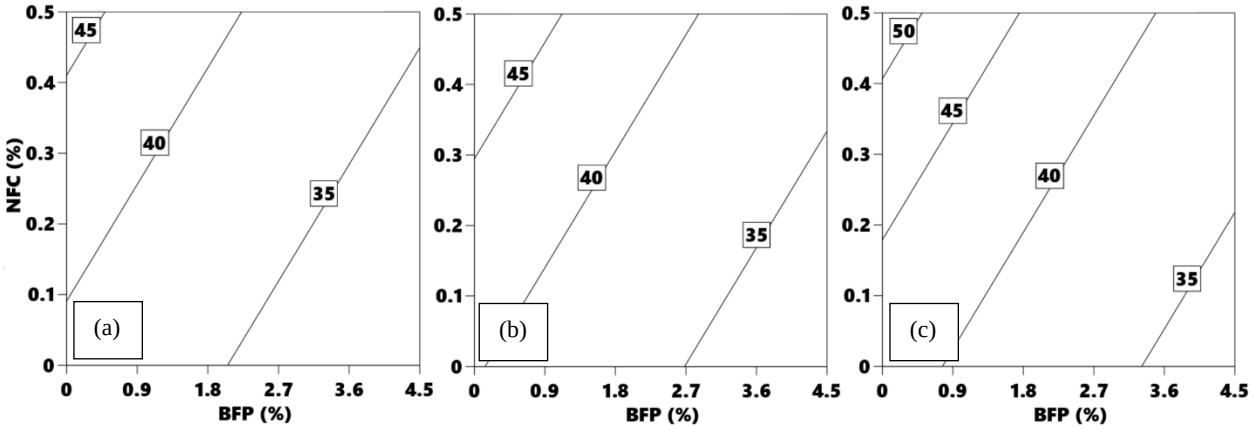

Figure 4. 3: 3-day compressive strength isoresponse curves (MPa): (a) 6% nano-silica, (b) 3% nano-silica with 0.05% nano-crystalline cellulose, and (c) 0.1% nano-crystalline cellulose.

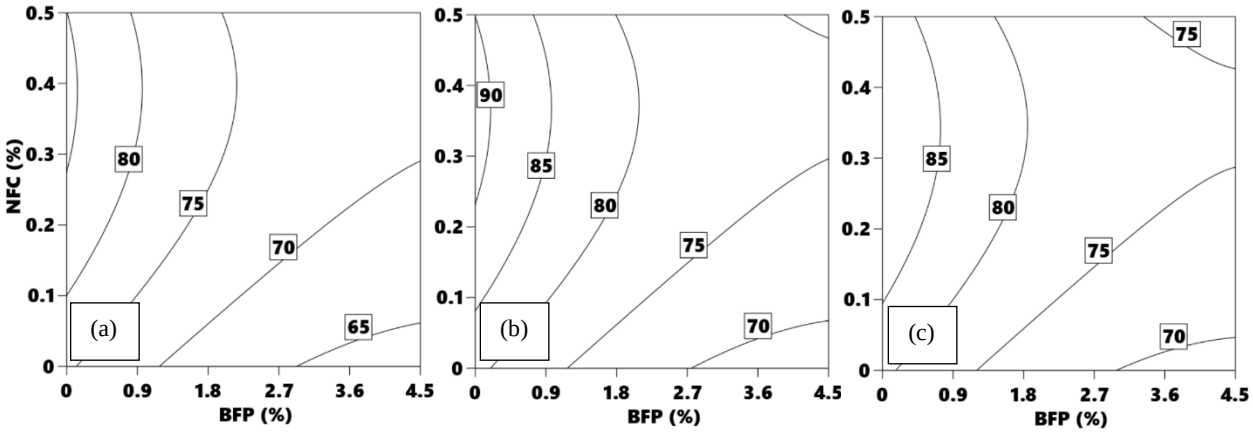

Figure 4. 4: 28-days compressive strength isoresponse curves (MPa): (a) 6% nano-silica, (b) 3% nano-silica with 0.05% nano-crystalline cellulose, and (c) 0.1% nano-crystalline cellulose.

4.4 Flexural Performance

Table 4.3 lists the flexural properties including first-peak flexural strength, residual strengths, post-cracking residual strength index, and toughness for all composites at 28 days following the guidelines stipulated by ASTM C1609/C1609M (2019). The flexural strengths for all composites were in the range of 5.7 to 14.7 MPa, which qualifies them to be employed in various construction applications such as bridge overlays, repair patches, joints, etc. (Mehta and Monteiro, 2014). The general trends of the tested design variables were similar to that of the compressive strength; hence, the first-peak flexural strength mainly depends on the mechanical capacity of the cementitious matrix, which is affected by the type of binder and fibers, as explained in the previous section.

Table 4. 3: Flexural properties of composites

Mixture ID	First-Peak Strength (MPa)	Residual Strength at *L/150* (MPa)	Residual Strength at *L/600* (MPa)	Post-Cracking Residual Strength Index (R_i)	Toughness (J)
B4.5-NFC0.5-C	7.3	6.4	5.6	0.9	43.0
B4.5-NFC0.5-S	6.8	6.7	5.9	1.1	45.0
B0-NFC0.5-C	13.8	0.0	0.0	0.0	0.8
B0-NFC0.5-S	11.6	0.0	0.0	0.0	2.1
B4.5-NFC0-C	6.8	6.2	6.3	1.0	42.0
B4.5-NFC0-S	5.7	6.6	6.0	1.2	43.0
B0-NFC0-C	10.4	0.0	0.0	0.0	1.6
B0-NFC0-S	10.0	0.0	0.0	0.0	1.5
B2.25-NFC0-SC	6.8	4.2	3.5	0.6	26.5
B2.25-NFC0.5-SC	9.8	4.0	3.8	0.4	26.7
B4.5-NFC0.25-SC	6.9	7.9	5.7	1.0	46.8
B0-NFC0.25-SC	14.7	0.0	0.0	0.0	2.6
B2.25-NFC0.25-C	9.9	4.4	4.1	0.4	25.5
B2.25-NFC0.25-S	7.0	4.0	3.8	0.6	26.0
B2.25-NFC0.25-SC	11.0	4.2	4.0	0.4	30.0
B2.25-NFC0.25-SC	11.1	4.2	4.0	0.4	29.0
B2.25-NFC0.25-SC	10.8	4.2	4.0	0.4	29.0

Figure 4.5 illustrates an exemplar post-cracking behavior (P- δ plot) of selected composites to comprehend the effect of each of the adopted parameters on the multi-scaled fibers incorporated in the nano-modified composites. After the first-cracking, a sharp decline in load capacity was observed, representing the transitional stage between matrix failure and engagement of BFP load-bearing mechanism in the post-peak stage (deflection softening or hardening), which is a typical trait of high-performance cementitious composites. The composites' post-cracking performance was enhanced, notably with higher BFP contents, as depicted in **Fig. 4.5** (B0-NFC0-NC, B2.25-NFC0.25-NC, B4.5-NFC0-NC), due to the pellets' pullout process. This was reflected by the tendency of composites containing low BFP dosage for exhibiting deflection softening in contrast to composites with 4.5% BFP dosage, which showed deflection hardening with higher ductility. It is worth noting despite the positive effect of NFC on the first-peak strength due to the improved mechanical capacity of the matrix, as mentioned in the compressive strength section, the overall post-peak behavior was comparable to composites without NFC, as shown in **Fig. 4.5** (B4.5-NFC0-NC vs. B4.5-NFC0.5-NC).

The residual post-cracking strength index (R_i), which assesses the performance of fiber-reinforced concrete (FRC) in bridges (CSA S6, 2019), was calculated for each composite. The R_i of composites containing 2.25% BFP was larger than 0.4, while it was greater than 0.9 for composites with 4.5% BFP. Depending on the application and the layers of cracking-control reinforcement, it is required that a suitable fiber content in FRC is chosen based on R_i to meet or surpass specified values ranging from 0 to 0.30 (CSA S6, 2019). According to those stipulations, the developed composites with BFP herein have acceptable flexural performance for bridge applications.

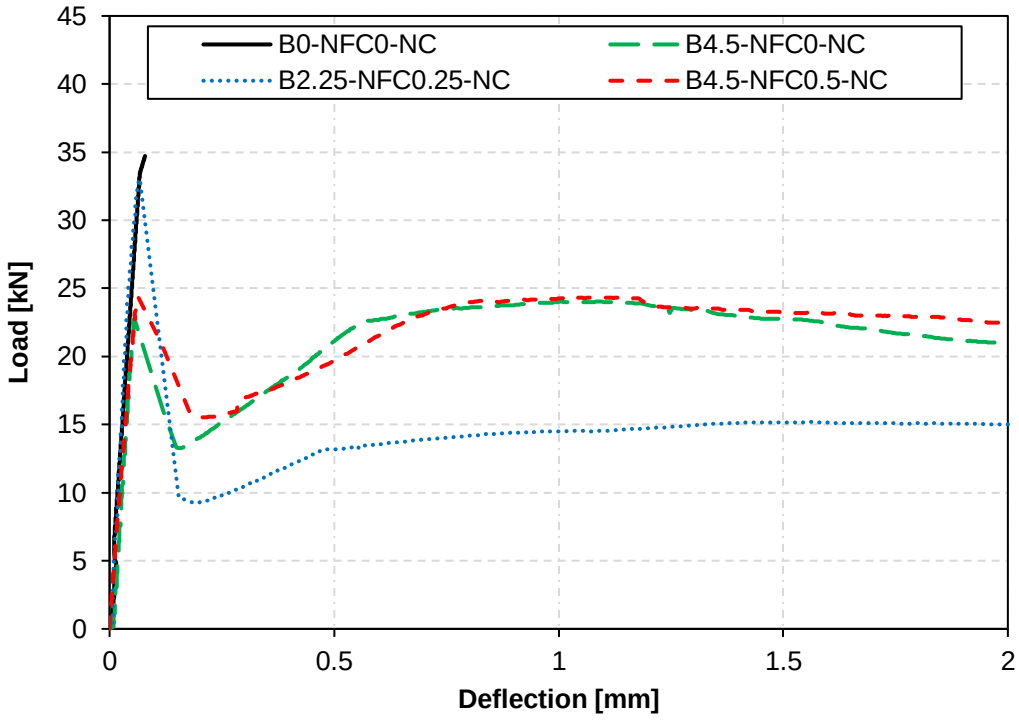

Figure 4. 5: Exemplar load-deflection (P-δ) curves.

The derived **Eq. 4.6** and corresponding isoresponse curves [**Fig. 4.6 (a-c)**], indicate that the toughness response was significantly influenced by BFP solely. Accordingly, the composites incorporating BFP experienced a significant increase in toughness. For instance, the addition of BFP at dosages of 2.25% and 4.5% to B0-NFC0-S composite to produce B2.25-NFC0-SC and B4.5-NFC0-S composites boosted the toughness from 1.5 J to 26.5 and 43 J, respectively. This can be linked to the effective control of BFP over the spread of macro-cracks resulting in higher ductility, which is reflected by an increase in toughness/ductility, especially with the higher BFP dosages owing to the abundance of the pellets in the specimens' failure plane leading to deflection hardening (**Fig. 4.5**). On contrary, NFC had a negligible impact on the composites' toughness; for instance, the addition of NFC to composite B4.5-NFC0-C to produce composite B4.5-NFC0.5-C increased the toughness by 1 J. Likewise, changing the type of used nano particles showed

an insignificant effect on the toughness. For example, composite B4.5-NFC0-S attained a toughness value of 43 J compared to 42J of the counterpart composite comprising NCC (B4.5-NFC0-C).

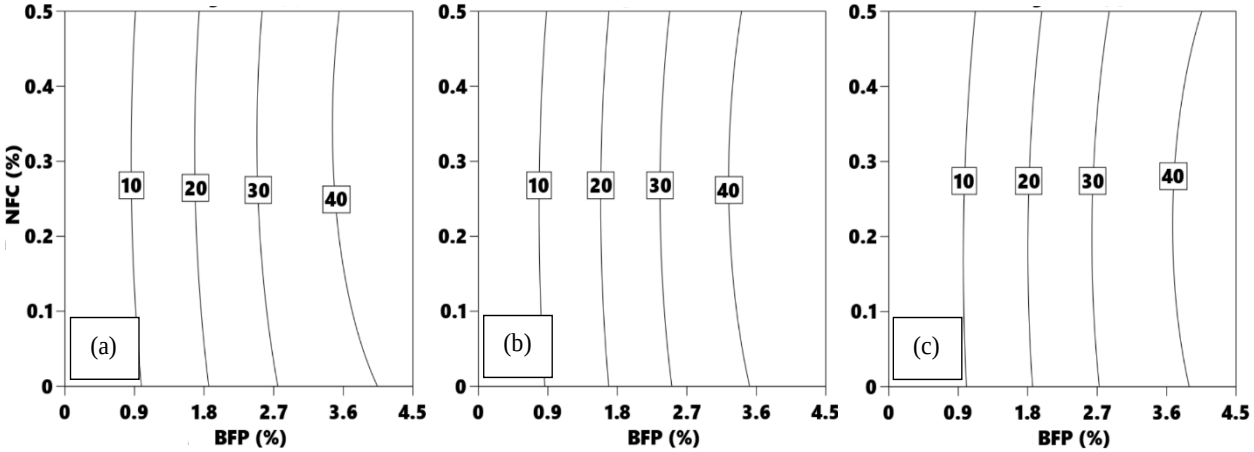

Figure 4. 6: Toughness isoresponse curves (J): (a) 6% nano-silica, (b) 3% nano-silica with 0.05% nano-crystalline cellulose, and (c) 0.1% nano-crystalline cellulose.

4.5 Durability Performance

The composites' durability performance was assessed based on its resistance to 300 cycles of freezing-thawing as stipulated by ASTM C666/C666M, (2015). The isoresponse curves mapped in **Figs. 4.7 (a-c)** and the corresponding **Eq. 4.7** show that the BFP and NFC dosages, in order of significance, had a dominant effect on the *DF* with regression coefficients of -2.2 and 1.5, respectively.

Composites comprising BFP achieved relatively lower *DF* compared to the counterpart composites without pellets. For instance, by adding BFP to mixture B0-NFC0-S to produce mixtures B4.5-NFC0-S, the *DF* was reduced by 10%. This can be ascribed to the creation of extra ITZs. However, the marginal effects of BFP on the composite's resistance to freezing-thawing cycles were mitigated by the combination of NFC and BFP to create a hybrid fiber system. For example, composites B0-NFC0-C, B4.5-NFC0-C, and

B4.5-NFC0.5-C achieved *DF* of 100, 93, and 98, respectively, which highlighted the capability of NFC to alleviate the negative effect of BFP due to its physical, chemical and internal curing effects, as explained earlier. Despite the insignificant effect of the nanoparticles type on the composites' response to frost action, their presence was essential to achieve high *DF* values. This can be attributed to the short circuit diffusion mechanism of NCC and the pozzolanic/filler effects of NS, which markedly enhanced the composites' microstructural characteristics as well as the discontinuity of the ITZs in the BFP mixtures; resulting in higher resistance to frost action.

It is worth noting that the composites tested herein, irrespective of the mixture design, reached a *DF* surpassing 90% and exceeding the 60% relative dynamic modulus of elasticity limit stipulated by ASTM C666/C666M, (2015), which qualifies them for exposed applications in cold regions. Indeed, the presence of adequate air content of 6±1%, as required by Canadian and American codes/guidelines for concrete (ACI 201.2R, 2016; CAN/CSA A231.1, 2019), was essential to accommodate the hydraulic/osmotic pressures in concrete caused by freezing-thawing cycles (Neville, 2011; Powers & Helmuth, 1953). In addition, the absorption percentages, which were in the narrow range of 2 to 2.5% without significant difference [overlapping error bars] (**Fig. 4.8)**, indicated very low penetrability. This is attributed to the fact that all composites tested herein had high binder contents ($\geq$ 700 kg/m^3) and low *w/b* (0.30), which would make them resistant to fluid ingress and in turn saturation, which is the necessary condition for frost damage of concrete. In particular, NCC, NFC, and NS densification effects improved the resistance of composites to the ingress of fluids; hence, little freezable water was present in the paste, resulting in composites with superior durability to frost action.

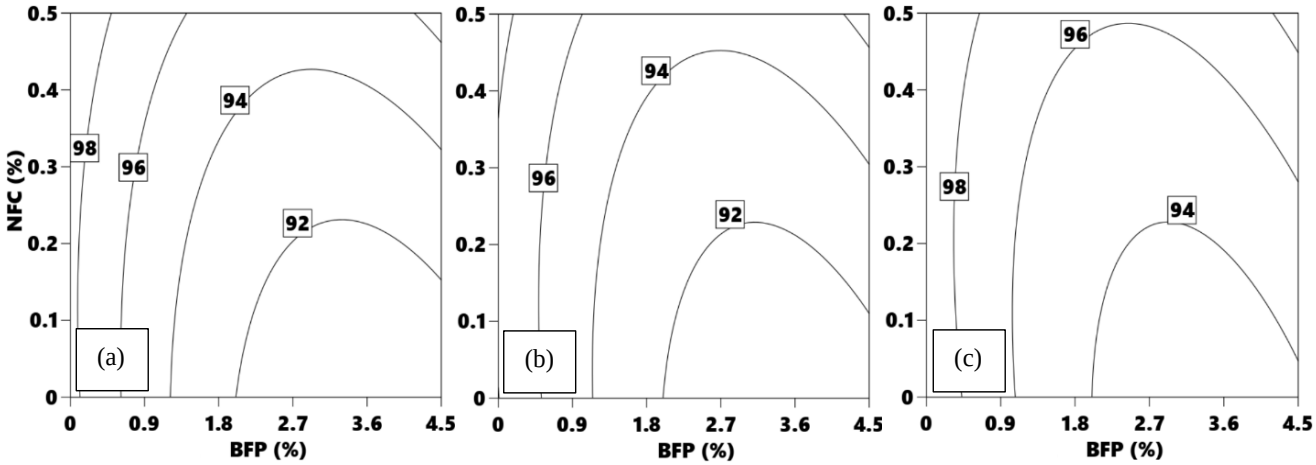

Figure 4. 7: Durability factor isoresponse curves (%): (a) 6% nano-silica, (b) 3% nano-silica with 0.05% nano-crystalline cellulose, and (c) 0.1% nano-crystalline cellulose.

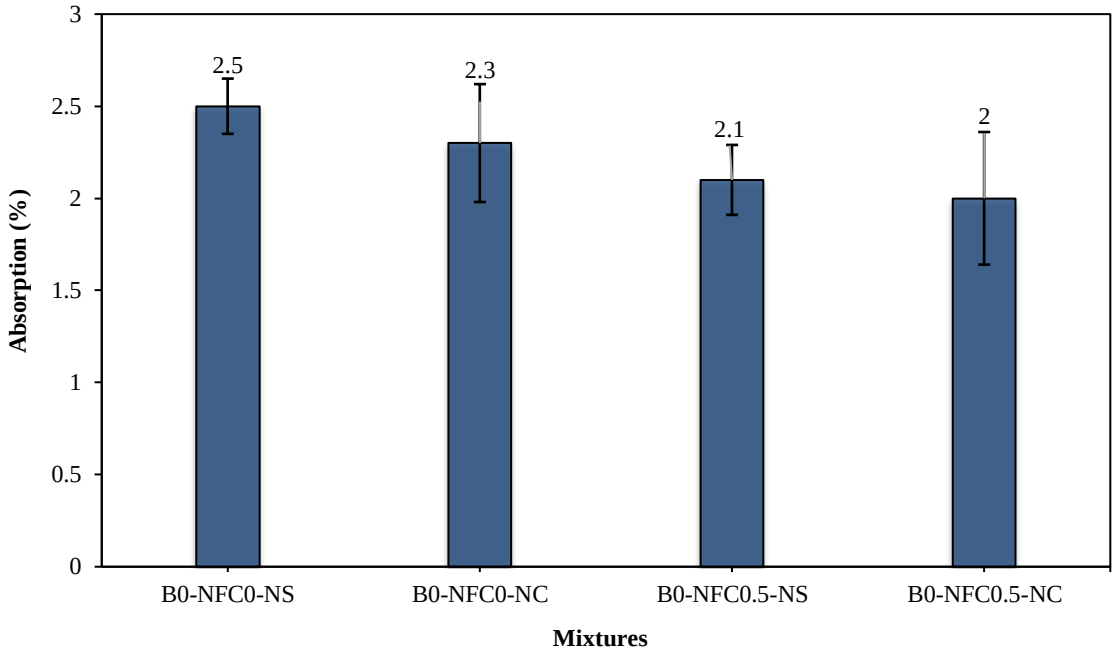

Figure 4. 8: Absorption results of the different mixtures after 28 days of curing. (Note: error bars represent standard deviations)

4.6 Thermogravimetric and Microscopy Analyses

4.6.1 Effect of nanomaterials on the slag-based binder

The contents of calcium hydroxide (CH) present in the nanomodified binders versus time are listed in **Table 4.4**. Irrespective of the different dosages of nanomaterials, it was observed that the mixtures incorporating nano-crystalline cellulose had consistently higher CH contents compared to the mixtures incorporating nano-silica in the slag-based binders at early- and late-ages. For example, after one day of curing, the CH contents in mixtures B0-NFC0-C and B0-NFC0-S was 4.11% and 3.86 % (i.e., 7% increase), respectively; the amount of CH in the matrix slightly increased when NCC was combined with NFC. For instance, the CH content at 7 days for mixtures B0-NFC0-C and B0-NFC0.5-C were 4.22 and 4.44, respectively.

Mixtures incorporating cellulose nanomaterials experienced a rise in CH contents for up to 14 days as they provide nucleation surfaces for the hydration products cementitious materials to precipitate on. In addition, they have omnipresence of superficial hydroxyl groups that can attract calcium ions (Kamasamudram et al., 2021a), causing cellulose to adhere to cement and slag particles. Therefore, selecting the optimum dosages of nanomaterials and dispersing them in the cementitious matrix are essential to minimize agglomeration and increase the area of cement–slag hydration surfaces. In addition, hydrophilic NCC/NFC which are intermixed with hydration shells around cement/slag grains created a network to diffuse water retained by NCC/NFC into the unhydrated core of particles [short circuit diffusion (Cao et al., 2015, 2016a)], hence improving the hydration process in the matrix and attaining a higher degree of maturity. This was reflected by high early-strength (above 30 MPa at 3 days) of these mixtures in spite of the high

content of slag (latent hydraulic binder). After 14 days the CH contents in the comprising cellulose nanomaterials decreased consistently up to 90 days (up to 26% reduction), indicating that NCC/NFC synergistically catalyzed pozzolanic reactivity of slag in the binder through consuming CH in the matrix and precipitating secondary C-S-H to densify the matrix. This conformed to the high strength (above 75 MPa at 28 days), low absorption (less than 2.5%), and improved durability (*DF* of 100%) of these composites.

Table 4. 4: TGA results for CH contents (temperature range of 400 – 450°C) in selected composites

Calcium Hydroxide Content (%)	Time (days)						
	1	3	7	14	28	56	90
B0-NFC0-C	4.1	4.2	4.2	4.4	4.0	3.8	3.7
B0-NFC0-S	3.9	3.7	3.1	2.9	2.3	1.9	1.7
B0-NFC0.5-C	4.2	4.2	4.4	4.5	3.9	3.5	3.3
B0-NFC0.5-S	3.9	3.7	3.8	2.6	2.1	1.8	1.6
B2.25-NFC0-SC	4.0	4.0	3.9	3.5	2.8	2.3	2.1
B2.25-NFC0.5-SC	4.0	3.9	3.7	3.5	2.7	2.1	2.0

Note: accuracy of TGA measurements is within ±0.2%.

Unlike the NCC/NFC mixtures, mixtures incorporating 6% NS alone had consistent reduction of CH from 1 to 90 days; for instance, B0-NFC0-S had a drop of 40% and 27% between 1 to 28 days, and 28 to 90 days respectively. A comparable trend was observed for mixtures comprising 6% NS with 0.5% NFC. Ultrafine nano-silica (specific surface of 80,000 m^2/g) acted as nuclei promoting the formation of hydration products. Sufficient CH contents (above 3%) in the presence of vigorously reactive nano-silica in the binder material led to rapid consumption of calcium hydroxide at very early-age, demonstrating a rapid pozzolanic activity to produce secondary and stiff C-S-H gel in the matrix, which

conformed to the high strength results at 3 (38 Pa) and 28 (78 MPa) days. In addition to the particle packing and physical filling effects of nano-silica agglomerates, the long-term pozzolanic reactivity of slag, as indicted by the lower rates of CH consumption between 28 to 90 days, in composites incorporating nano-silica which led to densification of the microstructure as reflected by the low absorption and high durability to frost action. Binders modified with 3% NS with 0.05% NCC (e.g., B2.25-NFC0-SC) benefited from the synergistic effects of improved hydration and pozzolanic reactivity (concurrent process of CH production and consumption to precipitate additional cement gel), especially with the addition of 0.5% NFC (e.g., B2.25-NFC0.5-SC), which achieved high strength (above 40 MPa and 75 MPa at 3 days and 28 days, respectively) and high resistance to freezing-thawing cycles (at least *DF* of 95%).

4.6.2 Effect of BFP

When BFP was incorporated into the composites, it resulted in decreasing the compressive and first-peak flexural strengths of composites, which are governed by the matrix quality. This effect is attributed to the formation of additional ITZs in the matrix, creating stress concentration regions and thus reduction of capacity. However, this adverse effect was partially offset with the addition of NCC and NFC, owing to the nucleation and internal curing effects that enhanced the degree of maturity of the matrix, as explained in Section 4.7.1. In addition, graded NFC could bridge micro-cracks in the matrix and further increase its capacity as observed in the compressive and flexural strength trends.

After the peak load/first-cracking, BFP had a positive effect on enhancing the post-cracking behavior of composites. The pellets were successful at actively restoring the load-bearing capacity experiencing a strain-hardening effect with increasing the dosage (**Fig.**

4.5). This can be ascribed to the presence of micro-grooves along the surface of the pellets, creating an efficient interlocking mechanism between the cementitious matrix and pellet's interface and resulting in a greater surface area of contact between them. Indeed, the precipitation of reaction products within the grooves enhanced the ductility of the composites by enhancing the bond between the pellets and matrix, as for example shown in **Figs. 4.9 (a-b)**. EDX was used to calculate the calcium-to-silicate ratio (*Ca/Si*) of the cement gel on and in the vicinity of micro-grooves. This relation is established to indicate whether the reaction products were hydraulic or pozzolanic as the C-S-H produced through hydration tends to 1.7, while the secondary C-S-H from pozzolanic reactions tends to 1 (Detwiler et al., 1996). For example, **Figs. 4.10 and 4.11** show that mixtures incorporation NS (vigorous pozzolanic reactivity) had an average *Ca/Si* of 1.1, while mixtures incorporating NCC (enhanced hydration reactions) had an average *Ca/Si* of 1.7, which complied with the TGA trends. This efficient bonding controlled the propagation of cracks in the matrix and impeded the process of the fiber pullout from the matrix, which is the chief toughening mechanism in the composites. Accordingly, a higher amount of BFP resulted in a greater chance for the pellets to be present across potential failure planes, and thus higher energy absorption/toughness.

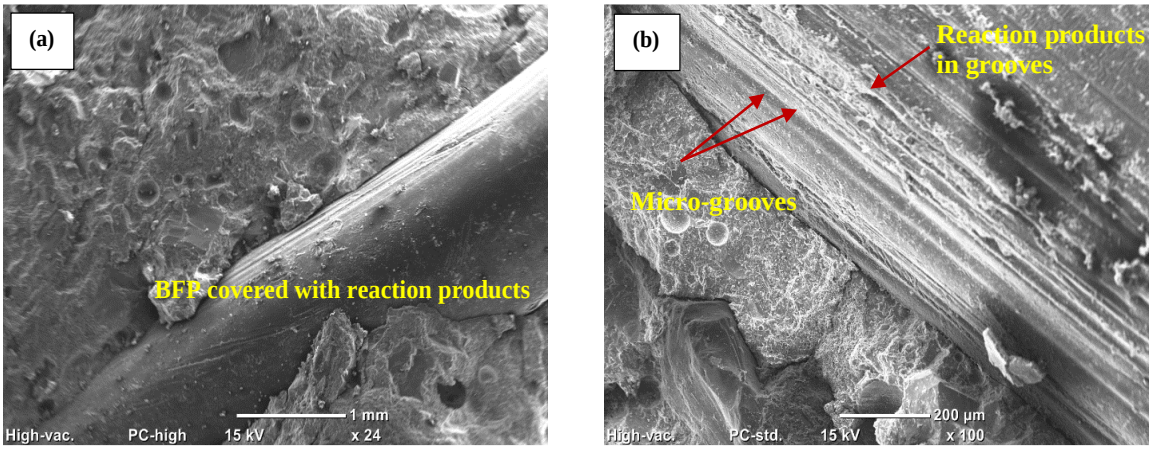

Figure 4. 9: Exemplar SEM micrographs of matrix showing ITZ with BFP for mixtures: (a) B4.5-NFC0.5-NS, and (b) B4.5-NFC0-NC.

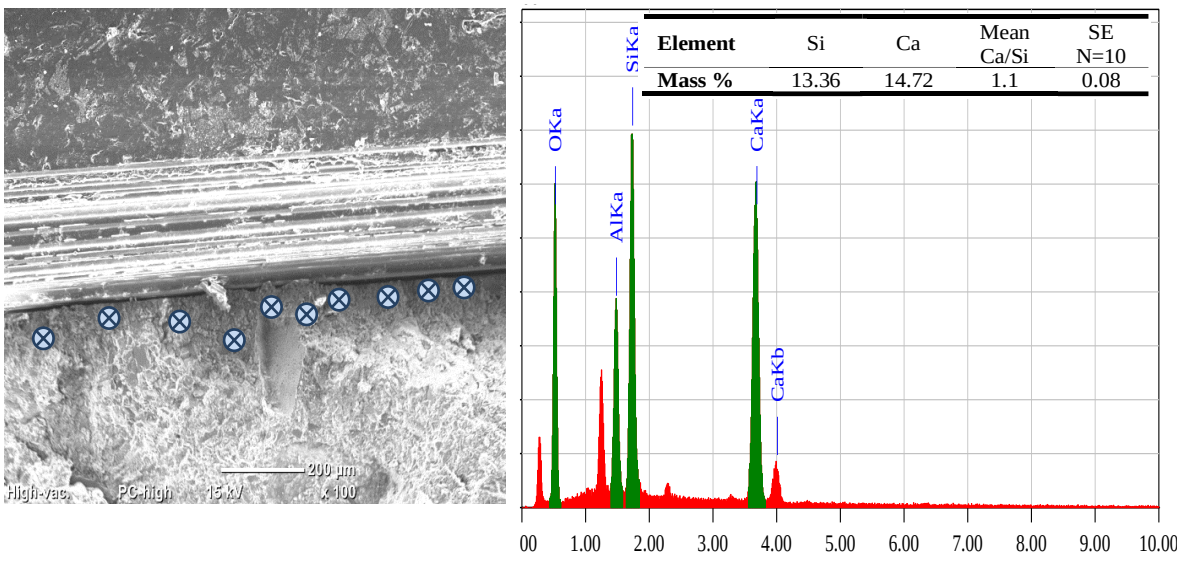

Figure 4. 10: Exemplar SEM micrograph and EDX spectrum of indicated points for samples extracted from mixture B4.5-NFC0-NS. (Note: SE is the standard error)

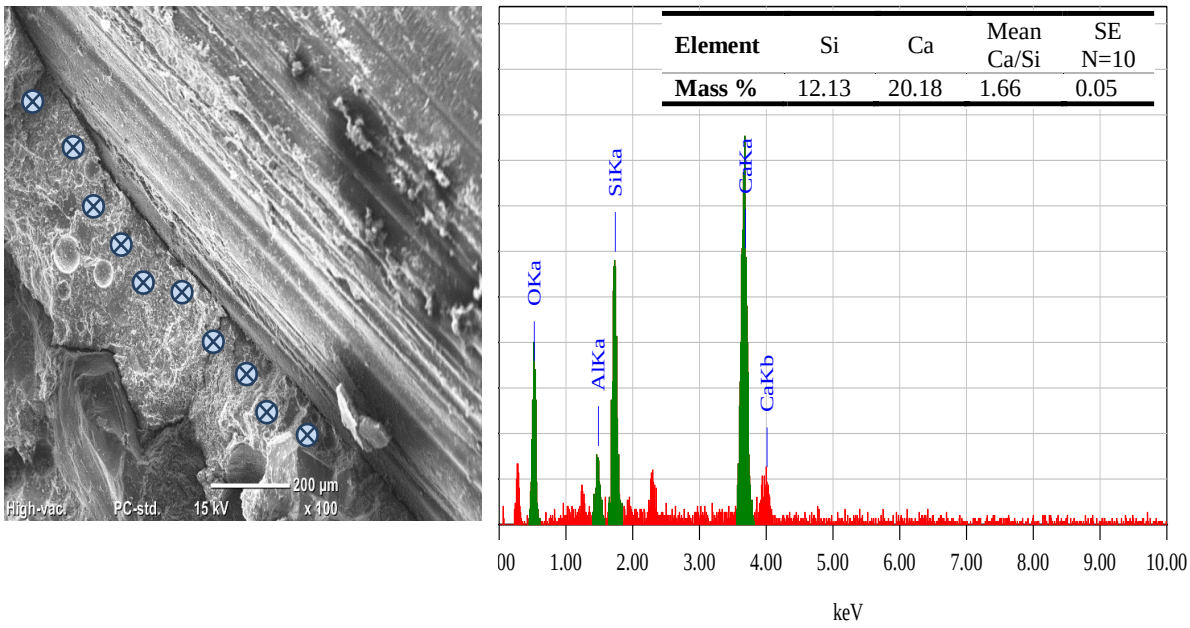

Figure 4. 11: Exemplar SEM micrograph and EDX spectrum of indicated points for samples extracted from mixture B4.5-NFC0-NC. (Note: SE is the standard error)

4.7 Numerical Optimization

Through numerical optimization, the generated models can be utilized to identify the mix design of cementitious composites that can be used for various construction applications. Accordingly, exemplar optimization scenarios were carried out considering the adopted parameters at the different levels in a manner to yield responses, which fulfill the target applications' performance criteria. Different goals, such as maximum, minimum, none, target, or within a certain range, were assigned to each response to achieve the intended use of the composite. Afterwards, the importance of each goal was graded on a scale of one to five reflecting the importance of each goal, with one being the least desired and five being the most important. Subsequently, a desirability function was calculated, which represents the best compromise that achieves a balance among all target goals through multi-objective optimization. The greatest desirability function was created by starting with 100 random points and proceeding forward to the sharpest slope until a maximum value

using statistical software [Design Expert], Due to the response surfaces' and their combinations' curvature, two or more maxima may be achieved. The desirability function has a range from 0 to 1, with 1 denoting the best possible outcome and 0 denoting that one or more responses are beyond the acceptable boundaries.

Two scenarios were developed, representing the use of composites as a viable option for repair/overlay applications in concrete pavements and bridge decks. For Scenario I, the criteria aimed to comply with the specifications of the COW-approved repair products list, which stipulates target 28 days compressive strength of 55 MPa, and durability factor of 95%. While for Scenario II, the criteria aimed to achieve a balance between the final setting time and 28 days strength, while maximizing the flexural and durability performance. The target criteria for the two scenarios adopted herein and their corresponding results are listed in **Table 4.5**. The obtained results showed desirability of 0.76 and 0.84 for Scenarios I and II, respectively.

The results of the optimization studies demonstrated that using the highest dosage of BFP (4.5%) was essential to obtaining the desired flexural performance for both scenarios. The other materials were adjusted to accommodate the performance requirements to fit each scenario. For Scenario, I, NS, NCC, and NFC were set at 3.75%, 0.0375%, and 0.375%, respectively, to reach a composite with a final setting time of 450 min and superior early and late compressive of 35 and 75 MPa, respectively, flexural toughness of 48.5 J and resistance to freezing-thawing with a durability factor of 95%. For Scenario II, only NCC and NFC were needed to reach a composite with optimized fresh properties (final setting time of 410 min), mechanical strength (28 days compressive strength of 74 MPa), and with emphasis on toughness reaching a value of 44 J and durability factor of 95%. It is worth noting that the optimized proportions would change

from the ones listed in **Table 4.5**, with the target performance criteria depending on the application defined by the user.

Table 4. 5: Selected criteria, goals, weights, and results of the numerical optimization

Criteria	Goal	Weight	Result
Scenario I			
NS (%)	Within range from 0 to 6%	-	3.75%
NCC (%)	Within range from 0 to 0.1%	-	0.0375%
NFC	Within range from 0 to 0.5%	-	0.375%
BFP	Within range from 0 to 4.5%	-	4.5%
Initial setting time	None	-	280 min
Final setting time	Minimize	3	450 min
f'_c 3d	In range 30 to 35 MPa	-	35 MPa
f'_c 28d	At least 55 MPa	5	75 MPa
Toughness	Maximize	5	48.5 J
Durability factor	At least 95%	5	95%
Scenario II			
NS (%)	Within range from 0 to 6%	-	0%
NCC (%)	Within range from 0 to 0.1%	-	0.1%
NFC	Within range from 0 to 0.5%	-	0.25%
BFP	Within range from 0 to 4.5%	-	4.5%
Initial setting time	2-4 h	-	240 min
Final setting time	4-8 h	-	410 min
f'_c 3d	None	-	35 MPa
f'_c 28d	At least 50 MPa	3	74 MPa
Toughness	Maximize	5	44 J
Durability factor	Maximize	5	95%

Note: Peak flexural strength surpassed 7 MPa for both scenarios

CHAPTER 5: RESULTS AND DISCUSSION OF PHASE II

5.1 Fresh Properties

Composites' fresh properties are represented in **Table 5.1**. All composites met the original target flow of 180±20 mm of the 100 mm base diameter of the test apparatus, which allowed for high consistency during casting, placement, compaction, and finishing. Flow values for composites remained over 100% of the mold's base diameter. This suggests that the materials are suitable for field deployment. Moreover, all mixtures maintained an adequate consistency for up to 60 minutes after mixing. For example, the average flow loss at 1 hour for all mixtures was 60% of the initial values, indicating sufficient placement times (typically 30 to 40 min) needed for quick batch repair operations in concrete pavement [e.g., Patel et al., 1993].

Depending on the binder used and the NFC doses employed, higher HRWRA dosages were needed for the nano-modified mixtures compared to standard concrete mixtures. This was attributed to NCC and NS's extremely large surface area, which increased the mixes' cohesion. Also, the angular structure of slag particles caused the constituents to interlock, which resulted in a harsher consistency (Neville, 2011), hence higher dosages of HRWRA were required to attain the desired flowability. Additionally, NFC altered the workability of mixtures as it is well known that adding fibers typically makes cementitious composites harder to work with due to the impacts of friction, interlocking, and clustering/balling effects (Mehta & Monteiro, 2014). In contrast, the stiffness of BFP used and the chosen dosage made mixing possible without any noticeable clustering or balling of the pellets. BFP was also used to substitute fine aggregate (0 to 600

μm), which has a larger specific surface than pellets, hence increasing the amount of free water available for lubricating and flowability of mixtures.

Air entrainment admixture was incorporated in the mixtures and fresh air content was recorded to ensure that the air content was set at 6%±1% in composites, which follows the recommended values indicated in the Canadian and American codes and guidelines for cement-based materials to resist freezing-thawing exposures (ACI 201.2R, 2016; CSA A23.1, 2019). The IST and FST results experienced an identical trend to that discussed in Phase I (Section 4.2). However, it is worth noting that the hardening rates reported here suggest the applicability of the composites for deployment in repair/overlay field applications. Indeed, the fresh properties of composites can be further altered by the use of accelerating or retarding admixtures to satisfy the specific needs of each project.

Table 5. 1: Summary of composites' fresh properties

Mixture ID	Flow (mm)					Air Content (%)	Setting time (min)	
	Time (min)							
	0	15	30	45	60		IST	FST
B4.5-NFC0.5-C	192	169	149	127	112	6.5	380	550
B4.5-NFC0.5-S	200	180	157	128	114	6.1	390	580
B4.5-NFC0-C	171	138	128	115	105	5.8	250	385
B4.5-NFC0-S	179	162	142	123	107	6.2	280	425
B4.5-NFC0.25-C	183	163	145	122	110	6.9	240	410
B4.5-NFC0.375-S3.75/C0.0375	185	168	148	121	112	6.4	280	450

5.2 Mechanical Properties

The average compressive strength at early- and late-ages as well as the flexural toughness at 28 days of the composites are presented in **Figs. 5.1 and 5.2**. According to Mehta & Monteiro (2014), blended binders that contain substantial volumes of slag (a latent hydraulic binder) often evolve slowly in terms of strength and microstructural development over time. The findings of this investigation demonstrated that all composites had high compressive strengths at early ages due to high binder content, low *w/b,* and employment of nanomaterials. The compressive strength of the nano-modified composites was between 31 and 38 MPa and 39 to 48 MPa after three and seven days, respectively. These early-age strength values satisfy the criteria for quick repairs and fast track overlays on concrete pavements and bridges, which requires a minimum strength of 15 to 25 MPa for early opening to traffic (e.g., CW3310 R17; Smith et al., 2014).

The addition of either NS, NCC, or a combination of both significantly increased the compressive strength of the composites with high-volume SCM at early ages (1, 3, and 7 days), conforming to the accelerated hardening rates discussed in the thermogravimetric analysis and microscopy section in Phase I (pozzolanic effect discussed in Section 4.6). Due to the extra surfaces that the ultrafine nature of NS provided for the early precipitation of the hydration products (nucleation effect), the hydration process of cement was ramped up (Kong et al., 2012). Additionally, agglomerates created by NS were reported to have a filling impact on the cementitious matrix [Oertel et al., 2013], which results in a densified microstructure. In addition, according to Kong et al., (2012), water can be absorbed in the highly present nano-pores of NS agglomerates, lowering the paste's *w/b* and resulting in a denser pore structure. Similarly, NCC offered additional nucleation surfaces for hydration

products to precipitate on, as well as the short circuit diffusion mechanism it provides led to a significantly higher improvement in the microstructure of the composites (Section 4.6).

The gain in strength was continued for composites at later ages (14 and 28 days) but at a lower rate. For instance, the average compressive strength of composites was within the range of 51 to 62 MPa at 14 days and 62 to 75 MPa at 28 days. These compressive strength ranges at later ages demonstrate the suitability of the composites for high-strength repair and overlay applications. For repair and overlay applications in concrete pavements and bridges, the compressive strength required is typically between 35 to 50 MPa after 28 days (e.g., ACI PRC-325.13-06; COW Tender 245-2020).

Moreover, as discussed in the flexural performance in Phase I (Section 4.4), BFP was the primary factor influencing the toughness of composites, hence all the mixtures employed the highest allowable dosage of BFP that enhanced the flexural toughness. For instance, the average toughness for all composites was within 42 to 49 J. This was attributed to the presence of a lot of pellets at the cracking planes, which restricted and bridged cracks, causing strain hardening and improving toughness beyond the first-cracking stage. Moreover, the microgrooves on the surface of the manufactured pellets were designed to infuse an interlocking effect between the matrix and the pellets by increasing the contact surface and providing host locations for the deposition of hydration products (**Fig. 5.3**). This consequently led to the BFP's high resistance to pullout, which is the primary toughening mechanism responsible for increasing the ductility of the composites.

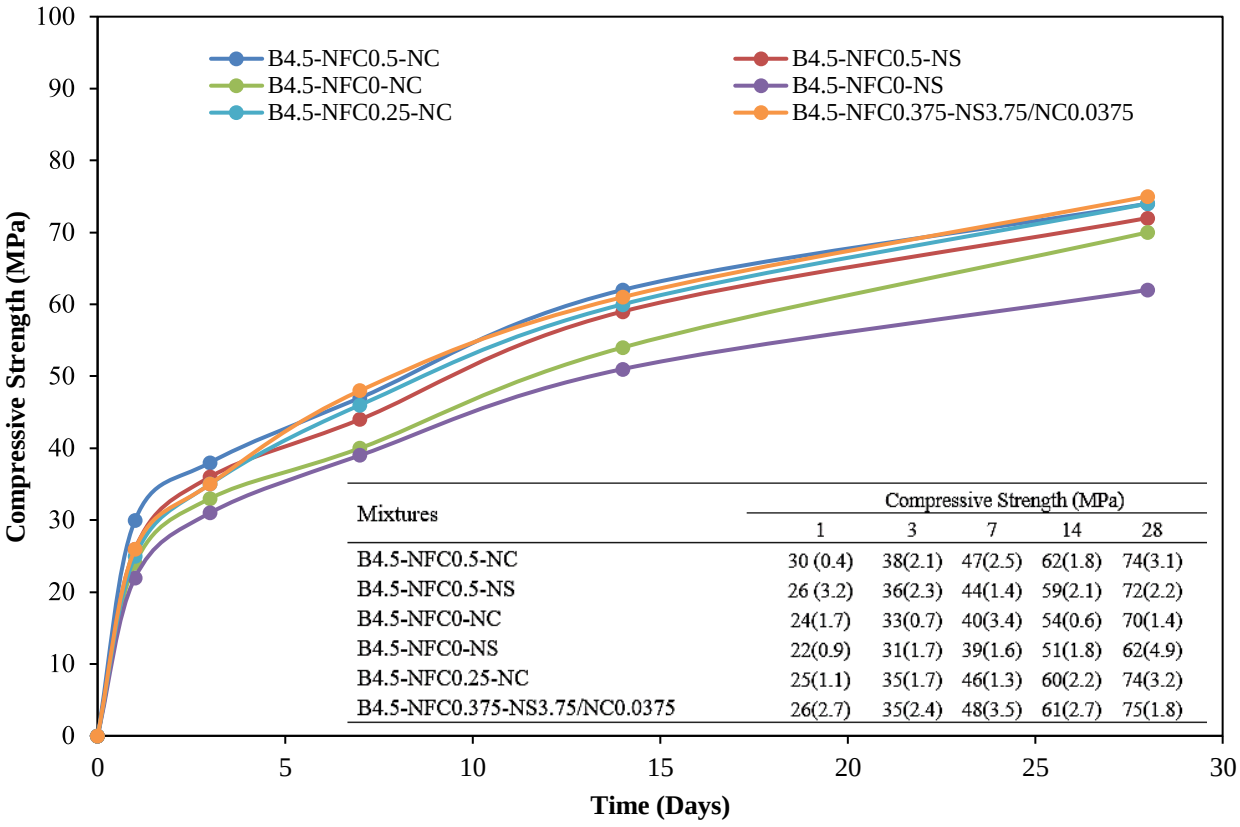

Mixtures	Compressive Strength (MPa)				
	1	3	7	14	28
B4.5-NFC0.5-NC	30 (0.4)	38(2.1)	47(2.5)	62(1.8)	74(3.1)
B4.5-NFC0.5-NS	26 (3.2)	36(2.3)	44(1.4)	59(2.1)	72(2.2)
B4.5-NFC0-NC	24(1.7)	33(0.7)	40(3.4)	54(0.6)	70(1.4)
B4.5-NFC0-NS	22(0.9)	31(1.7)	39(1.6)	51(1.8)	62(4.9)
B4.5-NFC0.25-NC	25(1.1)	35(1.7)	46(1.3)	60(2.2)	74(3.2)
B4.5-NFC0.375-NS3.75/NC0.0375	26(2.7)	35(2.4)	48(3.5)	61(2.7)	75(1.8)

Figure 5. 1: Compressive strength versus time. (Note: values in brackets represent the standard deviations)

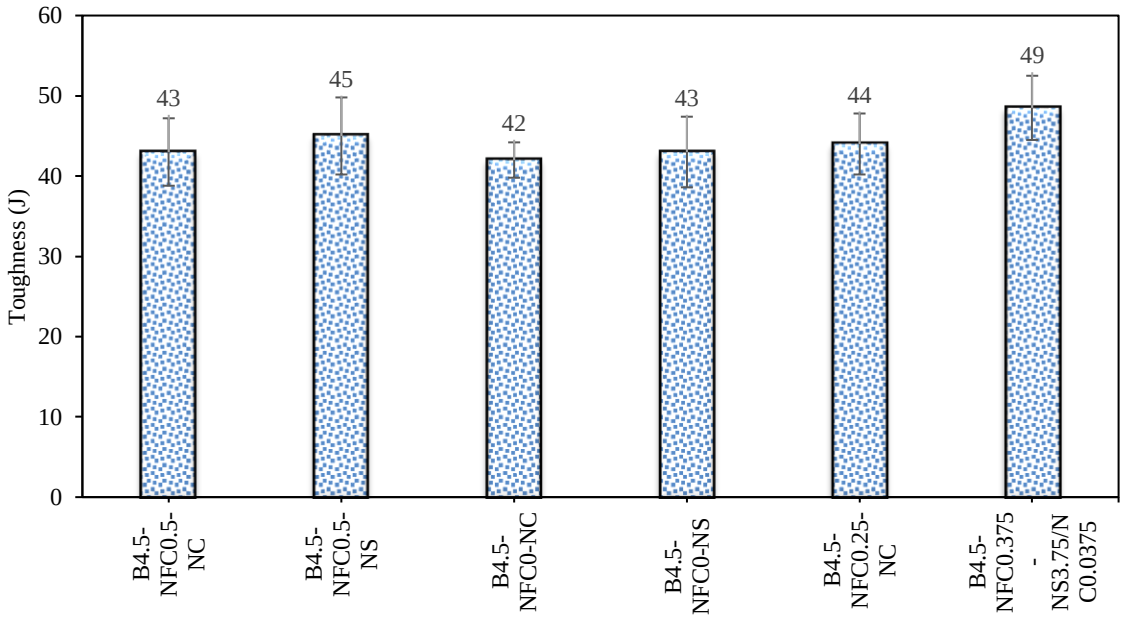

Figure 5. 2: Flexural toughness of the composites at 28 days. (Note: error bars represent standard deviation)

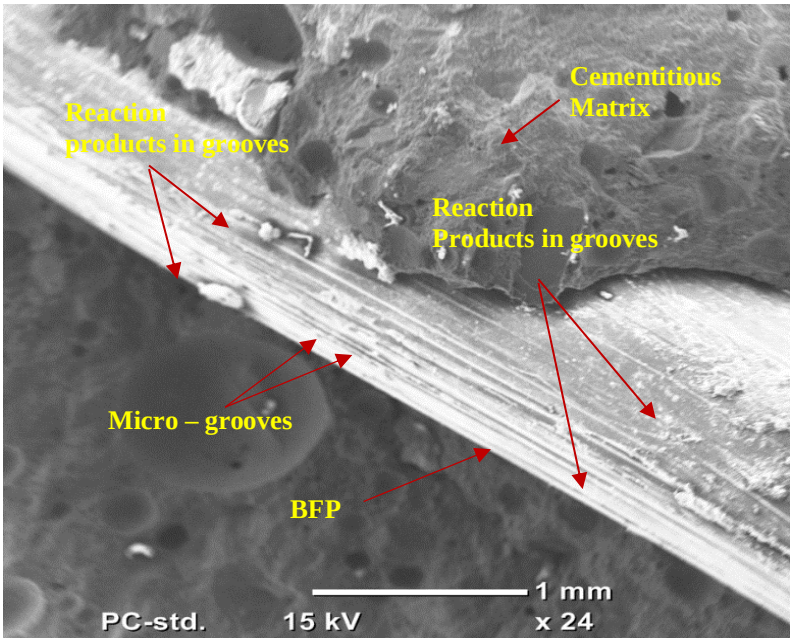

Figure 5. 3: Exemplar SEM micrograph of matrix showing deposition of reaction products in BFP microgrooves.

Due to the high ductility of the composites, it may be possible to withstand differential movement brought on by impact loading, structural/thermal stresses, and shrinkage. Thus, they could allow for thin overlays and/or longer junctions of joint spacing. This demonstrates the suitability of the composites for use as high-performance overlay for critical applications such as bridge decks and road joints.

5.3 Fluid Transport Properties

The fluid transport properties were assessed by performing the RCPT test, followed by the physical chloride penetration depth test. Results of both tests are shown in **Fig. 5.4**. All composites had passing charges less than 1000 coulombs at 28 days, classifying their penetrability as ‘very low’, as stipulated by ASTM C1202-22, (2022) categorizing table. This can be ascribed to the dense microstructure of the cementitious matrix due to high

binder content and low *w/b*. The physical chloride penetration depth, which ranged between 4.3 and 9.1 mm, confirmed the trends found in RCPT results.

The type of nanomaterials added influenced the test result of composites at different degrees. Composites incorporating NS had lower penetrability values. Several studies showed that micro-silica affects the ionic concentration of the pore solution, and reduces the free alkalis content, owing to binding free ions into cement gel (Dean et al., 2006; Shi, 2004). Therefore, when NS is present, it reduced passing charges, partially due to the decreased ionic concentration in the pore solution, i.e., decreased conductivity. Hence, the RCPT passing charge indication has been criticized for showing a substantial preference for pozzolanic additives (Streicher & Alexander, 1995). Generally, all composites had a very low penetrability, which proves the enhanced densification process in microstructure of composites incorporating NFC, NCC, and/or NS. Complying with the findings of the mechanical performance and TGA results. This can be attributed to the short circuit diffusion mechanism of NCC, NFC and the pozzolanic/filler effects of NS, which markedly enhanced the composites' microstructural characteristics as well as the discontinuity of the pore structure including BFP interfacial transitional zones. Hence, resulting in higher resistance to infiltration of fluids.

Low penetrability is required by several guidelines and specifications for repair/overlay systems in concrete pavements and bridges to decrease moisture infiltration into the cementitious matrix and increase the material's durability against damage mechanisms such as de-icing salt and frost action. For concrete construction applications at ages later than 28 days, the proposed maximum passing charges in accordance with ASTM C1202 are fewer than 1500/1000 coulombs (COW Tender 245-

2020; Smith et al., 2014), which makes all the composites herein a robust option for concrete repair works.

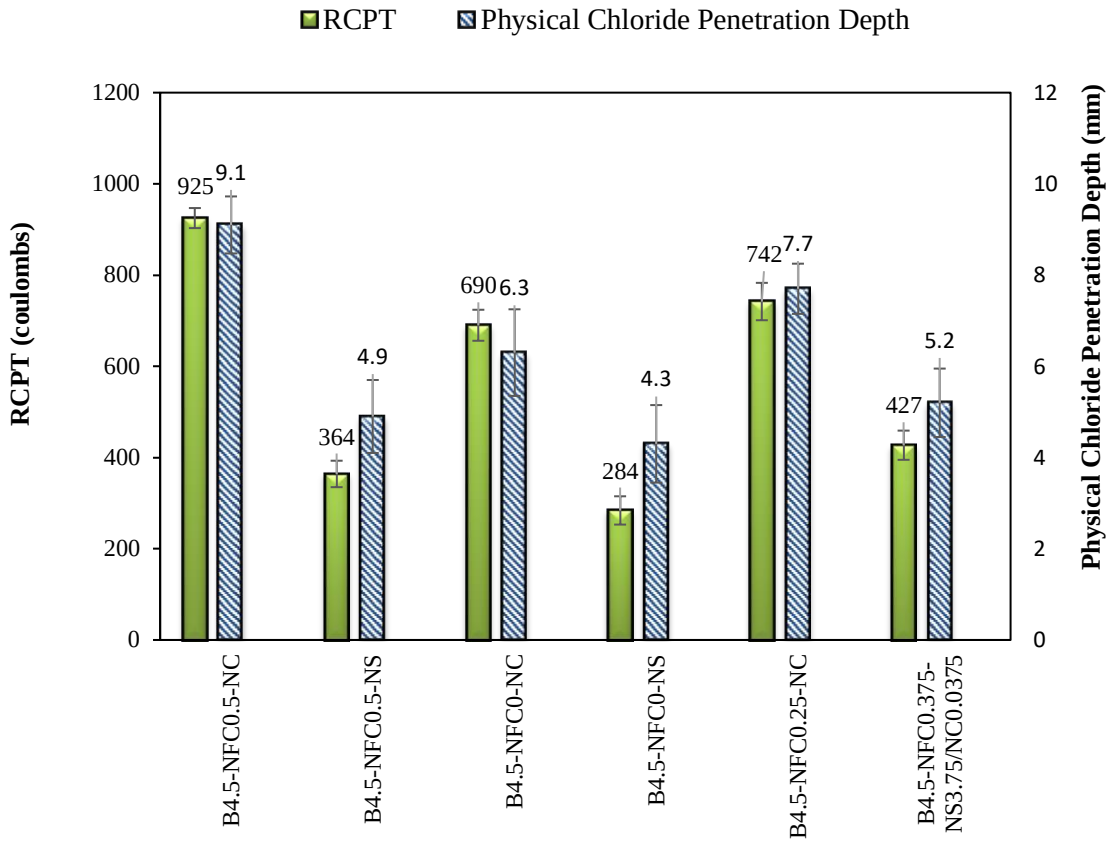

Figure 5. 4: Fluid transport properties evaluated according to RCPT and physical chloride penetration depth.

5.4 Salt Frost Scaling

Figures 5.5 and 5.6, respectively, depict the surface condition and mass loss of the specimens as a result of simultaneous exposure to salt solution and frost action. The Ministry of Transportation of Ontario (MTO LS-412 1997) and Bureau du normalization du Québec (BNQ NQ 2621-900 2002) specify that the salt-frost scaling tests should be limited to a mass loss of 500 and 800 g/m^2, respectively, but both jurisdictions employ a solution of 3% sodium chloride, which is a less aggressive solution compared to the one used in this study.

Generally, all mixtures showed acceptable performance with a total mass loss in the range of 8.2 to 27.6 g/m^2 and the visual rating was 0 for all mixtures. This can be attributed to the mix design parameters (high binder content, low *w/b*, and dosages of nanomaterials employed) selected, which led to sufficient microstructural development after 28 days of moist curing, and very low penetrability as discussed in Section 5.3.

Incorporating nanomaterials (NCC or NS) in binary binder mixtures led to the noticeable low surface scaling and mass loss of composites. Mixtures B4.5-NFC0.375-NS3.75/NC0.0375 and B4.5-NFC0.25-NC had the lowest scaled mass of 8.2 and 12.2 g/m^2, respectively. This enhanced resistance to salt-frost scaling conforming to the low fluid penetration values obtained from RCPT results, which can be ascribed to the nanomaterials pore blocking action as well as the refined pore structure, which discounted the ingress of salt solution into the concrete surface, and in turn its vulnerability to critical saturation. This was confirmed by the greater degree of hydration and pozzolanic reactivity of nano-modified binders within 28 days shown in Section 4.3. The resistance of nano-modified composites to stresses brought on by hydraulic and osmotic pressures resulting from frost action (Karagöl et al. 2015; Prado et al. 1998; Powers & Helmuth, 1953) was also augmented by the high flexural toughness, due to the existence of BFP.

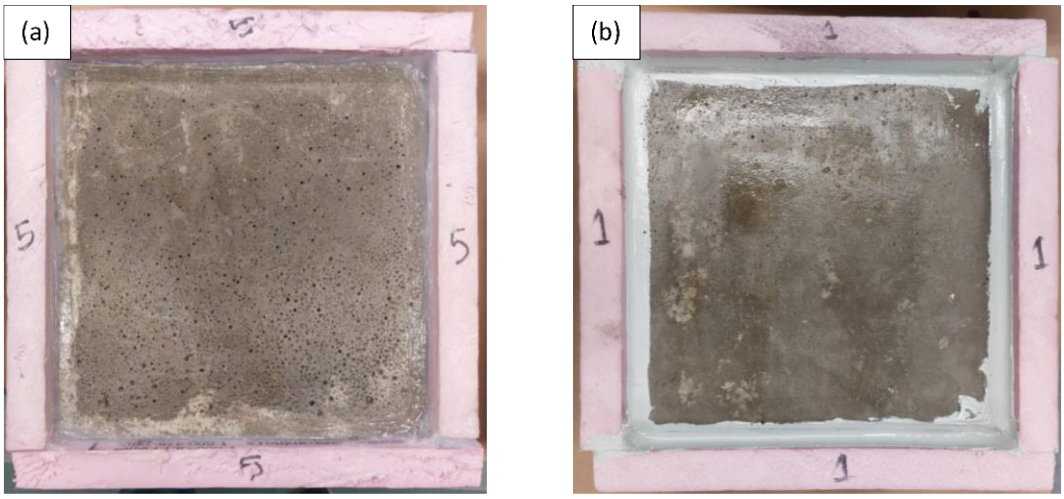

Figure 5. 5: Exemplar surface condition of frost surface scaling test specimens after exposure: (a) B4.5-NFC0-NS, and (b) B4.5-NFC0-NC.

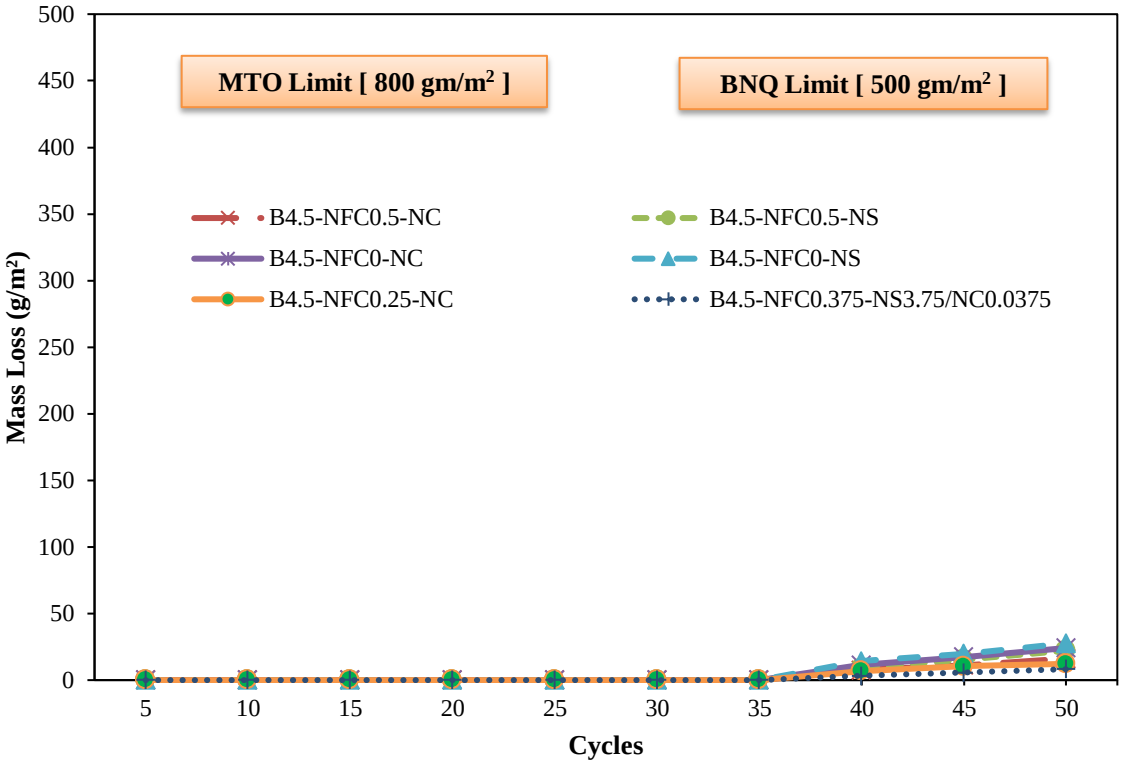

Figure 5. 6: Cumulative mass loss of slabs under salt-frost scaling.

5.5 Compatibility with Parent Concrete

5.5.1 Restrained Shrinkage

The results of the restrained shrinkage test are listed in **Table 5.2**, where cumulative restrained shrinkage of the composites up to 180 days was measured under an aggressive exposure in a hot/dry condition for 152 days after 28 days in conventional curing conditions. This test was performed to account for any surface cracking and de-bonding at the interface that can result from significant differential deformations between the repair/overlay layer and the substrate concrete (ACI PRC 546R-14, 2014; ACI PRC-325.13-06, 2020). In contrast to the rigorous drying conditions used herein, it is plausible that alternative field conditions, such as frequent increases in RH, precipitation, and/or temperature drops, can partially reverse or lessen the total shrinkage of composites. In order to predict performance concerns or restrictions that might exist with composites in the field, this exposure scenario was chosen.

At early and late-ages the cumulative shrinkage values were influenced by the type of nanomaterials employed. Mixtures incorporating NCC generally yielded slightly lower shrinkage rates than their counterpart mixtures incorporating NS. For instance, mixtures B4.5-NFC0-NC and B4.5-NFC0-NS had a restrained shrinkage value of 187 and 199 micro-strain, respectively at 28 days. This trend was sustained for all ages, which can be ascribed to the boosting effect of both NCC and NS on the hydration of the slag-based composites. It is worth noting that composite B4.5-NFC0.375-NS3.75/NC0.0375 had the lowest restrained shrinkage values at all ages due to the amalgamated effects of NCC and NS to achieve a higher reactivity binder particularly with the coexistence of NFC, as explained earlier.

The presence of BFP had an impact on the shrinkage behavior of the composites regardless of the type of nanomaterial(s) employed. As discussed in the flexural toughness section earlier, the chosen BFP dose was in charge of limiting the composites' shrinkage by bridging micro-cracks present in specimens, which resulted in low shrinkage values (**Table 5.2**) without any evidence of surface cracking. This demonstrated how BFP helped prevent the composites from shrinking in relation to the parent concrete, hence preventing the possibility of early-age surface cracking that would jeopardize the integrity of the repair/overlay system. The harsh drying conditions for 152 days, resulted in the amplification of shrinkage values. However, due to the restraining effect of BFP, no cracks were found on the specimens after this drying regime (**Fig. 5.7**).

Table 5. 2: Cumulative restrained shrinkage test results

Mixtures	**Shrinkage (micro-strain)**							
	Time (days)							
	1	**3**	**7**	**14**	**28**	**56**	**90**	**180**
B4.5-NFC0.5-NC	61	78	144	154	169	200	302	370
B4.5-NFC0.5-NS	65	82	152	163	179	212	320	392
B4.5-NFC0-NC	68	93	159	170	187	221	334	409
B4.5-NFC0-NS	72	98	169	181	199	235	355	435
B4.5-NFC0.25-NC	50	59	118	127	139	165	249	305
B4.5-NFC0.375-NS3.75/NC0.0375	43	50	101	109	119	141	213	261

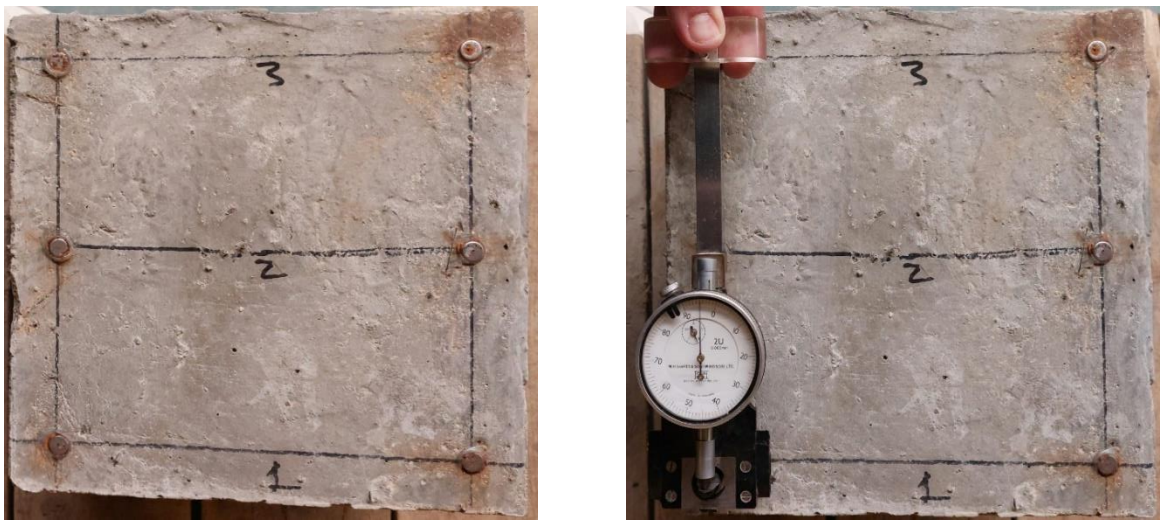

Figure 5. 7: Exemplar surface condition of restrained shrinkage specimen with demic points for mixture B4.5-NFC0.5-NC.

5.5.2 Pull-Off (Bonding Capability)

The bond strength between the repair/overlay material and parent concrete is one of the most important criteria in repair/overlay applications. The employment of different materials may result in compatibility failure at the interface as a result of distinct qualities, such as modulus of elasticity, thermal, and elastic mismatch (Li et al. 1999). Hence, the bond strength between the proposed repair/overlay composites and parent concrete was evaluated by means of a direct tension test (pull-off test) to mimic the worst-case loading configuration that may occur in the field. **Figure 5.8** demonstrates the bond strength values of composites.

Irrespective of the nanomaterials or NFC dosage employed, all composites had a close range of 1.06 to 1.57 MPa bond strength, and the pull-off failure location was captured at the substrate layer, where the assembly failed at the specimen's weakest region (10 to 20 mm below the interface). Therefore, the bond strength herein reflected the tensile strength of the substrate layer (identical mix design) in the test assembly, which

explains the narrow ranged results obtained for this test. Indeed, the applied curing regime adopted in this study led to the microstructural growth of mixtures due to high degree of maturity. It also demonstrated that BFP didn't have any preferential plastic sedimentation in the interface region, otherwise it would have resulted in failure at the interface, which demonstrates the effective compatibility between the repair/overlay layer and substrate concrete, as well as the robust integrity of the suggested composite to be employed as a repair/overlay option.

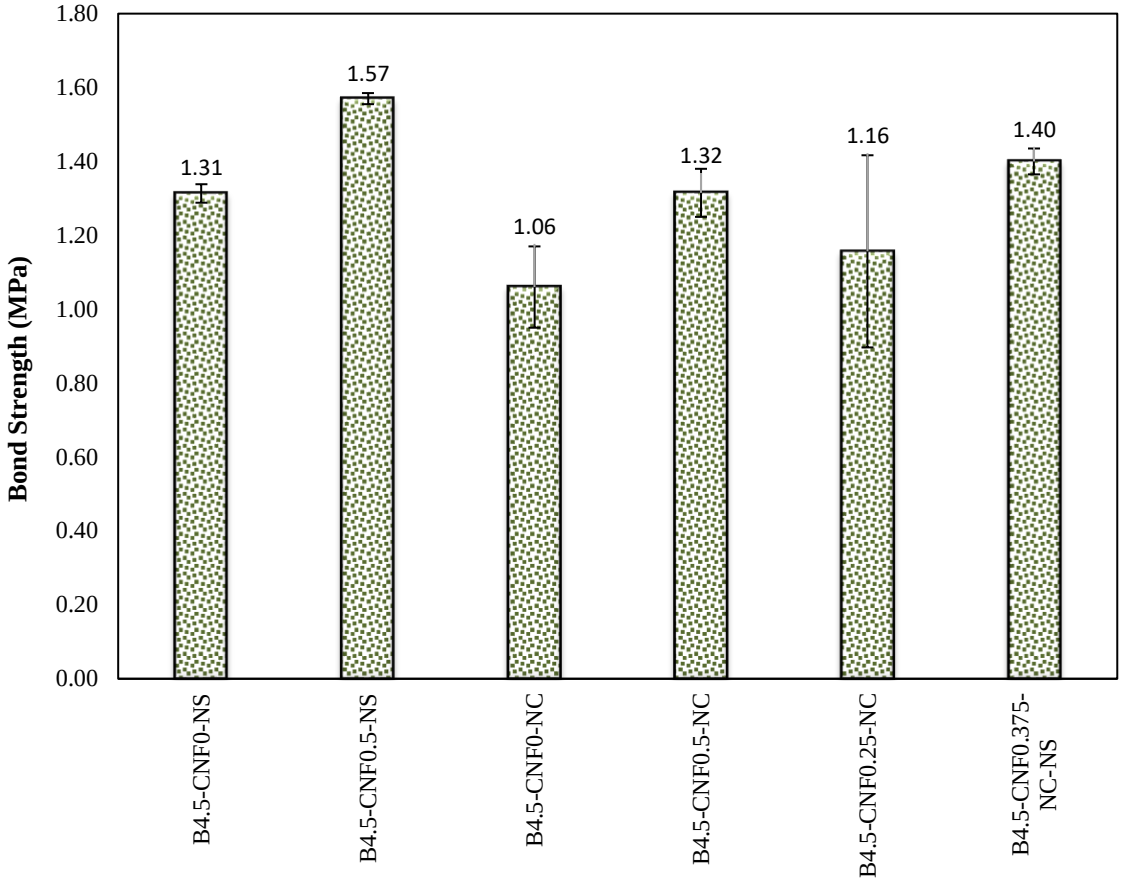

Figure 5. 8: Bond strength results from pull-off test.

CHAPTER 6: SUMMARY, CONCLUSIONS, AND RECOMMENDATIONS

6.1 Summary

This study responds to the need for improving the overall performance of concrete infrastructure to achieve longer service life, fewer cycles of repair, and reduced life-cycle costs. Novel high-performance fiber-reinforced cementitious composites were developed, which comprised high content (50%) slag by mass of the base binder as well as nano-silica (NS) or nano-crystalline cellulose (NCC). In addition, nano-fibrillated cellulose (NFC), and a novel form of basalt fiber strands protected by polymeric resins: basalt fiber pellets (BFP), representing nano-/micro- and macro-fibers, respectively were incorporated in the composites.

In Phase I, 15 mixtures were cast, and the mixtures' performance was assessed based on fresh properties (air content and setting time), hardened properties (compressive strength and flexural behavior (pre-and post-cracking at 28 days), as well as durability (absorption, freezing/thawing resistance), which were augmented by thermogravimetry and microscopy analyses. Moreover, a statistical model was established from the experimental program to evaluate the effect of the parameters used herein on the chosen responses.

Three parameters adopted in the developed models were: nano-particles type (NCC/NS), nano-fibrillated cellulose (NFC) dosage, and basalt fiber pellets (BFP) dosage. The Response Surface Method (RSM), based on Face-Centered Composite Design (FCCD) was used to evaluate the influence of mixture design parameters on the performance of

composites. Hence, the independent responses modeled were: initial (IST) and final (FST) setting times, 7 and 28 days compressive strengths, flexural toughness, and resistance to freezing and thawing cycles (durability factor) which represent the composites' fresh, hardened and durability properties. After yielding the relationship between the parameters and responses of the model, numerical optimization exercises were conducted to deduce the optimum mix-design for repair/overlay applications of concrete flatwork.

In Phase II, four selected HPFRCC mixtures, as well as the two optimized mixtures derived from the optimization scenarios were extracted from Phase I to investigate their potential to be used as a repair/overlay option for concrete flatwork. These composites were evaluated in an integrated manner to ensure the suitability of selected mixtures to be used in the field. Hence, the composites were assessed based on fresh properties (air content, mortar flow/flow-retention, and setting time), hardened properties (compressive strength and flexural toughness at 28 days), fluid transport properties (RCPT), durability (salt-frost scaling) and compatibility (restrained shrinkage and pull-off) with substrate concrete.

6.2 Conclusions

6.2.1 Slag-based cementitious composites incorporating nano-silica, nano-cellulose material, and basalt pellets (Phase I)

- The statistical models generated showed high reliability due to their strong dependency on data from the experimental work. Therefore, they can serve as a tool for predicting responses, enhancing efficiency by tracking changes in any of the factors selected, and defining the characteristics of nano-modified cementitious composites.

- Incorporating nanomaterials (NCC/NS) in the binder enhanced the properties of composites which led to an overall shortening of setting times, increased mechanical properties, densification of the matrix, and resistance to frost action.
- NCC and/or NFC incorporation in mixtures improved the hydration process in the matrix and attained a higher degree of maturity. This was reflected by the high early-strength (above 30 MPa at 3 days) of these mixtures in spite of the high content of slag (latent hydraulic binder).
- NCC/NFC amalgamation resulted in superior hardened and durability traits of composites, due to the presence of superficial hydroxyl groups that can attract calcium ions, causing cellulose to adhere to cement and slag particles and creating a network to diffuse water retained by NCC/NFC into the unhydrated core of particles.
- Increasing the dosage of BFP demonstrated its significance in improving the post-cracking flexural behavior of composites, imposing a strain-hardening effect when incorporated at a dosage of 4.5% (by volume of composite).
- SEM highlighted the optimum design of the micro-grooved BFP, which allowed for the deposition of hydration/pozzolanic products in the grooves resulting in a superior bond between the matrix and BFP.
- In addition to the particle packing and physical filling effects of NS, thermogravimetric analysis showed the role of NS in densifying the microstructure of composites, owing to the rapid pozzolanic activity to produce secondary and stiff C-S-H gel in the matrix, which conformed to the high strength results at 3 (38 Pa) and 28 (78 MPa) days.

- Based on the results in this phase, the incorporation of (up to 3.75%) NS and (0.0375–0.1) NCC in slag-based composites, with (0.25–0.375) NFC and (4.5%) BFP, obtained balanced fresh, mechanical, and durability properties. Hence, these sets of nano-modified composites can present an option for specialty concrete applications.

6.2.2 Nano-modified slag-based cementitious composites reinforced with multi-scale fiber systems as a repair/overlay option (Phase II)

- Based on the result from Phase I, six HPFRCC were chosen for repair testing, including two mixtures obtained from the numerical optimization exercise performed in that phase.
- The selected mixtures demonstrated adequate fresh properties that are compatible with products used by different jurisdictions in field applications. This was reflected by the results of setting times and flow retention tests.
- All the selected mixtures experienced high mechanical properties, conforming to the early, and late-age compressive strength, and flexural toughness of many jurisdictions, which yielded results up to 38 MPa, 75 MPa, and 49 J, respectively.
- Composites showed high durability traits in resisting moisture infiltration with penetrability values less than 1000 coulombs (very low penetrability class in RCPT), making the proposed mixtures a robust repair/overlay option.
- The synergistic effects of NCC, NFC and NS markedly enhanced the discontinuity of the pore structure, hence resulting in high mechanical, and durability properties.

- The resistance of nano-modified composites to stresses brought on by hydraulic and osmotic pressures, as well as the pore blocking effects of nanomaterials resulted in the resistance of composites to salt-frost action, which was demonstrated in the very low mass loss (below 30 gm) and visual rating values (Zero rating) of specimens.
- High compatibility features were observed between the proposed repair materials and the substrate. This is attributed to the presence of BFP, which controls and bridges cracks. Therefore, the restrained shrinkage test yielded low cumulative shrinkage results between 261 and 435 micro-strain with no presence of cracks on the surface of specimens at the end of the test. Moreover, the pull-off failure location for all composites was captured at the substrate layer, which indicated that all mixtures had a high bond strength with the parent concrete.
- Overall, the outcomes of this phase demonstrate the reliability of the proposed mixtures, especially B4.5-NFC0.375-NS3.75/NC0.0375, to be employed as a repair/overlay option for a suite of infrastructural repair applications due to its high fresh, mechanical, durability, and compatibility properties.

6.3 Recommendations for Future Research

- Different mixtures developed in the current thesis present a viable option for a suite of repair/overlay applications. However, a life-cycle cost analysis should be conducted in the future, as well as a comparative study to evaluate their economics relative to other repair products, commercially available.

- The potential for using NFC/NCC at low temperatures should be explored as it would extend repair and maintenance seasons, if successful.
- The proposed composites should be studied under different physical and chemical exposures to explore their stability under severe conditions.
- Conducting field trials to assess the performance of the composites in an uncontrolled environment is necessary for the acceptance of these composites by the industry.

REFERENCES

Abtahi, S. M., Sheikhzadeh, M., & Hejazi, S. M. (2010). Fiber-reinforced asphalt-concrete – A review. *Construction and Building Materials*, *24*(6), 871–877. https://doi.org/10.1016/j.conbuildmat.2009.11.009

ACI 201.2R. (2016). 201.2R-16 Guide to Durable Concrete. *Technical Documents*.

ACI, 2020. Concrete Overlays for Pavement Rehabilitation (Reapproved 2020). ACI PRC-325.13-06, American Concrete Institute, Farmington Hills, Michigan, USA, 39 p.

ACI, 2014. Concrete Repair Guide. ACI PRC-546R-14, American Concrete Institute, Farmington Hills, Michigan, USA, 70 p.

Akhlaghi, M. A., Bagherpour, R., & Kalhori, H. (2020). Application of bacterial nanocellulose fibers as reinforcement in cement composites. *Construction and Building Materials*, *241*, 118061. https://doi.org/10.1016/j.conbuildmat.2020.118061

Al-alaily, H. S., & Hassan, A. A. A. (2016). Refined statistical modeling for chloride permeability and strength of concrete containing metakaolin. *Construction and Building Materials*, *114*, 564–579. https://doi.org/10.1016/j.conbuildmat.2016.03.187

Al-Saleh, S. A. (2015). Analysis of total chloride content in concrete. *Case Studies in Construction Materials*, *3*, 78–82. https://doi.org/10.1016/j.cscm.2015.06.001

Angst, U., Elsener, B., Larsen, C. K., & Vennesland, Ø. (2009). Critical chloride content in reinforced concrete — A review. *Cement and Concrete Research*, *39*(12), 1122–1138. https://doi.org/10.1016/j.cemconres.2009.08.006

Ardanuy, M., Claramunt, J., & Toledo Filho, R. D. (2015). Cellulosic fiber reinforced cement-based composites: A review of recent research. *Construction and Building Materials*, *79*, 115–128. https://doi.org/10.1016/j.conbuildmat.2015.01.035

Ardanuy, M., Clarmunt, J., & Toledo Filho, R. D. (2012). Evaluation of durability to wet/dry cycling of cement mortar composites reinforced with nanofibrillated cellulose. In *Brittle Matrix Composites 10* (pp. 33–41). Elsevier. https://doi.org/10.1533/9780857099891.33

ASTM C39/C39M. (2018). Standard Test Method for Compressive Strength of Cylindrical Concrete Specimens. In *ASTM International*.

ASTM C128. (2014). Standard Test Method for Relative Density (Specific Gravity) and Absorption of Fine Aggregate 1. In *ASTM International*. ASTM International. https://doi.org/10.1520/C0128-15

ASTM C136/136M. (2014). Standard Test Method for Sieve Analysis of Fine and Coarse Aggregates. In *ASTM International*. https://doi.org/10.1520/C0136_C0136M-19

ASTM C230/C230M. (2014). Standard Specification for Flow Table for Use in Tests of Hydraulic Cement. In *ASTM International*. ASTM International.

ASTM C260. (2010). Standard Specification for Air-Entraining Admixtures for Concrete. In *ASTM International*. https://doi.org/10.1520/C0260_C0260M-10AR16

ASTM C403/C403M. (2016). Standard Test Method for Time of Setting of Concrete Mixtures by Penetration Resistance. In *ASTM International*.

ASTM C494/C494M. (2017). Standard Specification for Chemical Admixtures for Concrete. In *ASTM International*. https://doi.org/10.1520/C0494_C0494M-19

ASTM C597. (2016). Standard Test Method for Pulse Velocity Through Concrete1. In *ASTM International*. ASTM International. https://doi.org/10.1520/C0597-16

ASTM C666/C666M. (2015). Standard Test Method for Resistance of Concrete to Rapid Freezing and Thawing. In *ASTM International*. ASTM International. https://doi.org/10.1520/C0666_C0666M-15

ASTM, 2012. Standard Test Method for Scaling Resistance of Concrete Surfaces Exposed to Deicing Chemicals. ASTM C672/ C672M -12, American Society for Testing and Materials, West Conshohocken, PA, USA.

ASTM C1202-22. (2022). Standard Test Method for Electrical Indication of Concrete's Ability to Resist Chloride Ion Penetration. In *ASTM International*. https://doi.org/10.1520/C1202-22

ASTM C1609/C1609M. (2012). Standard Test Method for Flexural Performance of Fiber-Reinforced Concrete (Using Beam With Third-Point Loading). In *ASTM International*.

Azzam, A., Bassuoni, M. T., & Shalaby, A. (2019a). Properties of High-Volume Fly Ash and Slag Cementitious Composites Incorporating Nano-silica and Basalt Fiber Pellets. *Advances in Civil Engineering Materials*, *8*(3), 20190018. https://doi.org/10.1520/ACEM20190018

Azzam, A., Bassuoni, M. T., & Shalaby, A. (2021). Nanomodified Cementitious Composites Incorporating Basalt Fiber Pellets under Tensile and Impact Loads. *Journal of Materials in Civil Engineering*, *33*(10), 4021260. https://doi.org/10.1061/(ASCE)MT.1943-5533.0003913

Azzam, A., Bassuoni, M. T. and Shalaby, A. (Nov. 2022) "Durability of Nano-modified Cementitious Composites Reinforced with Basalt Fiber Pellets to Alkaline and Salt-Frost Exposures" Cement and Concrete Composites, V. 134, 104761, 17 p.

Bakharev, T., Sanjayan, J. G., & Cheng, Y.-B. (2001). Resistance of alkali-activated slag concrete to alkali–aggregate reaction. *Cement and Concrete Research*, *31*(2), 331–334. https://doi.org/10.1016/S0008-8846(00)00483-X

Bakkari, M. el, Bindiganavile, V., Goncalves, J., & Boluk, Y. (2019). Preparation of cellulose nanofibers by TEMPO-oxidation of bleached chemi-thermomechanical pulp for cement applications. *Carbohydrate Polymers*, *203*, 238–245. https://doi.org/10.1016/j.carbpol.2018.09.036

Balagopal, V., Panicker, A. S., Arathy, M. S., Sandeep, S., & Pillai, S. K. (2022). Influence of fibers on the mechanical properties of cementitious composites - a review. *Materials Today: Proceedings*, *65*, 1846–1850. https://doi.org/10.1016/j.matpr.2022.05.023

Balea, A., Fuente, E., Blanco, A., & Negro, C. (2019a). Nanocelluloses: Natural-Based Materials for Fiber-Reinforced Cement Composites. A Critical Review. *Polymers*, *11*(3), 518. https://doi.org/10.3390/polym11030518

Barnat-Hunek, D., Szymańska-Chargot, M., Jarosz-Hadam, M., & Łagód, G. (2019). Effect of cellulose nanofibrils and nanocrystals on physical properties of concrete. *Construction and Building Materials*, *223*, 1–11. https://doi.org/10.1016/j.conbuildmat.2019.06.145

Bedwiy, A. G., Bassuoni, M. T., and El-Salakawy, E. (Oct. 2021) "Residual Mechanical Properties of BPRCC under Cyclic Environmental Conditions," Journal of Materials in Civil Engineering, ASCE, V. 33, No. 4, 04021290: 10 p.

Bentz., D. P., Sato, T., de la Varga, I. and Weiss, J. W. (2012) “Fine Limestone Additions to Regulate Setting in High Volume Fly Ash Mixtures,” Cement and Concrete Composites, V. 34, No. 1, pp. 11-17.

BNQ NQ 2621-900, 2002. Determination of the scaling resistance of concrete surfaces exposed to freezing-and-thawing cycles in the presence of de-icing chemicals. Bureau de Normalisation du Québec, Annexe A, Québec, Canada.

Branston, J., Das, S., Kenno, S. Y., & Taylor, C. (2016). Influence of basalt fibres on free and restrained plastic shrinkage. *Cement and Concrete Composites*, *74*, 182–190. https://doi.org/10.1016/j.cemconcomp.2016.10.004

Canadian Standard Association. (2019). Canadian Highway Bridge design code CAN/CSA-S6. In *CSA, 2019. Canadian Highway Bridge design code. CAN/CSA-S6, Canadian Standard Association, Mississauga, Ontario, Canada.* (Vol. 19). CSA.

Canadian Standards Association. (2013). Cementitious Materials for Use in Concrete CAN/CSA-A3001. In *Canadian Standards Association*. Canadian Standards Association.

Canadian Standards Association. (2019). CAN/CSA A231.1. In *Canadian Standards Association*. CSA group.

Canadian Standards Association. (2019). Determination of Bond Strength of Bonded Toppings and Overlays and of Direct Tensile Strength of Concrete, Mortar, and Grout. CSA A23.2-6B, Canadian Standards Association, Mississauga, ON, Canada.

Cao, Y., Gehlen, C., Angst, U., Wang, L., Wang, Z., & Yao, Y. (2019). Critical chloride content in reinforced concrete — An updated review considering Chinese experience. *Cement and Concrete Research*, *117*, 58–68. https://doi.org/10.1016/j.cemconres.2018.11.020

Cao, Y., Zavaterri, P., Youngblood, J., Moon, R., & Weiss, J. (2015). The influence of cellulose nanocrystal additions on the performance of cement paste. *Cement and Concrete Composites*, *56*, 73–83. https://doi.org/10.1016/j.cemconcomp.2014.11.008

Cao, Y., Zavattieri, P., Youngblood, J., Moon, R., & Weiss, J. (2016a). The relationship between cellulose nanocrystal dispersion and strength. *Construction and Building Materials*, *119*, 71–79. https://doi.org/10.1016/j.conbuildmat.2016.03.077

Castellano, C. C., Bonavetti, V. L., Donza, H. A., & Irassar, E. F. (2016). The effect of w/b and temperature on the hydration and strength of blastfurnace slag cements. *Construction and Building Materials*, *111*, 679–688. https://doi.org/10.1016/j.conbuildmat.2015.11.001

Claramunt, J., Ardanuy, M., & Fernandez-Carrasco, L. J. (2015). Wet/Dry Cycling Durability of Cement Mortar Composites Reinforced with Micro- and Nanoscale Cellulose Pulps. *BioResources*, *10*(2). https://doi.org/10.15376/biores.10.2.3045-3055

Claramunt, J., Ventura, H., Toledo Filho, R. D., & Ardanuy, M. (2019). Effect of nanocelluloses on the microstructure and mechanical performance of CAC cementitious matrices. *Cement and Concrete Research*, *119*, 64–76. https://doi.org/10.1016/j.cemconres.2019.02.006

CW, 2015. Portland Cement Concrete Pavement Works. CW3310-R17, City of Winnipeg Specification, Winnipeg, Manitoba, Canada.

Da Costa Correia, V., Santos, S. F., Soares Teixeira, R., & Savastano Junior, H. (2018). Nanofibrillated cellulose and cellulosic pulp for reinforcement of the extruded cement based materials. *Construction and Building Materials*, *160*, 376–384. https://doi.org/10.1016/j.conbuildmat.2017.11.066

Dean, S., Bassuoni, M., Nehdi, M., & Greenough, T. (2006). Enhancing the Reliability of Evaluating Chloride Ingress in Concrete Using the ASTM C 1202 Rapid Chloride

Penetrability Test. *Journal of ASTM International*, *3*(3), 13403. https://doi.org/10.1520/JAI13403

E. Yang, Yingzi Yang, & v. Li. (2007). Use of High Volumes of Fly Ash to Improve ECC Mechanical Properties and Material Greenness. *ACI Materials Journal*, *104*(6). https://doi.org/10.14359/18966

Eco Smart Foundation (2007), Assessment of Greenhouse Gas (GHG) Savings Achieved Through the Increased Use of SCMs, AP2K Assessment Project, Final Report for Natural Resources Canada, 23 p.

Eyley, S., & Thielemans, W. (2014). Surface modification of cellulose nanocrystals. *Nanoscale*, *6*(14), 7764–7779. https://doi.org/10.1039/C4NR01756K

Ferdosian, I., & Camões, A. (2017). Eco-efficient ultra-high performance concrete development by means of response surface methodology. *Cement and Concrete Composites*, *84*, 146–156. https://doi.org/10.1016/j.cemconcomp.2017.08.019

Fonseca, C. S., Silva, M. F., Mendes, R. F., Hein, P. R. G., Zangiacomo, A. L., Savastano, H., & Tonoli, G. H. D. (2019). Jute fibers and micro/nanofibrils as reinforcement in extruded fiber-cement composites. *Construction and Building Materials*, *211*, 517–527. https://doi.org/10.1016/j.conbuildmat.2019.03.236

Frentress, D.P. and Harrington, D.S., 2012. Guide for partial-depth repair of concrete pavements. Iowa State University Institute for Transportation.

Ghafari, E., Costa, H., & Júlio, E. (2014). RSM-based model to predict the performance of self-compacting UHPC reinforced with hybrid steel micro-fibers. *Construction and Building Materials*, *66*, 375–383. https://doi.org/10.1016/j.conbuildmat.2014.05.064

Ghazy, A., Bassuoni, M., Maguire, E., & O'Loan, M. (2016). Properties of Fiber-Reinforced Mortars Incorporating Nano-Silica. *Fibers*, *4*(1), 6. https://doi.org/10.3390/fib4010006

Ghazy, A., Bassuoni, M. T., & Shalaby, A. (2016). Nano-Modified Fly Ash Concrete: A Repair Option for Concrete Pavements. *ACI Materials Journal*. https://doi.org/10.14359/51688642

Ghazy, A., Bassuoni, M. T., Shalaby, A. and Hamilton, R., 2017. Nano-modified fly ash concrete as a repair material for concrete pavements: field trial. ACI Concrete international, 39(2), pp. 38-44.

Ghezal, A., & Khayat, K. H. (2002). Optimizing self-consolidating concrete with limestone filler by using statistical factorial design methods. *ACI Materials Journal*, *99*(3), 264–272.

Goncalves, J., Boluk, Y., & Bindiganavile, V. (2020). Cellulose nanofibres mitigate chloride ion ingress in cement-based systems. *Cement and Concrete Composites*, *114*, 103780. https://doi.org/10.1016/j.cemconcomp.2020.103780

Goncalves, J., El-Bakkari, M., Boluk, Y., & Bindiganavile, V. (2019). Cellulose nanofibres (CNF) for sulphate resistance in cement based systems. *Cement and Concrete Composites*, *99*, 100–111. https://doi.org/10.1016/j.cemconcomp.2019.03.005

Gruyaert, E., van den Heede, P., & de Belie, N. (2013). Carbonation of slag concrete: Effect of the cement replacement level and curing on the carbonation coefficient – Effect of carbonation on the pore structure. *Cement and Concrete Composites*, *35*(1), 39–48. https://doi.org/10.1016/j.cemconcomp.2012.08.024

Guimarães, M., Botaro, V. R., Novack, K. M., Flauzino Neto, W. P., Mendes, L. M., & Tonoli, G. H. D. (2015). Preparation of Cellulose Nanofibrils from Bamboo Pulp by

Mechanical Defibrillation for Their Applications in Biodegradable Composites. *Journal of Nanoscience and Nanotechnology*, *15*(9), 6751–6768. https://doi.org/10.1166/jnn.2015.10854

Habibi, Y., Lucia, L. A., & Rojas, O. J. (2010). Cellulose Nanocrystals: Chemistry, Self-Assembly, and Applications. *Chemical Reviews*, *110*(6), 3479–3500. https://doi.org/10.1021/cr900339w

He, X., Ma, M., Su, Y., Lan, M., Zheng, Z., Wang, T., Strnadel, B., & Zeng, S. (2018). The effect of ultrahigh volume ultrafine blast furnace slag on the properties of cement pastes. *Construction and Building Materials*, *189*, 438–447. https://doi.org/10.1016/j.conbuildmat.2018.09.004

Heidari, A., & Tavakoli, D. (2013). A study of the mechanical properties of ground ceramic powder concrete incorporating nano-SiO2 particles. *Construction and Building Materials*, *38*, 255–264. https://doi.org/10.1016/j.conbuildmat.2012.07.110

Hisseine, O. A., Omran, A. F., and Tagnit-Hamou, A., 2018. "Influence of Cellulose Filaments on Cement Paste and Concrete. Journal of Materials in Civil Engineering, 30(6), pp. 04018109-14.

Hisseine, O. A., Soliman, N. A., Tolnai, B., & Tagnit-Hamou, A. (2020). Nano-engineered ultra-high performance concrete for controlled autogenous shrinkage using nanocellulose. *Cement and Concrete Research*, *137*, 106217. https://doi.org/10.1016/j.cemconres.2020.106217

Hisseine, O. A., & Tagnit-Hamou, A. (2020). Nanocellulose for ecological nanoengineered strain-hardening cementitious composites incorporating high-volume ground-glass pozzolans. *Cement and Concrete Composites*, *112*, 103662. https://doi.org/10.1016/j.cemconcomp.2020.103662

Hisseine, O. A., Wilson, W., Sorelli, L., Tolnai, B., & Tagnit-Hamou, A. (2019). Nanocellulose for improved concrete performance: A macro-to-micro investigation for disclosing the effects of cellulose filaments on strength of cement systems. *Construction and Building Materials*, *206*, 84–96. https://doi.org/10.1016/j.conbuildmat.2019.02.042

Hoyos, C. G., Cristia, E., and Vázquez, A., 2013. "Effect of Cellulose Microcrystalline Particles on Properties of Cement-Based Composites." Materials and Design, 51, pp. 810-818.

Hoyos, C. G., Zuluaga, R., Gañán, P., Pique, T. M., & Vazquez, A. (2019). Cellulose nanofibrils extracted from fique fibers as bio-based cement additive. *Journal of Cleaner Production*, *235*, 1540–1548. https://doi.org/10.1016/j.jclepro.2019.06.292

Hsie, M., Tu, C., & Song, P. S. (2008). Mechanical properties of polypropylene hybrid fiber-reinforced concrete. *Materials Science and Engineering: A*, *494*(1–2), 153–157. https://doi.org/10.1016/j.msea.2008.05.037

Islam, A., Alengaram, U. J., Jumaat, M. Z., & Bashar, I. I. (2014). The development of compressive strength of ground granulated blast furnace slag-palm oil fuel ash-fly ash based geopolymer mortar. *Materials & Design (1980-2015)*, *56*, 833–841. https://doi.org/10.1016/j.matdes.2013.11.080

Iyer, P., Kenno, S. Y., & Das, S. (2015). Mechanical Properties of Fiber-Reinforced Concrete Made with Basalt Filament Fibers. *Journal of Materials in Civil Engineering*, *27*(11). https://doi.org/10.1061/(ASCE)MT.1943-5533.0001272

Jalasutram, S., Sahoo, D. R., & Matsagar, V. (2017). Experimental investigation of the mechanical properties of basalt fiber-reinforced concrete. *Structural Concrete*, *18*(2), 292–302. https://doi.org/10.1002/suco.201500216

Jang, S.-Y., Karthick, S., & Kwon, S.-J. (2017). Investigation on Durability Performance in Early Aged High-Performance Concrete Containing GGBFS and FA. *Advances in Materials Science and Engineering*, *2017*, 1–11. https://doi.org/10.1155/2017/3214696

Jennings, H. M., Thomas, J. J., Rothstein, D., & Chen, J. J. (2002). Cements as Porous Materials. In *Handbook of Porous Solids* (pp. 2971–3028). Wiley-VCH Verlag GmbH. https://doi.org/10.1002/9783527618286.ch40

Jhatial, A. A., Sohu, S., Bhatti, N.-K., Lakhiar, M. T., & Oad, R. (2018). Effect of steel fibres on the compressive and flexural strength of concrete. *International Journal of ADVANCED AND APPLIED SCIENCES*, *5*(10), 16–21. https://doi.org/10.21833/ijaas.2018.10.003

Jiang, C., Fan, K., Wu, F., & Chen, D. (2014). Experimental study on the mechanical properties and microstructure of chopped basalt fibre reinforced concrete. *Materials & Design*, *58*, 187–193. https://doi.org/10.1016/j.matdes.2014.01.056

Jiang, X., Xiao, R., Bai, Y., Huang, B., & Ma, Y. (2022). Influence of waste glass powder as a supplementary cementitious material (SCM) on physical and mechanical properties of cement paste under high temperatures. *Journal of Cleaner Production*, *340*, 130778. https://doi.org/10.1016/j.jclepro.2022.130778

Kaïkea, A., Achoura, D., Duplan, F., & Rizzuti, L. (2014). Effect of mineral admixtures and steel fiber volume contents on the behavior of high performance fiber reinforced concrete. *Materials & Design*, *63*, 493–499. https://doi.org/10.1016/j.matdes.2014.06.066

Kamasamudram, K. S., Ashraf, W., & Landis, E. N. (2021). Cellulose nanofibrils with and without nano-silica for the performance enhancement of Portland cement systems.

Construction and Building Materials, *285*, 121547. https://doi.org/10.1016/j.conbuildmat.2020.121547

Kamasamudram, K. S., Ashraf, W., & Landis, E. N. (2021). Cellulose Nanocomposites for Performance Enhancement of Ordinary Portland Cement-Based Materials. *Transportation Research Record: Journal of the Transportation Research Board*, *2675*(9), 11–20. https://doi.org/10.1177/0361198120958421

Kang, S.-C., Koh, H.-M., & Choo, J. F. (2010). An efficient response surface method using moving least squares approximation for structural reliability analysis. *Probabilistic Engineering Mechanics*, *25*(4), 365–371. https://doi.org/10.1016/j.probengmech.2010.04.002

Kang, S.-T., & Kim, J.-K. (2011). The relation between fiber orientation and tensile behavior in an Ultra High Performance Fiber Reinforced Cementitious Composites (UHPFRCC). *Cement and Concrete Research*, *41*(10), 1001–1014. https://doi.org/10.1016/j.cemconres.2011.05.009

Kayali, O., Haque, M. N., & Zhu, B. (2003). Some characteristics of high strength fiber reinforced lightweight aggregate concrete. *Cement and Concrete Composites*, *25*(2), 207–213. https://doi.org/10.1016/S0958-9465(02)00016-1

Ke, X., Bernal, S. A., & Provis, J. L. (2017). Uptake of chloride and carbonate by Mg-Al and Ca-Al layered double hydroxides in simulated pore solutions of alkali-activated slag cement. *Cement and Concrete Research*, *100*, 1–13. https://doi.org/10.1016/j.cemconres.2017.05.015

Khan, Md. N. N., & Sarker, P. K. (2019). Alkali silica reaction of waste glass aggregate in alkali activated fly ash and GGBFS mortars. *Materials and Structures*, *52*(5), 93. https://doi.org/10.1617/s11527-019-1392-3

Klemm, D., Cranston, E. D., Fischer, D., Gama, M., Kedzior, S. A., Kralisch, D., Kramer, F., Kondo, T., Lindström, T., Nietzsche, S., Petzold-Welcke, K., & Rauchfuß, F. (2018). Nanocellulose as a natural source for groundbreaking applications in materials science: Today's state. In *Materials Today* (Vol. 21, Issue 7, pp. 720–748). Elsevier B.V. https://doi.org/10.1016/j.mattod.2018.02.001

Köksal, F., Altun, F., Yiğit, İ., & Şahin, Y. (2008). Combined effect of silica fume and steel fiber on the mechanical properties of high strength concretes. *Construction and Building Materials*, *22*(8), 1874–1880. https://doi.org/10.1016/j.conbuildmat.2007.04.017

Köksal, F., Beycioğlu, A., & Dobiszewska, M. (2022). Optimization Based on Toughness and Splitting Tensile Strength of Steel-Fiber-Reinforced Concrete Incorporating Silica Fume Using Response Surface Method. *Materials*, *15*(18), 6218. https://doi.org/10.3390/ma15186218

Kong, D., Du, X., Wei, S., Zhang, H., Yang, Y., & Shah, S. P. (2012). Influence of nano-silica agglomeration on microstructure and properties of the hardened cement-based materials. *Construction and Building Materials*, *37*, 707–715. https://doi.org/10.1016/j.conbuildmat.2012.08.006

Karagöl, F., Demirbog, R., and Khushefati, W.H., 2015. Behavior of fresh and hardened concretes with antifreeze admixture in deep-freeze low temperatures and exterior winter conditions. *Construction and Building Materials*, *76*, pp. 388–395.

Lavoine, N., Desloges, I., Dufresne, A., & Bras, J. (2012). Microfibrillated cellulose – Its barrier properties and applications in cellulosic materials: A review. *Carbohydrate Polymers*, *90*(2), 735–764. https://doi.org/10.1016/j.carbpol.2012.05.026

Lee, H.-J., Kim, S.-K., Lee, H.-S., & Kim, W. (2019). A Study on the Drying Shrinkage and Mechanical Properties of Fiber Reinforced Cement Composites Using Cellulose Nanocrystals. *International Journal of Concrete Structures and Materials*, *13*(1), 39. https://doi.org/10.1186/s40069-019-0351-2

Lee, J. J., Song, J., & Kim, H. (2014). Chemical stability of basalt fiber in alkaline solution. *Fibers and Polymers*, *15*(11), 2329–2334. https://doi.org/10.1007/s12221-014-2329-7

Lee, N. K., & Lee, H. K. (2013). Setting and mechanical properties of alkali-activated fly ash/slag concrete manufactured at room temperature. Construction and Building Materials, 47, 1201–1209. https://doi.org/10.1016/j.conbuildmat.2013.05.107

Li, S. E., Frantz, G. C., & Stephens, J. E., 1999. Bond performance of rapid-setting repair materials subjected to deicing salt and freezing-thawing cycles. *ACI Materials Journal*, *96*(6), 692-697.

Malhotra, V.M., Zhang, M.H., Read, P.H. and Ryell, J., 2000. Long-term mechanical properties and durability characteristics of high-strength/high-performance concrete incorporating supplementary cementing materials under outdoor exposure conditions. Materials Journal, 97(5), pp.518-525.

Mazlan, D., Krishnan, S., Din, M. F. M., Tokoro, C., Khalid, N. H. A., Ibrahim, I. S., Takahashi, H., & Komori, D. (2020). Effect of Cellulose Nanocrystals Extracted from Oil Palm Empty Fruit Bunch as Green Admixture for Mortar. *Scientific Reports*, *10*(1), 6412. https://doi.org/10.1038/s41598-020-63575-7

Mechtcherine, V. (2012). Towards a durability framework for structural elements and structures made of or strengthened with high-performance fibre-reinforced

composites. *Construction and Building Materials*, *31*, 94–104. https://doi.org/10.1016/j.conbuildmat.2011.12.072

Mehta, P. K., & Monteiro, P. J. M. (2014). *Concrete: Microstructure, Properties, and Materials* (4th ed.). McGraw-Hill Education. https://www.accessengineeringlibrary.com/content/book/9780071797870

Mejdoub, R., Hammi, H., Suñol, J. J., Khitouni, M., M'nif, A., & Boufi, S. (2017). Nanofibrillated cellulose as nanoreinforcement in Portland cement: Thermal, mechanical and microstructural properties. *Journal of Composite Materials*, *51*(17), 2491–2503. https://doi.org/10.1177/0021998316672090

Mexasa, Z. S., Konsta-Gdoutos, M. S., & Shah, S. P. (2011). *Crack Free Concrete Made With Nanofiber Reinforcement*.

Mitchell, M. R., Link, R. E., Sappakittipakorn, M., & Banthia, N. (2012). Corrosion of Rebar and Role of Fiber Reinforced Concrete. *Journal of Testing and Evaluation*, *40*(1), 103873. https://doi.org/10.1520/JTE103873

Mohamed, O. A. (2019). A Review of Durability and Strength Characteristics of Alkali-Activated Slag Concrete. *Materials*, *12*(8), 1198. https://doi.org/10.3390/ma12081198

Montgomery, D. C. (2017). Design and analysis of experiments . In *Design and analysis of experiments* (Ninth edition.). John Wiley & Sons, Inc.

Moon, R. J., Martini, A., Nairn, J., Simonsen, J., & Youngblood, J. (2011). Cellulose nanomaterials review: Structure, properties and nanocomposites. *Chemical Society Reviews*, *40*(7), 3941–3994. https://doi.org/10.1039/c0cs00108b

Motahari Karein, S. M., Ramezanianpour, A. A., Ebadi, T., Isapour, S., & Karakouzian, M. (2017). A new approach for application of silica fume in concrete: Wet

granulation. *Construction and Building Materials, 157, 573–581. https://doi.org/10.1016/j.conbuildmat.2017.09.132*

MTO LS-412, 1997. Method of test for scaling resistance of concrete surfaces exposed to deicing chemicals. Ontario Lab Testing Manual, Ministry of Transportation, Ontario, Canada.

Nataraja, M. C., Dhang, N., & Gupta, A. P. (1999). Stress–strain curves for steel-fiber reinforced concrete under compression. *Cement and Concrete Composites, 21*(5–6), 383–390. https*://doi.org/10.1016/S0958-9465(99)00021-9*

Neville, A. M. (2011). Properties of Concrete. Pearson. https://books.google.ca/books?id=vsztgAEACAAJ

Oertel, T., Hutter, F., Tänzer, R., Helbig, U. and Sextl, G., 2013. Primary particle size and agglomerate size effects of amorphous silica in ultra-high performance concrete. Cement and Concrete Composites, 37, pp.61-67.

Onuaguluchi, O., Panesar, D. K., & Sain, M. (2014). Properties of nanofibre reinforced cement composites. Construction and Building Materials, 63, 119–124. https://doi.org/10.1016/j.conbuildmat.2014.04.072

Patel, A.J., Mojab, C.A.G. and Romine, A.R., 1993. Materials and procedures for rapid repair of partial depth spalls in concrete pavements-Manual of practice. Strategic highway research report No. SHRP-H-349, National research council, Washington, D.C.

Peters, S. J., Rushing, T. S., Landis, E. N., & Cummins, T. K. (2010). Nanocellulose and Microcellulose Fibers for Concrete. *Transportation Research Record: Journal of the Transportation Research Board, 2142*(1), 25–28. https://doi.org/10.3141/2142-04

Powers, T. C., & Helmuth, R. A. (1953). *Theory of Volume Changes in Hardened Portland Cement Paste During Freezing*. Portland Cement Association. https://books.google.ca/books?id=9GDvngEACAAJ

Prado, P. J., Balcom, B. J., Beyea, T. W., Armstrong, R. L., and Grattan-Bellew, P. E., 1998. Concrete freeze/thaw as studied by magnetic resonance imagine. *Cement and Concrete Research, 2*(28), pp. 261–70.

Reixach, R., Claramunt, J., Chamorro, M. À., Llorens, J., Pareta, M. M., Tarrés, Q., Mutjé, P., & Delgado-Aguilar, M. (2019). On the Path to a New Generation of Cement-Based Composites through the Use of Lignocellulosic Micro/Nanofibers. *Materials*, *12*(10), 1584. https://doi.org/10.3390/ma12101584

Safiuddin, Md., Kaish, A., Woon, C.-O., & Raman, S. (2018). Early-Age Cracking in Concrete: Causes, Consequences, Remedial Measures, and Recommendations. *Applied Sciences*, *8*(10), 1730. https://doi.org/10.3390/app8101730

Samad, S., & Shah, A. (2017). Role of binary cement including Supplementary Cementitious Material (SCM), in production of environmentally sustainable concrete: A critical review. *International Journal of Sustainable Built Environment*, *6*(2), 663–674. https://doi.org/10.1016/j.ijsbe.2017.07.003

Sanchez, F., & Sobolev, K. (2010). Nanotechnology in concrete – A review. *Construction and Building Materials*, *24*(11), 2060–2071. https://doi.org/10.1016/j.conbuildmat.2010.03.014

Santos, R. F., Ribeiro, J. C. L., Franco de Carvalho, J. M., Magalhães, W. L. E., Pedroti, L. G., Nalon, G. H., & Lima, G. E. S. de. (2021). Nanofibrillated cellulose and its applications in cement-based composites: A review. *Construction and Building Materials*, *288*, 123122. https://doi.org/10.1016/j.conbuildmat.2021.123122

Said, A.M., Zeidan, M.S., Bassuoni, M.T. and Tian, Y., 2012. Properties of concrete incorporating nano-silica. Construction and building materials, 36, pp.838-844.

Smith, K.D., Harrington, D.S., Pierce, L., Ram, P. and Smith, K.L., 2014. Concrete Pavement Preservation Guide. No. FHWA-HIF-14-014. Federal Highway Administration, USA.

Shahab-ud-Din, Ahmad, M. Z., Qureshi, K., Bhatti, I. A., Zahid, M., Nisar, J., Iqbal, M., & Abbas, M. (2018). Hydrothermal synthesis of molybdenum trioxide, characterization and photocatalytic activity. *Materials Research Bulletin*, *100*, 120–130. https://doi.org/10.1016/j.materresbull.2017.11.044

Sharip, N. S., & Ariffin, H. (2019a). Cellulose nanofibrils for biomaterial applications. *Materials Today: Proceedings*, *16*, 1959–1968. https://doi.org/10.1016/j.matpr.2019.06.074

Shi, C. (2004). Effect of mixing proportions of concrete on its electrical conductivity and the rapid chloride permeability test (ASTM C1202 or ASSHTO T277) results. *Cement and Concrete Research*, *34*(3), 537–545. https://doi.org/10.1016/j.cemconres.2003.09.007

Siddique, R., & Mehta, A. (2014). Effect of carbon nanotubes on properties of cement mortars. *Construction and Building Materials*, *50*, 116–129. https://doi.org/10.1016/j.conbuildmat.2013.09.019

Spadea, S., Farina, I., Carrafiello, A., & Fraternali, F. (2015). Recycled nylon fibers as cement mortar reinforcement. *Construction and Building Materials*, *80*, 200–209. https://doi.org/10.1016/j.conbuildmat.2015.01.075

Stephenson, K. (2011). *Characterizing the Behavior and Properties of Nanocellulose Reinforced Ultra High Performance Concrete*.

Streicher, P. E., & Alexander, M. G. (1995). A chloride conduction test for concrete. *Cement and Concrete Research*, *25*(6), 1284–1294. https://doi.org/10.1016/0008-8846(95)00121-R

Sun, X., Wu, Q., Lee, S., Qing, Y., & Wu, Y. (2016). Cellulose Nanofibers as a Modifier for Rheology, Curing and Mechanical Performance of Oil Well Cement. *Scientific Reports*, *6*(1), 31654. https://doi.org/10.1038/srep31654

Sun, X., Wu, Q., Zhang, J., Qing, Y., Wu, Y., & Lee, S. (2017). Rheology, curing temperature and mechanical performance of oil well cement: Combined effect of cellulose nanofibers and graphene nano-platelets. *Materials & Design*, *114*, 92–101. https://doi.org/10.1016/j.matdes.2016.10.050

Teng, S., Lim, T. Y. D., & Sabet Divsholi, B. (2013). Durability and mechanical properties of high strength concrete incorporating ultra fine Ground Granulated Blast-furnace Slag. *Construction and Building Materials*, *40*, 875–881. https://doi.org/10.1016/j.conbuildmat.2012.11.052

Tiznobaik M, and Bassuoni M. T., 2018. A test protocol for evaluating absorption of joints in concrete pavements. *Journal of Testing and Evaluation, 46*(4), pp. 1636-1649.

Wawrzeńczyk, J., Molendowska, A., & Juszczak, T. (2018). Determining k-Value with Regard to Freeze-Thaw Resistance of Concretes Containing GGBS. *Materials*, *11*(12), 2349. https://doi.org/10.3390/ma11122349

Yasien, A. M., & Bassuoni, M. T. (2022). Nano-modified concrete at sub-zero temperatures: experimental and statistical modelling. *Magazine of Concrete Research*, *74*(1), 2–21. https://doi.org/10.1680/jmacr.19.00437

Yi, Y., Guo, S., Li, S., Zillur Rahman, M., Zhou, L., Shi, C., & Zhu, D. (2021). Effect of alkalinity on the shear performance degradation of basalt fiber-reinforced polymer

bars in simulated seawater sea sand concrete environment. *Construction and Building Materials*, *299*, 123957. https://doi.org/10.1016/j.conbuildmat.2021.123957

Zhang, M.-H., Islam, J., & Peethamparan, S. (2012). Use of nano-silica to increase early strength and reduce setting time of concretes with high volumes of slag. *Cement and Concrete Composites*, *34*(5), 650–662. https://doi.org/10.1016/j.cemconcomp.2012.02.005

Zhao, Y.-R., Wang, L., Lei, Z.-K., Han, X.-F., & Xing, Y.-M. (2017). Experimental study on dynamic mechanical properties of the basalt fiber reinforced concrete after the freeze-thaw based on the digital image correlation method. *Construction and Building Materials*, *147*, 194–202. https://doi.org/10.1016/j.conbuildmat.2017.02.133

Zheng, Z. (1995). Synthetic fibre-reinforced concrete. *Progress in Polymer Science*, *20*(2), 185–210. https://doi.org/10.1016/0079-6700(94)00030-6

Zhu, Y., Yang, Y., & Yao, Y. (2012). Use of slag to improve mechanical properties of engineered cementitious composites (ECCs) with high volumes of fly ash. *Construction and Building Materials*, *36*, 1076–1081. https://doi.org/10.1016/j.conbuildmat.2012.04.031

APPENDIX A: SUPPLEMENTAL RESULTS FOR PHASE I

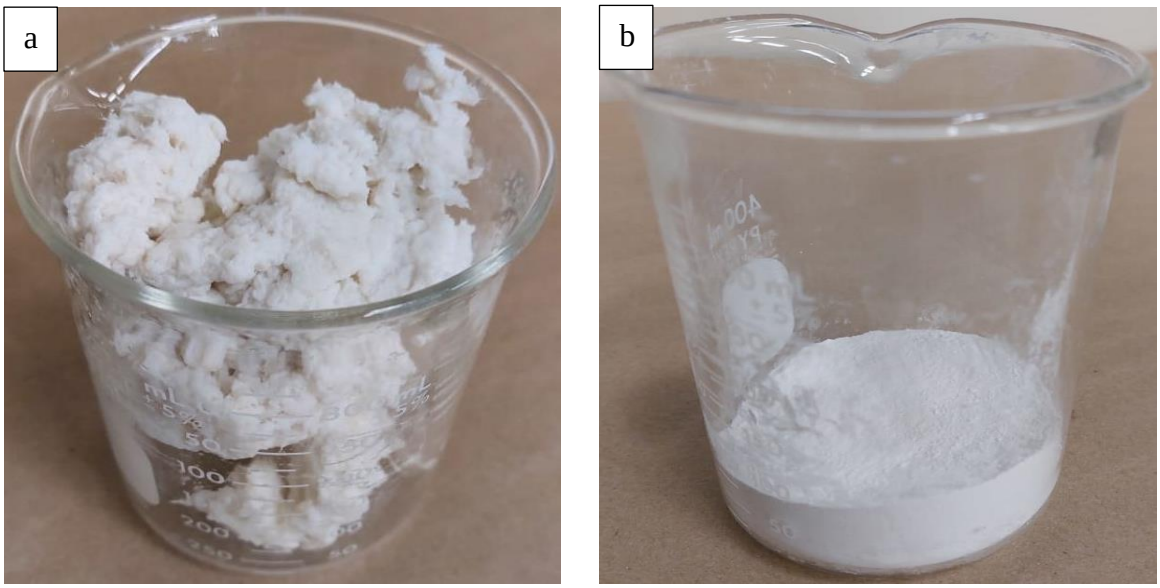

Figure A. 1: Sample of nano-cellulose materials: (a) Nano-fibrillated cellulose (NFC), and (b) Nano-crystalline cellulose.

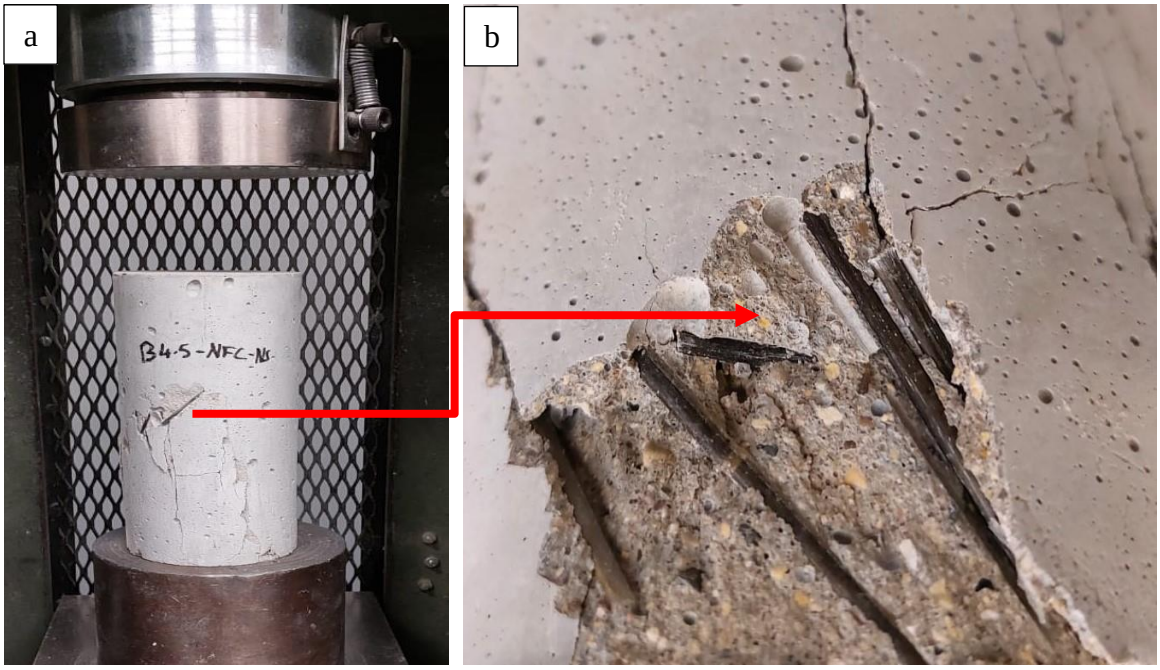

Figure A. 2: BFP crack bridging mechanism captured after conducting compressive strength test for specimen B4.5-NFC0.5-NS: (a) specimen after test ended, and (b) BFP bridging cracks.

Figure A. 3: Carbon coating machine.

Figure A. 4: Carbon coated specimens for SEM.

APPENDIX B: SUPPLEMENTAL RESULTS FOR PHASE II

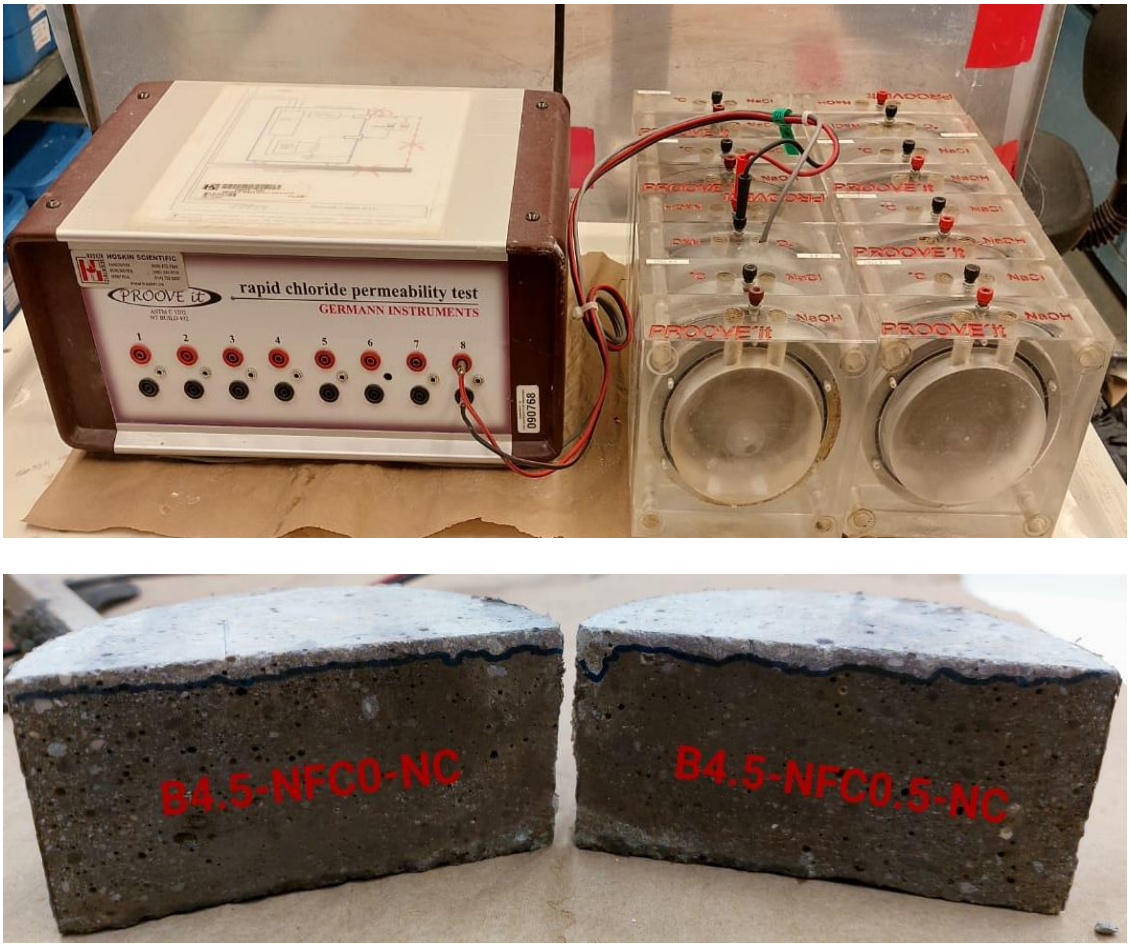

Figure B. 1: RCPT test set-up and exemplar sample after spraying 0.1M silver nitrate.

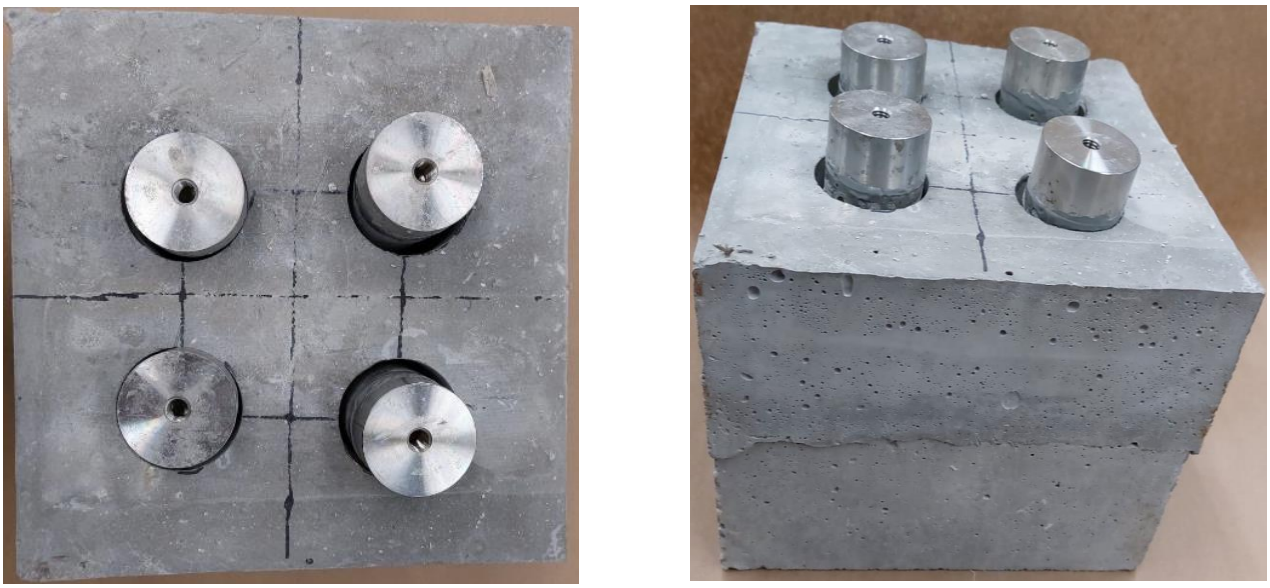

Figure B. 2: Pull off test sample.

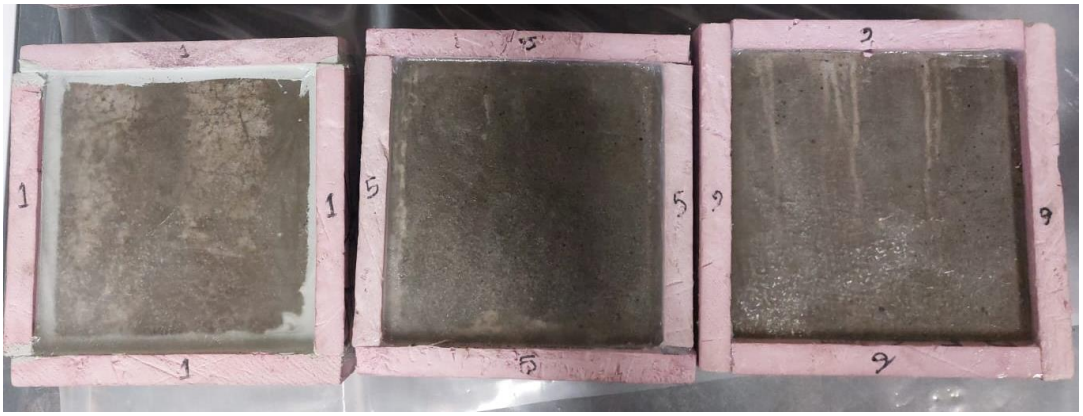

Figure B. 3:Exemplar surface scaling samples.

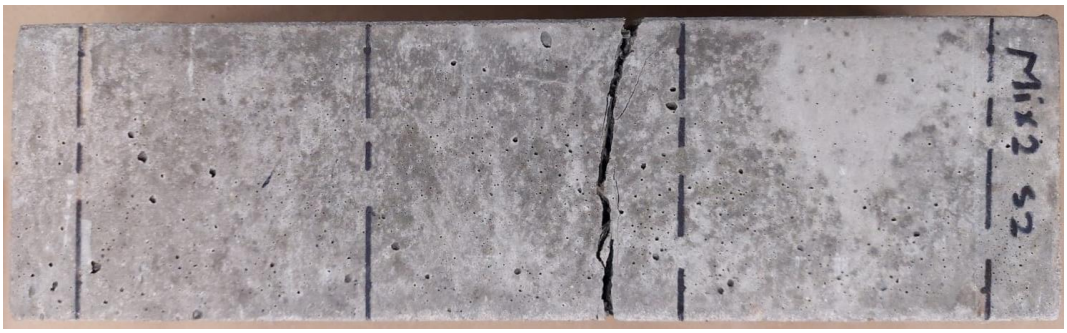

Figure B. 4:Exemplar specimens after flexural test cracked at mid-span as stipulated by ASTM C1609.

Figure B. 5:Exemplar of restrained shrinkage specimen.